QUANTUM MECHANICAL PHASE OF PARTICLES AND MOLECULES IN VARIOUS ELECTROMAGNETIC CONFIGURATIONS: MOLECULAR AND NANO-SCALE INTERFEROMETRIC DEVICES

A Thesis Submitted

To

Sikkim University

In Partial Fulfillment of the Requirement for the Degree of Doctor of Philosophy in Physics

By

Yam Prasad Rai

Department of Physics

School of Physical Sciences

July 2022

CERTIFICATE

This is to certify that the Ph.D. thesis entitled **"Quantum Mechanical Phase of Particles and Molecules in Various Electromagnetic Configurations: Molecular and Nano-scale Interferometric Devices"**, submitted to Sikkim University in partial fulfillment of the requirement for the degree of Doctor of Philosophy in Physics, represents the work carried out by **Mr. Yam Prasad Rai** in the Department of Physics, Sikkim University, Gangtok, Sikkim. The results are original and have not been submitted anywhere else for any other degree. It is recommended that this Ph.D. thesis be placed before the Examiners for evaluation.

Head of the Department
(Dr. Ajay Tripathi)
Department of Physics
School of Physical Sciences
Sikkim University
Gangtok- 737102

Place: Gangtok, Sikkim, India

Date:

CERTIFICATE

This is to certify that the work presented in the dissertation **"Quantum Mechanical Phase of Particles and Molecules in Various Electromagnetic Configurations: Molecular and Nano-scale Interferometric Devices"**, being submitted by **Mr. Yam Prasad Rai** for the award of Ph.D. in Physics was carried out by him under my supervision.

Dr. Dhurba Rai
Ph.D. Supervisor
Department of Physics
School of Physical Sciences
Sikkim University

Place: Gangtok, Sikkim, India

Date:

Declaration

I, **Yam Prasad Rai**, declare that this thesis titled **"Quantum Mechanical Phase of Particles and Molecules in Various Electromagnetic Configurations: Molecular and Nano-scale Interferometric Devices"** submitted by me for the award of **Doctor of Philosophy** in Physics at **Sikkim University** is my original work. It is further declared that the present thesis does not contain materials previously published. I do confirm that

- The content of this Ph.D. thesis is based on the work which I have performed myself while in candidature for a Ph.D. degree at this University.
- This thesis has not been submitted for any degree to any other University or institution.
- The content of this thesis has been subjected to anti-plagiarism software **(URKUND)** and was found satisfactory.

(Yam Prasad Rai)
Roll No.: 14PDPY04
Regn. No.:14/Ph.D/PHY/04

Date:

Recommended that the thesis be placed before the Examiners for evaluation

(Dr. Dhurba Rai)
Ph.D. Supervisor

Date:

In the memory of my Parents

Late Ratna Bahadur Rai , Late Fif Rani Rai..

Dedicated *to my Elder Sister Tulasa Rai , Elder Brother Ram Kumar Rai , Bhawju Jasnita Rai , Nani Ninamcha Rai, Nani Samridhi Shree Chettri and to my only friend Umesh Dhakal . . .*

Acknowledgements

This thesis has been a long and adventurous journey for me. Although I value my accomplishments and privileges, the most important lesson I've learned during this journey has come from multiple setbacks I've experienced. Having stated that, I would like to express my deep sense of gratitude to my supervisor Dr. Dhurba Rai, Assistant Professor, Department of Physics, Sikkim University, India. Without him, this thesis would have remained a dream and seemingly impossible feat to conquer. His dedication, timely advice and rigorous scrutiny have inspired and motivated me to advance to where I am today.

I owe my deepest gratitude to all the faculty members of the Physics Department for their kind support, advice and cooperation throughout my career as a research scholar. My heartfelt thanks to all my friends, brothers, sisters and colleagues who endured this long process with me, always offering the much-needed support and care. I'll always cherish the time we spent together in the research lab, and in social settings.

I am thankful to my friend Umesh Dhakal whom I met during the undergraduate course in physics at St. Joseph's College, Darjeeling. Since then our journey continued on the same path to the end of this thesis and for many more years to go ahead together. He has been a constant companion, offering advice and encouragement with a perfect blend of insight and humor.

I would also like to acknowledge the funding agency, University Grants Commission (UGC), Government of India for providing financial assistance through the UGC CSIR Direct-SRF. Special thanks to Alexandra Elbakyan, the founder of the website Sci-Hub aimed at removing all the barriers in the way of science, thereby making worldwide accessibility to virtually all scientific research papers.

I am indebted to my elder brother and sister who took the role of parents for helping me through the toughest times. They were the ones providing me with the enormous emotional and financial support in need, to which I shall ever remain grateful.

Lastly, to my late parents who were immensely proud of me for pursuing Ph.D., though it didn't make much sense to them in essence. I wish they could see me accomplishing this.

Despite how little I was able to accomplish during my research activities, which I accept, nonetheless, I hope that the efforts I have made as presented in this thesis have in some way contributed to the advancement of science.

Yam Prasad Rai
July, 2022

Preface

This thesis deals with the quantum mechanical phase of particles and molecules in various electro-magnetic configurations that may be exploited in the molecular and nano-scale interferometric setup. The thesis consists of five chapters that flow seamlessly into the next as one reads. Every chapter begins with an abstract that gives a brief summary of the work presented there. The background material on the subject covered in each chapter is provided with relevant classic and recent references. This is followed by motivations as presented in the section, "Scope of the Work", leading to investigations as presented in the "Results and Discussion" section in Chapters 2 through 4. Each of these chapters ends with the "Summary and Concluding Remarks", followed by a list of references. At places, additional studies and figures that are not the part of the published article are also presented. The last chapter provides a brief summary of the work covered in the thesis with a future outlook and suggestions for future work on some selected topics.

Chapter 1 gives a brief review of the necessary background materials for the work carried out in this thesis starting with a preamble to the various quantum mechanical topological phases of the neutral and charged particles. This includes the Aharonov-Bohm (AB) phase of a charged particle, the dual-AB phase of a fluxon, the Aharonov-Casher (AC) phase of magnetic moment and the He-McKellar-Wilkens phase of electric dipole moment in the various electromagnetic field configurations. A brief overview of various excitons is presented to the effect that how the exciton-based optoelectronic devices exploiting the HMW phase might benefit from the significant electric dipole moment of the inter-layer excitons in the bilayer heterostructures of transition-metal dichalcogenides (TMDs).

Chapter 2 presents a systematic investigation of the locality aspects of the various quantum topological phase shift effects that include the AB, AC and HMW effects. A unified coherent description is presented emphasizing that the topological effects are exclusively local phenomena. Absence of force on the charged particle passing by a "perfectly shielded" long and narrow current carrying solenoid establish that the AB phase shift is truly non-classical in origin. The AB phase shift from energy consideration is presented.

Chapter 3 focuses on the HMW phase of the neutral particles endowed with an electric dipole moment. Derivation of the HMW phase with explicit consideration of the interaction between current associated with the moving dipole and the magnetic vector potential is presented. Various field configurations are explored and conditions laid down for the observation of the HMW phase in its original essence with radial magnetic field alone. A practical setup is proposed for the observation of the HMW phase in a radial magnetic field.

Chapter 4 opens with the possibility of modulating the HMW phase acquired by the excitons in suitably designed light-driven molecular ring junctions. Influence of magnetic field on the transmission probability of exciton transport in a 1D continuum ring and polyacetylene macrocycle (PAM) dimer ring is demonstrated within the model based calculations. The possible modulation of exciton photoluminescence (PL) at the output by the applied magnetic field in the ring is discussed.

Chapter 5 briefly summarizes the main conclusions of the study carried out in this thesis. The future direction of research and development in this area is explored. A list of future works on a few selected topics is given, along with an outline and explanation.

The thesis concludes with a list of index that fills the last pages.

List of Publications

(A) Referred Journals:

- Yam P. Rai and Dhurba Rai, "On the He–McKellar–Wilkens phase of an electric dipole", Ann. Phys. **383**, 196 (2017).
  doi.org/10.1016/j.aop.2017.05.007

(B) Submitted:

- Yam P. Rai and Dhurba Rai, "A Unified View On The Quantum Topological Phase Shifts".
- Yam P. Rai, Umesh Dhakal, and Dhurba Rai, "Magnetic field control of exciton transport through the stacked PAM junction".

(C) Other work of author (in preparation):

- Umesh Dhakal, Yam P. Rai, and Dhurba Rai, "Magnetic field effects on thermoelectric properties of ring structure molecular junctions".

Presentations in National/ International Conferences/Workshops

- **Poster Presentation** on the topic "Quantum Phase of an Electric Dipole in a Static Magnetic Field" in International Conference on Nanotechnology : Ideas, Innovation and Initiatives - 2017 at IIT Roorkee, Dec 06th – 08th, Uttarakhand, India.
- **Oral Presentation** on the topic "Quantum Phase of an Electric Dipole in a Static Magnetic Field" in National Conference on Trends in Science and Technology 27th -28th Feb, 2018, at Salesian College, Siliguri, W.B, India.
- **Participated** Refresher Course on Basic Physics and Topology organized by Deptt. of Physics Sikkim University, Gangtok, Jan 29, 2018 to Feb 09, 2018, India.

Contents

List of Figures

List of Tables

Chapter1

Introduction: The Background

Abstract

This chapter provides an overview of the most relevant topics concerning the work carried out in this thesis. Background materials are presented, and the strategy of the work is outlined, with details addressed later in the respective chapters.

1.1 Preamble

The quest for understanding particle-field interaction is as much old as Maxwell's classical theory of the electromagnetic field, which is one of the important pillars of modern physics. Maxwell's electromagnetic theory played a fundamental role in the development of Einstein's special theory of relativity. It is important to realize that Maxwell's equations in vacuum implicitly contain the special theory of relativity. The advent of quantum theory, however, revealed the need of addressing additional significance to the quantities introduced in classical physics. An issue concerning such redressal constitutes the part of the theme subscribed herein. We here begin with the classical notion of the electromagnetic fields that otherwise are considered the fundamental quantities responsible for every effect.

In classical physics, a charged particle q moving with a velocity $\vec{v}$ in an electromagnetic field $(\vec{E}, \vec{B})$ experiences a force described by the Lorentz,

$$\vec{F} = q\left(\vec{E} + \frac{\vec{v}}{c} \times \vec{B}\right). \tag{1.1}$$

The classical notion is that the behaviour of charged particles in the electromagnetic field can entirely be described by the fields $(\vec{E}, \vec{B})$, while the associated potentials, viz., the scalar electric potential ϕ and the magnetic vector potential $\vec{A}$ are introduced only as a means of obtaining $\vec{E}$ and $\vec{B}$ as, $\vec{E} = -\vec{\nabla}\phi - \frac{\partial \vec{A}}{\partial t}$ and $\vec{B} = \vec{\nabla} \times \vec{A}$. The potentials $(\phi, \vec{A})$ have no physical significance of their own,

and are determined only up to a transformation known as *gauge transformation.* Under the gauge transformation, viz., $\phi \rightarrow \phi' = \phi - \frac{\partial \chi}{\partial t}$ and $\vec{A} \rightarrow \vec{A'} = \vec{A} + \vec{\nabla}\chi$, where χ is a scalar function called gauge function, the potentials $(\phi, \vec{A})$ undergo transformation attaining a new value, while the fields $(\vec{E}, \vec{B})$ remain unaffected.

The above viewpoint, however, shattered when Yakir Aharonov and David Bohm in 1959 made a fascinating and remarkable prediction in their seminal paper on the *"Significance of Electromagnetic Potentials in the Quantum Theory"*,[1] that the behavior of the charged particles cannot entirely be described by the fields $(\vec{E}, \vec{B})$. Instead, the scalar and vector potentials $(\phi, \vec{A})$ play an important role and thus bring about the fundamental importance of potentials over the fields. Among the two proposed experiments to verify the effect of the potentials $(\phi, \vec{A})$ on the motion of the charged particles, the prediction of a phase difference between the counter-propagating electron's wave function outside a long current-carrying solenoid is extensively studied for if the vector potential $\vec{A}$ is more fundamental than the field $\vec{B}$. Another important defining feature of the Aharonov-Bohm (AB) effect is the independence of the phase on particle velocity and path taken, which makes the effect topological in nature. The study not only revealed the importance of the vector potential but also engendered analogous topological effects, viz., the Aharonov-Casher (AC) [2] and the He-McKellar-Wilkens (HMW) [3, 4] effects. Moreover, the investigation and exploitation of the AB effect resulting from the potential-induced phase difference remain far from finished.

In what follows, we outline the various topological effects and the interrelation between them. The physical origins of each effect will be briefly explored, while a more in-depth understanding of the mechanism as studied in this work will be discussed later in the related chapters, viz., Chapters 2 and 3. The model calculation for possible exploitation of one of the topological effects in the optoelectronic devices is presented in Chapter 4. Finally, the key conclusions of the work in the thesis are summarized in Chapter 5, and future prospects are discussed.

1.2 Sagnac Effect

The Sagnac effect is a phase-induced effect in the rotating atom or optical interferometers that leads to the difference in travel time between the two counter-propagating particles or optical waves.[5] The path difference between the counter-propagating waves differs by an amount proportional to the angular velocity ω of rotation of the interferometer, and the area S enclosed by the paths of interfering waves, leading to a shift of the interference fringe positions when the interfering waves overlap.[6] The effect is universal and experimentally observed for both light and particle waves. A sketch of the Sagnac interferometer mounted on a turntable rotating with a constant angular velocity ω is shown in Fig. 1.1. While the entire interferometer setup is made to rotate, the light or particle beam from a source is split into two beams by a beam splitter (usually a half-silvered mirror) which in conjunction with an arrangement of beam reflectors allows them to propagate in opposite directions. These beams are constrained to make round trips, which are

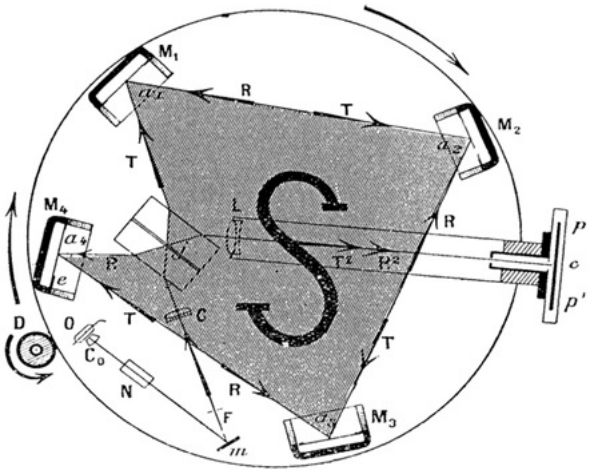

FIGURE 1.1: Sagnac interferometer mounted on a turntable. M's indicate the beam reflectors, while the letter S denotes the area (shaded region) enclosed by the interfering waves. Figure adapted from Ref.[5]

then, reunited back for overlap to produce the interference pattern. The difference in the round-trip time for these counter-propagating beams leads to a phase difference with a consequent shift in the position of the fringes in the interference pattern. The phase difference induced due to the difference in path lengths between the counter-propagating waves in the rotating interferometer is known as the Sagnac phase, and the phase-induced effect as the Sagnac effect, named after its discoverer in 1913. It turns out that the Sagnac phase is expressible as the closed line integral of the linear velocity $\vec{v}$ of rotation of the interferometer, which is then transformed into the surface integral form involving the physical quantities that are easily accessible to experimental measurements,

$$\phi_{Sag} = \frac{m}{\hbar}\oint \vec{v}\cdot d\vec{l} = \frac{2m}{\hbar}\int \vec{\omega}\cdot d\vec{S} = \frac{2m}{\hbar}\omega S, \tag{1.2}$$

where m is the inertial mass of the interfering particles ($m = h/\lambda c$ for photons). Note that the constancy of the angular velocity ω of the interferometer is employed in obtaining the last equality. Also, the phase acquired is independent of the velocity of the interfering waves and the path taken.

Concerning the theoretical perspectives behind the Sagnac phase, the interaction energy associated with the local coupling of velocity field $\vec{v}$ to a component of the canonical momentum, the hidden momentum $\vec{p}_{hidden} = m\vec{v}$, is $U = -\vec{v} \cdot \vec{p}_{hidden}$. Therefore, the Sagnac phase is

$$\begin{aligned} \phi_{Sag} &= \frac{1}{\hbar} \oint -\frac{\partial U}{\partial \vec{v}} \cdot \vec{dl}, \\ &= \frac{m}{\hbar} \oint \vec{v} \cdot \vec{dl}, \\ &= \frac{2m}{\hbar} \int \vec{\omega} \cdot \vec{dS}, \\ &= \frac{2m}{\hbar} \omega S. \end{aligned} \tag{1.3}$$

Yet another elegant way to look at the Sagnac phase is due to Sakurai.[7] As shown, the Sagnac phase can be obtained from the AB phase by exploiting the two-fold analogy, between the Lorentz force on a charged particle and the Coriolis force in the rotating frame, and that between the canonical momentum of the charged particle and that in the rotating frame. The Sagnac effect is a well studied phenomenon with numerous applications including the most common technical application in the fibre-optic gyroscope (FOG) systems that sense changes in orientation of an object by measuring the angular velocity utilizing the Sagnac effect

occurring in an optical fiber loop or a ring laser in the setup.[8]

1.3 Aharonov-Bohm Effect

An interesting and far-reaching aspect of Maxwell's electrodynamics of particle-field interactions involves both the classical fields $(\vec{E}, \vec{B})$ as well as potentials $(\phi, \vec{A})$. However, the potentials are introduced only as a convenient means of evaluating the fields whenever symmetry of a system permits, particularly in the case of evaluating magnetic field $\vec{B}$ from the vector potential $\vec{A}$. The defining equations for the potentials $(\phi, \vec{A})$ are $\vec{E} = -\vec{\nabla}\phi - \frac{\partial \vec{A}}{\partial t}$ and $\vec{B} = \vec{\nabla} \times \vec{A}$. As is evident that unlike the fields $(\vec{E}, \vec{B})$, the potentials are subject to change under the gauge transformations $\phi \to \phi' = \phi - \frac{\partial \chi}{\partial t}$ and $\vec{A} \to \vec{A}' = \vec{A} + \vec{\nabla}\chi$. As a consequence, any physical significance, as otherwise, in the sense of ordinary physical quantities, cannot be deduced for potential.

Notwithstanding the above, in 1959, in the most influential paper, Aharonov and Bohm (hereafter AB), drew attention to the significance of potentials and their role in the quantum mechanics of the charged particles.[1] Ever since their seminal work, our perception of the potentials as exclusively the mathematical construction for the calculation of fields has changed. Moreover, it has raised considerable interest and speculation too, with never-ending debate. The crux of the AB's work hinges on the conclusion that the interference fringes formed by the interfering charged particles get shifted by the potentials $(\phi, \vec{A})$, though the charged

particles never come in direct contact with the physical fields $(\vec{E}, \vec{B})$. Thus, there is no electromagnetic force whatsoever on the moving charged particles. However, in the electric (or scalar) AB effect, the charged particles indeed pass through time-dependent scalar electric potential, while in the magnetic (or vector) AB effect, they traverse through spatially varying, but static, magnetic vector potential outside a long current-carrying solenoid. With no force acting on the particles, the AB effects are essentially quantum-mechanical in nature, and the non-classical explanation is that the potentials influence the canonical momentum of the charged particle leading to the wave function of the particle acquire phase that affects the interference fringes.

In the following sections, we describe the electric and magnetic AB effects with due attention to the latest works on the subject.

1.3.1 Electric Aharonov–Bohm effect

In the seminal paper,[1] AB proposed the interference experiment to test the influence of scalar electric potential ϕ on the motion of electrons through a region where there are no physical fields, i.e., $\vec{E} = 0$, $\vec{B} = 0$. As shown in Fig. 1.2, the proposed experimental setup has two long cylindrical metal tubes within which the electrons are subjected to time-varying electric potentials, $\phi_1(t)$ and $\phi_2(t)$. A coherent electron wavepacket travelling towards the tubes is split into two wavepackets. Subsequently, each wavepacket is allowed to enter a long cylindrical metal tube wherein the potentials are varied only when the electron wave packets are well

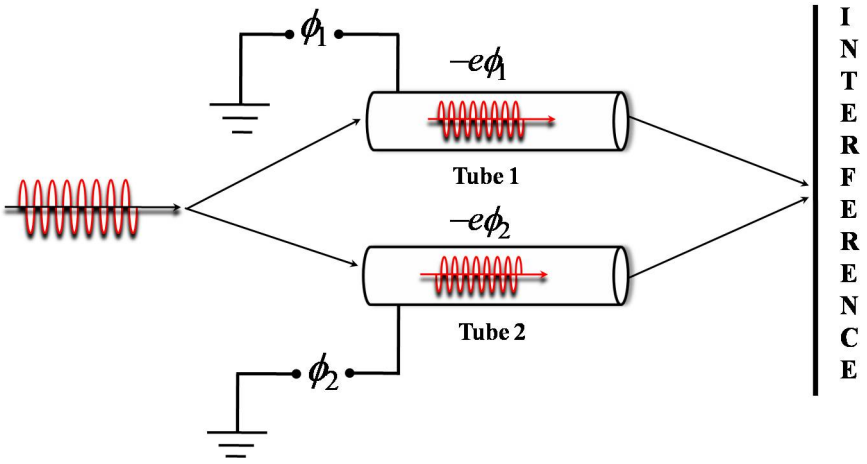

FIGURE 1.2: Schematic diagram of electric Aharonov-Bohm effect. ϕ_1 and ϕ_2 are the time-varying electric potentials that are switched on to influence the electron wavepackets only when the wavepackets are well within the metallic tubes.

inside the tubes so as not to have any effect of the stray or fringe fields at the ends of the tubes. The wavepackets are then superimposed to give an interference pattern. The proposed experimental setup is expected to show a phase difference due to the time-dependent scalar potential, even though no electromagnetic force is ever exerted on the wave packets. Consequently, the interference pattern will show the displacement of the interference fringes, with a magnitude proportional to the phase difference, within the undeflected diffraction envelope. This is known as the electric AB effect (EAB). The electric AB phase reads [1]

$$\begin{aligned} \phi_{EAB} &= \frac{e}{\hbar} \oint \phi(t) dt, \\ &= \frac{et}{\hbar} \Delta\phi(t), \end{aligned} \tag{1.4}$$

where $\Delta\phi(t) = \phi_2(t) - \phi_1(t)$ is the potential difference between the two tubes. A rigorous proof of quantum mechanical prediction of the existence of the electric AB effect under some conditions can be found in Ref. [9]. It must be mentioned here that the electric AB effect is much less studied both theoretically [9] and experimentally,[10] and its very existence is still a controversial issue.[11–14]

1.3.2 Magnetic Aharonov–Bohm effect

Owing to the comparatively much easier and technically attractive experimental setup for the magnetic AB effect, it is no surprise that there exists a huge volume of literature on the magnetic version of the AB effect. In what follows, we shall limit our discussion to the magnetic AB effect only (hereafter, just AB effect). As shown in Fig. 1.3, the AB setup consists of a long, narrow and tightly wound current-carrying solenoid that produces uniform magnetic field $\vec{B}$ within it, while no field in its exterior. The incoming electron beam is split into two, which are then made to overlap at the other end after traversing past the solenoid from opposite sides, thereby enclosing the magnetic flux Φ of the solenoid within the interfering paths. The amount of fringe shift in the interference pattern is predicted to be proportional to the amount of magnetic flux Φ enclosed by the interfering paths. This effect is known as the AB effect, and the associated induced phase ϕ_{AB} is the AB phase. As there is no magnetic field and electric field either, the charged particle does not experience force whatsoever, and the non-classical explanation for the AB effect is that the vector potential $\vec{A}$ enters into the canonical momentum of

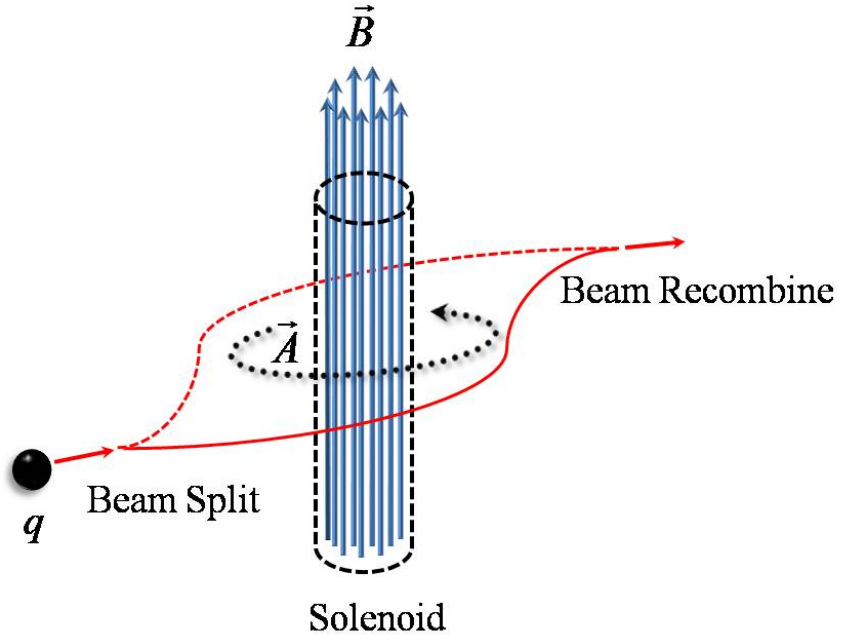

FIGURE 1.3: Schematic diagram of Aharonov-Bohm effect. The long, narrow and tightly wound solenoid carries a steady current to produce a uniform magnetic field $\vec{B}$ inside the solenoid, however, no magnetic field outside the solenoid. The vector potential $\vec{A}$ mimics the direction of current flow in the solenoid.

the moving charged particle leading to the wave function of the particle acquiring phase that affects the interference fringes. The difference in phase accumulated on either path around the solenoid is the line integral of the electromagnetic momentum. The Lagrangian for the charged particle q moving with velocity $\vec{v}$ outside the solenoid, where there is only the magnetic vector potential $\vec{A}$, is given by

$$L = \frac{1}{2}m|\vec{v}|^2 + q\vec{A}\cdot\vec{v}. \tag{1.5}$$

The canonical momentum is

$$\begin{aligned}\vec{p}_{canonical} &= \frac{\partial L}{\partial \vec{v}}, \\ &= \frac{\partial}{\partial \vec{v}}\left(\frac{1}{2}m\vec{v}^2 + q\vec{A}\cdot\vec{v}\right), \\ &= m\vec{v} + q\vec{A}. \end{aligned} \tag{1.6}$$

As $\vec{p}_{canonical} = \vec{p}_{kinetic} + \vec{p}_{em}$, the electromagnetic momentum is identified as $\vec{p}_{em} = q\vec{A}$. The associated interaction energy is $U = -\vec{v}\cdot\vec{p}_{em}$, and the AB phase is

$$\begin{aligned}\phi_{AB} &= \frac{1}{\hbar}\oint -\frac{\partial U}{\partial \vec{v}}\cdot d\vec{l}, \\ &= \frac{q}{\hbar}\oint \vec{A}\cdot d\vec{l}, \\ &= \frac{q}{\hbar}\int \vec{B}\cdot d\vec{s}, \end{aligned} \tag{1.7}$$

where $\vec{B} = \vec{\nabla}\times\vec{A}$ is the magnetic field that exists only inside the solenoid. Thus, the AB phase is proportional to the amount of flux $\Phi = \int \vec{B}\cdot d\vec{s}$ enclosed by the interfering paths.

Although the very existence of the AB effect was demonstrated in an early experiment by Chambers,[15] a conclusive demonstration was made in the electron holography interferometry experiments by Tonomura et al.,[16–18] with due attention to the magnetic field leakage if any. Nevertheless, the theory behind the AB effect has generated two longstanding fundamental issues that continue till today. First, since the physical field $\vec{B}$ is confined inside the solenoid, the

charged particle is as if interacting with the field from a finite distance away, i.e., non-locally, thereby causing the interference fringes to shift in accordance with the amount of magnetic flux inside the solenoid. Second, since locally only the vector potential $\vec{A}$ is present, the interaction it causes must be local. And since, $\vec{A}$ enters in the Schrödinger equation for the particles, the status of $\vec{A}$ must be promoted to a quantity of fundamental importance, from erstwhile, a merely mathematical construction for the evaluation of magnetic field whenever symmetry of a system permits. This in turn suggests that $\vec{A}$, though non-gauge invariant, may be regarded as a physical quantity more fundamental than the physical field $\vec{B}$. These issues have been fiercely debated in the literature, and continue unabated, constituting the subject explored in the next chapter.

1.4 The AB Conundrum: Classical or Quantum? Does it Exist?

From the very beginning, the validity of the AB effect, as proposed in the seminal paper by Aharonov and Bohm,[1] has been questioned and uncertainty continues to date. Among others,[19–25] a sound semi-classical interpretation of the AB put forward by Boyer has always inspired the opponents of the AB effect, thereby doubting the AB effect as a force-based classical effect.[26–29] No doubt, this has remained an elegant method ever proposed to explain the supposedly quantum phenomenon advocated by the proponents of the AB effect.[30–32] The

tug of war is often complicated by the proposals of radically different interpretations over time.[33–37] Notwithstanding the above, some doubt if the AB effect really exists![13, 28, 38] Nevertheless, limiting our interest in the subject of maintaining the existence of the AB effect, we here discuss only the main three perspectives on the AB effects, viz., Boyer's reactionary force-based analysis,[27, 28] Vaidman's interpretation of the role of potential,[39] and Wang's energy-based interpretation.[40]

1.4.1 Boyer's reactionary force-based analysis

In consonance with some of the earliest objections against the AB effect,[19–23] a series of papers due to Boyer [26–29] has revolutionized our perception of the AB effect, particularly due to the surprising match between his reactionary force-based induced phase and the genuine AB phase. The basic idea is that the magnetic field $\vec{B}_q$ of a charge q, mass m, and moving with a velocity $\vec{v}$ overlaps with the magnetic field $\vec{B}_S$ inside a narrow and tightly wound long solenoid having a cross-sectional area $\mathcal{A}$. The interaction energy corresponding to the overlapping of the magnetic fields is

$$U_{BB} = \frac{1}{\mu_0} \int \vec{B}_q \cdot \vec{B}_S \, d\tau. \tag{1.8}$$

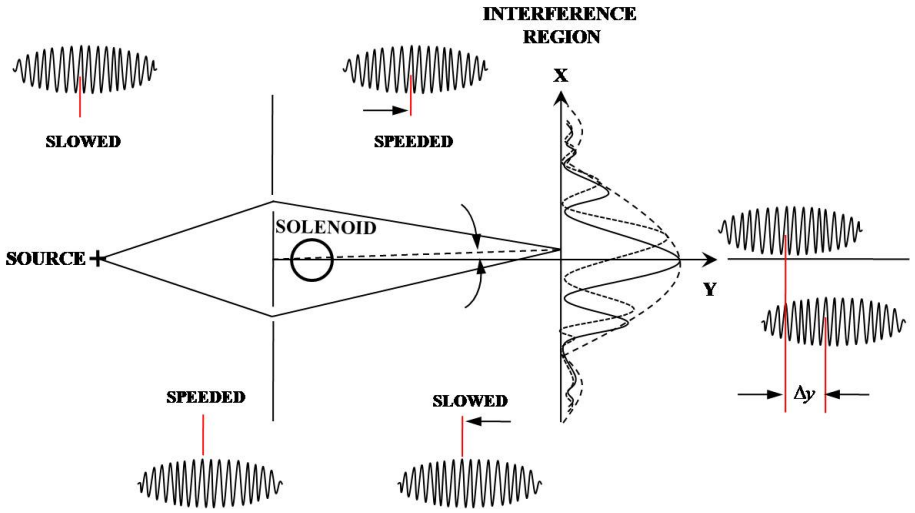

FIGURE 1.4: A schematic of the AB effect showing the path difference Δy developed between the wave packets when they pass the solenoid enclosing the magnetic field in its interior.

The back-action force on the charged particle is $\vec{F} = -\vec{\nabla} U_{BB}$, which can be shown to be [20, 21, 28]

$$\vec{F} = q\vec{\nabla}(\vec{v} \cdot \vec{A}), \tag{1.9}$$

where $\vec{A}$ is the vector potential outside the narrow and tightly wound current-carrying solenoid. For the solenoid oriented along the z-axis and the charged particle moving along the y-axis, the analysis of the longitudinal component $F_y = q\vec{\nabla}(\vec{v} \cdot \vec{A})_y$ of the force reveals that the charge q is first *speeded up* as it approaches the solenoid along one of the interfering paths, and then *slowed down* as it recedes away. As shown in Fig. 1.4, this action of the longitudinal component F_y gets reversed for the interfering path on the other side of the solenoid, leading to a relative time lag and the path difference, $\Delta y = qB_S\mathcal{A}/mv$, between the charges reaching the interference region.[27, 28, 32] The associated phase difference is,

$$\phi = \frac{2\pi}{\lambda}\Delta y = \frac{qB_S\mathcal{A}}{\hbar} = \frac{q\Phi}{\hbar}, \tag{1.10}$$

where $\Phi = B_S\mathcal{A}$ is the magnetic flux in the solenoid. It must be noted that $\lambda = h/mv$ is the de Broglie wavelength associated with the moving particle. This is the only non-classical idea Boyer employed in obtaining the above expression for the induced phase, which is precisely the AB phase, Eq. 1.7. This surprising match between the force-based expression ϕ and the quantum mechanical expression ϕ_{AB} is the greatest triumph of the semi-classical force-based analysis of the genuine AB effect. Ironically, a recent experiment aimed at measuring any time delay between the charged particles traversing opposite sides of the current-carrying solenoid showed a null result.[32]

Finally, Boyer's force-based analysis of the AB effect has led to the classification of the force-based interference effect into type I and type II classes.[27, 32] In the type I interference, the interfering particles experience deflecting transverse force resulting in a shift of the entire interference pattern, i.e., the double-slit fringe pattern as well as the single-slit envelope. Whereas in the type II interference, the interfering particles suffer time lag due to longitudinal force, resulting in path difference and hence the fringe shift in the interference pattern, i.e., only the double-slit pattern (the wavy structure in the interference pattern in Fig. 1.4) gets shifted, while the single-slit envelope (the broad outline hump) remains undisplaced. Thus, within Boyer's analysis, the AB phase belongs to the type II interference effect. A deeper discussion on this issue in conjunction with the

genuine AB phase is relegated to the next chapter.

1.4.2 Vaidman's interpretation on the role of potential

Consideration of a local theory for the AB effect at the cost of accepting the vector potential $\vec{A}$ as a physical quantity entails that $\vec{A}$ is more fundamental than the physical field $\vec{B}$, a view expressed in the influential paper of Aharonov and Bohm.[1] The vector potential is non-gauge invariant, however, its closed line integral, i.e., the magnetic flux, and hence the AB phase ϕ_{AB} is gauge invariant. Amid persisting issue of whether or not $\vec{A}$ is more fundamental than $\vec{B}$, Vaidman [39] proposed a quantum mechanical explanation of the AB effect without the use of vector potential. The main idea is the local interaction between the magnetic field of the moving charged particle and the source of the potential, the solenoid when treated quantum mechanically. According to Vaidman, the charged particle q and the source S of the potential can be considered as a composite system described by one state, i.e., an entangled state represented by the total wave function

$$|\Psi\rangle_{tot} = \frac{1}{\sqrt{2}} \left(|L\rangle_q |\Psi_L\rangle_S + |R\rangle_q |\Psi_R\rangle_S \right), \tag{1.11}$$

where $\{|L\rangle_q, |R\rangle_q\}$ are the states of charged particles moving past the solenoid from the left and right sides, while $\{|\Psi_L\rangle_S, |\Psi_R\rangle_S\}$ are the quantum states of the source (solenoid) for the corresponding left/right side motion of the particles. Due

to local interaction between the magnetic field of the moving charged particle and the source of the potential, the states of the source evolve, however, they differ only in their phase. At the end of the evolution, the states $\{|\Psi_L\rangle_S, |\Psi_R\rangle_S\}$ are identical except for the AB phase factor $e^{\frac{i}{\hbar}\phi_{AB}}$, i.e., the total wave function becomes

$$|\Psi\rangle_{tot} = \frac{1}{\sqrt{2}}|\Psi\rangle_S \left(|L\rangle_q + e^{\frac{i}{\hbar}\phi_{AB}}|R\rangle_q\right). \tag{1.12}$$

Such an evolution of the total wave function leads to a shift of fringes in the interference pattern, which is the AB effect.

1.4.3 Wang's energy-based interpretation

Yet another non-classical interpretation of the AB phase due to Wang [40, 41] emanated from the consideration of the magnetic interaction energy associated with the overlap of magnetic field $\vec{B}_q$ of the moving charged particle with the field $\vec{B}_S$ inside the solenoid. The field configurations are shown in Fig. 1.5. The interaction energy corresponding to the overlap of the magnetic fields as expressed in Eq. 1.8 is shown to be $U_{BB} = q\vec{v}\cdot\vec{A}$.[31, 40] A subtle difference that exists between Wang's energy-based interpretation [40, 41] and Boyer's force-based interpretation [27, 28] is that in Wang's consideration there is no reactionary back-action non-Lorentz force $\vec{F}_q = -\vec{\nabla}U_{BB}$, on the charged particle. Instead, the magnetic interaction energy $U_{BB} = q\vec{v}\cdot\vec{A}$, which is precisely the form of the interaction energy appearing in the Lagrangian for the charged particle, directly leads to the

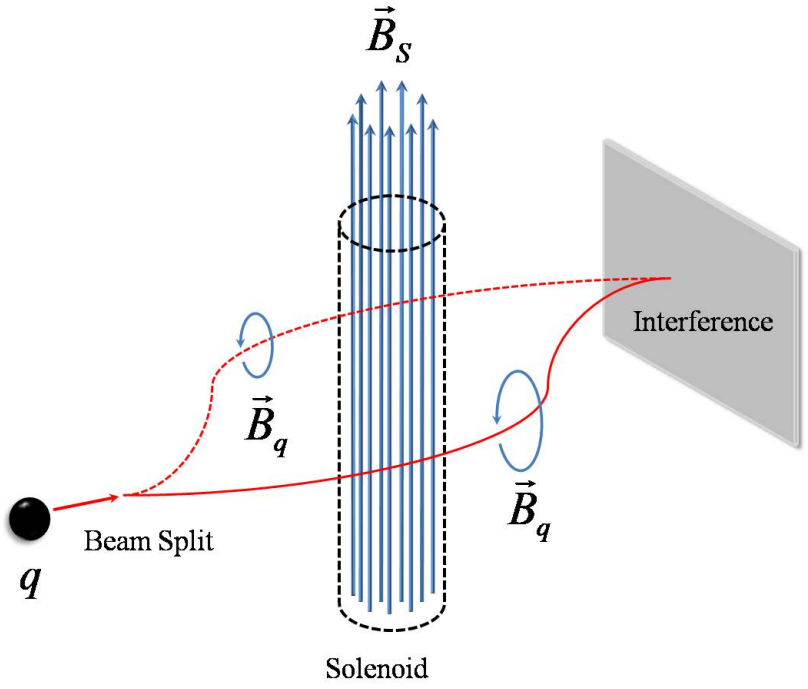

FIGURE 1.5: Schematic diagram of AB setup showing the magnetic field $\vec{B}_q$ due to a moving charged particle and the field $\vec{B}_S$ within the solenoid.

AB phase given by Eq. 1.7. To us, this is a little obscure, that how this interaction energy is accessible to the charged particle moving outside the solenoid? We will revisit this problem later in Chapter 2 in the context of AB effect with imperfect shielding. Nevertheless, the essence of Wang's analysis is that the AB effect is the energy-based effect, and not the force-based effect as advocated by Boyer.[27, 28]

1.5 Aharonov-Casher Effect

After about 25 years of discovery of the AB effect, Y. Aharonov and A. Casher, in 1984, discovered an analogous topological effect, in which a moving neutral particle possessing a magnetic dipole moment $\vec{m}$ in a radial electric field $\vec{E}(\vec{r})$

acquires phase independent of its velocity and path taken. This is known as the Aharonov-Casher (AC) effect,[2] and the setup is shown in Fig. 1.6. Just as in the AB effect, the neutral particles experience no force or torque in their entire journey along the paths. Idealizing a perfect source of a cylindrically symmetric

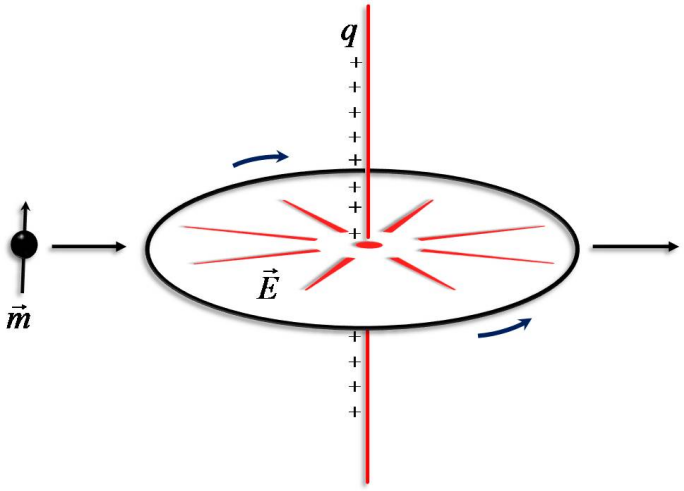

FIGURE 1.6: The Aharonov-Casher setup, wherein neutral particles having magnetic dipole moment $\vec{m}$ move past the radial electric field $\vec{E}$ produced by a line of electric charges, q.

radial electric field, Aharonov and Casher consider an infinitely long and straight line of electric charges in which coherent neutral particles possessing permanent magnetic dipole moment move past the line distribution of charges from both sides to interfere on a reunion at the other end. Physically, in the co-moving frame, the magnetic moment $\vec{m}$ of the neutral particle interacts locally with the Lorentz transformed magnetic field, $\vec{B}' = (\vec{E} \times \vec{v})/c^2$, and the associated interaction energy is $U = -\vec{m} \cdot \vec{B}'$. Viewed in the lab frame, the moving magnetic moment appears as an electric dipole moment $\vec{d}' = (\vec{v} \times \vec{m})/c^2$, that interacts locally with the electric field $\vec{E}$ produced by the line of charge and the associated interaction energy is $U = -\vec{d}' \cdot \vec{E}$. The interaction energy is the same in the co-moving frame of the

particle as it is in the lab frame. Thus, the Lagrangian for the particle is

$$L = T - U = \frac{1}{2}m|\vec{v}|^2 + \vec{v} \cdot \left(\frac{\vec{m} \times \vec{E}}{c^2}\right), \tag{1.13}$$

and the AC phase of the particle's wavefunction that affects the interference fringes is

$$\begin{aligned} \phi_{AC} &= \frac{1}{\hbar} \oint -\frac{\partial U}{\partial \vec{v}} \cdot \vec{dl}, \\ &= \frac{1}{\hbar c^2} \oint (\vec{m} \times \vec{E}) \cdot \vec{dl}. \end{aligned} \tag{1.14}$$

The AC phase was experimentally demonstrated for the thermal neutrons, in 1989, by Cimmino et al. [42] using a neutron interferometer with 30KV/mm vacuum electrode system in the setup. The observed phase acquired by the particles in the setup was measured to be 2.19 ± 0.52 mrad which is roughly the same order of magnitude as the theoretical value, 1.52 mrad, estimated for the geometry and experimental conditions of the setup. The AC phase is also reported to be observed in the interference of magnetic vortices around an induced charge.[43]

1.6 He-McKellar-Wilkens Effect

After about 8 years of discovery of the AC effect, a third topological effect was predicted in 1993 by He and McKellar,[3] and independently by Wilkens,[4] a year later, in which a neutral particle endowed with a permanent electric dipole

moment $\vec{d}$ traversing through a region of radial magnetic field $\vec{B}$ undergoes a relative phase shift in its wave function. This effect is known as He-McKellar-Wilkens (HMW) effect, and the induced phase difference between the interfering waves is the HMW phase, ϕ_{HMW}. The setup is shown in Fig. 1.7. Since the

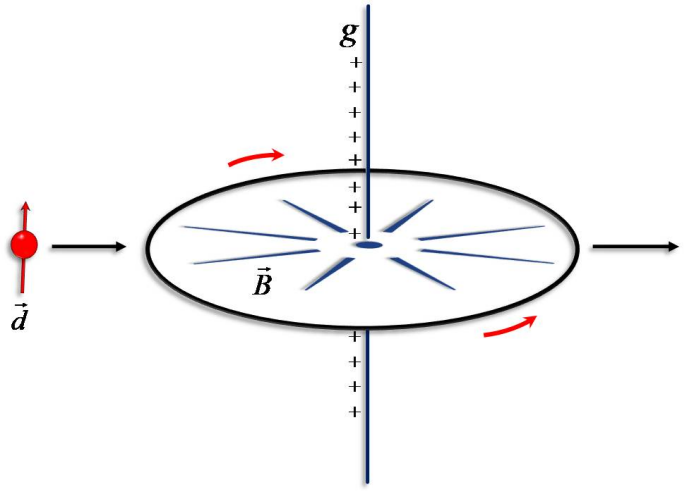

FIGURE 1.7: A simplified view of the HMW setup, in which neutral particles having permanent electric dipole moment $\vec{d}$ traverse through the radial magnetic field $\vec{E}$ produced by a line of magnetic charges, g.

HMW effect is the electromagnetic dual of the AC effect, a role reversal of the pair $(\vec{m}, \vec{E})$ in the AC setup with $(\vec{d}, \vec{B})$ in the HMW setup leads to interaction energy, $U = -\vec{d} \cdot \vec{E}' = -\vec{d} \cdot (\vec{v} \times \vec{B})$, in the rest frame of an electric dipole, or equivalently, $U = -\vec{m}' \cdot \vec{B} = -(\vec{d} \times \vec{v}) \cdot \vec{B}$, in the lab frame. The Lagrangian for the particle is then

$$L = T - U = \frac{1}{2} m |\vec{v}|^2 + \vec{v} \cdot \left(\vec{B} \times \vec{d} \right), \tag{1.15}$$

and the HMW phase is

$$\begin{aligned}\phi_{HMW} &= \frac{1}{\hbar}\oint -\frac{\partial U}{\partial \vec{v}}\cdot \vec{dl}, \\ &= \frac{1}{\hbar}\oint (\vec{B}\times\vec{d})\cdot\vec{dl}. \end{aligned} \tag{1.16}$$

A major hurdle in the experimental verification of the HMW phase is the need for a radial magnetic field. Starting from Wilkens' proposal [4] of the setup consisting of a thin magnetic sheet that one of the interfering paths straddles the sheet through a small hole on it where the field is nearly radial, several others [44–48] have proposed a wide variety of setups and field configurations to meet the demand that both force and torque on the moving dipole are identically zero.[49–52] It took almost two decades for the experimental verification of the HMW effect when Lepoutre et al. [53–56] confirmed the effect in a Li-atom interferometer with an interaction region consisting of crossed electric and magnetic fields similar to that proposed by Wei-Han-Wei.[44] The measured values for the three mean velocities in the range 744-1520 m/s are in excellent agreement with the calculated value $\phi^{cal}_{HMW}(IV) = 1.28 \pm 0.03$ mrad$/IV$, as a function of current-voltage (IV) used in the experiment.[54]

It must be mentioned here that the measurement of the HMW phase also requires the electric dipole moment of the particles as large as possible. The electric dipole moment of the stable atoms is usually small. Instead, as suggested in Ref. [46], one may use some polar molecules like BaS having a permanent dipole moment of 10.76 Debye [57] which is about 6-fold the value for an isolated

water molecule ($|\vec{d}|$=1.85 Debye). We note in passing that the permanent dipole moment of dipolar molecules does not exceed 12 Debye.[58] Furthermore, a study of a neutral composite particle consisting of an electron-hole pair, called an exciton, has proven a promising candidate for the study and exploitation of the HMW phase due to exceedingly large dipole moment over several hundreds of Debye in some cases. A brief introduction to the physics of excitons will be covered in the next few sections.

1.7 Dowling's Unified Description of the Topological Phases

It is realized quite early that the AC and HMW phases are the Maxwell's electromagnetic dual of each other with the duality pair transformations ($\vec{E} \to c\vec{B}, \vec{m} \to -c\vec{d}$) and ($c\vec{B} \to -\vec{E}, c\vec{d} \to \vec{m}$). In an attempt at providing a unified description of the three topological phases, viz., AB, AC and HMW, Dowling et al.[45] discovered the Maxwell dual of the AB phase, called the dual AB (DAB) phase, in which a moving magnetic charge g past a line of electric dipoles $\vec{d}$ acquires phase, such that the phase difference between the interfering magnetic charges is

$$\phi_{DAB} = -\frac{g}{\hbar c^2}\phi_E, \tag{1.17}$$

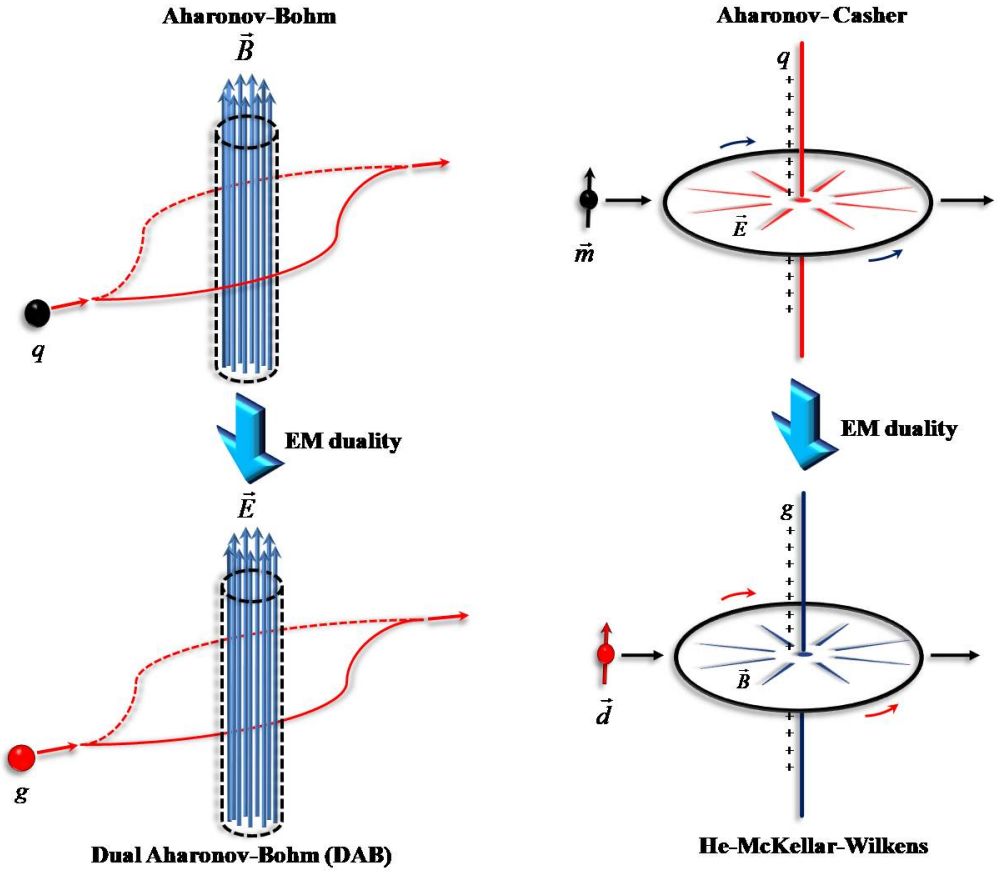

FIGURE 1.8: Maxwell electromagnetic duality relations between the pair topological effects (a) Aharonov-Bohm and (c) Dual Aharonov-Bohm, and that between (b) Aharonov-Casher and (d) He-McKellar-Wilkens. The confined magnetic and electric fluxes in the configurations (a) and (c) are considered due to a linear array of magnetic and electric dipoles.

where ϕ_E is the electric flux of the line of electric dipole enclosed by the interfering paths. The AB phase in terms of magnetic flux is

$$\phi_{AB} = \frac{q}{\hbar}\phi_B, \tag{1.18}$$

where the magnetic flux ϕ_B, as otherwise confined inside a solenoid, can be considered as due to a line of magnetic dipoles $\vec{m}$. The two topological phases ϕ_{AB} and ϕ_{DAB} are related by the duality pair transformations ($\vec{E} \to c\vec{B}, g \to -cq$)

and $(c\vec{B} \rightarrow -\vec{E}, cq \rightarrow g)$. A schematic of the duality pairs is presented in Fig. 1.8. It must be noted that the DAB effect is already been demonstrated if the magnetic fluxon are considered as the magnetic charges.[43] Of interest to us here is the generalization of the duality relations among the various effects, however, the pair effects (AB & AC) and (DAB & HMW) are found to relate only through "reference frame correspondence". This is discussed in Chapter 2.

Since, we consider potential exploitation of the HMW phase in the excitonic optoelectronic devices, in what follows, we discuss very succinctly the different types of excitons while we restrict ourselves to a class of excitons of interest and suitable materials where such excitons manifest to exist.

1.8 Excitons

Excitons are neutral bound electron-hole pairs that exist in dielectrics, semiconductors, and also in some molecular materials. When incident photons are absorbed by the materials, the electrons are excited to the conduction band generating vacancies for electrons in the valence band, called holes, which are considered as positive charges in the valence band. The attractive Coulomb interaction between an excited electron in the conduction band and a hole in the valence band binds them together to form a bound electron-hole pair, i.e., an exciton. Excitons are capable of diffusion through the materials and eventually, the electron and hole pair recombine, thereby releasing the recombination energy in the form of

photons, often at wavelengths different from that of the absorbed photons. Since excitons can be regarded as the intrinsic electronic excitations in the materials, their motion can be viewed as the transport of energy through the materials without transporting the net charges.

The idea of an exciton as a quasiparticle formed by the association of an electron and a hole with an attractive force between them was first proposed by Frenkel in 1931.[59] As such, the excitons represent a wide class of electronic excitations in a variety of materials, which we classify as follows.

1.8.1 Types of excitons

1.8.1.1 Classification based on size

Excitons are generally classified into three categories based on their size (Bohr radius) relative to the interatomic or intermolecular distances in the material. [60] We briefly describe them as follows.

(a) Frenkel excitons

Frenkel excitons are tightly bound electron-hole pairs localized in atoms or molecules and have size (exciton Bohr radius $\sim$ 10 Å) same order as the size of the unit cell of the material. Frenkel excitons are usually generated in the materials having a relatively small dielectric constant, so that the strong Coulomb interaction between the electron and hole would make them tightly bound and localized. These

excitons have binding energy on the order of 0.1 to 1 eV, and are typically found in alkali halide crystals and in organic molecular crystals composed of aromatic molecules, such as anthracene and tetracene.

Because of their small size and site localization, their wave functions do not overlap, and thus the interaction between the Frenkel excitons at different sites can be neglected in many cases. Also, due to small size the Frenkel excitons have vanishingly small permanent electric dipole moments, however, a finite dipole moment can be induced by an externally applied electric field. Frenkel excitons have well-defined spin states (singlet and triplet) and travel by hopping process with the associated energy transfer described by the Förster or Dexter mechanism. These mechanisms will be briefly reviewed and discussed shortly.

(b) Warnier-Mott Excitons

Warnier-Mott excitons are loosely bound electron-hole pairs having a size (exciton Bohr radius ~ 100 Å) larger than the interatomic spacing due to dielectric screening of the Coulomb interaction between the electron-hole pairs. These excitons are found in most of the typical inorganic semiconductors having small energy band gap and high dielectric constants such as indium antimonide (InSb, 0.17 eV), germanium (Ge, 0.66 eV), silicon (Si, 1.11 eV), and gallium arsenide (GaAs, 1.43 eV). Owing to a small Coulombic binding energy (typically < 0.1 eV), these excitons tend to dissociate very quickly even at temperatures around room temperature. For example, the lifetime of such an exciton in Ge is of the order of 10^{-5} sec. The

spin state of Wannier-Mott excitons is not well defined due to the rapid exchange of singlet-triplet states.

(c) Charge-Transfer Excitons

Charge-transfer (CT) excitons are the excitons intermediate between the Frenkel and Wannier-Mott excitons. The CT excitons are formed when the electron and hole occupy the adjacent molecules called the donor and acceptor molecules in regards to electron or hole transfer between the donors and acceptors. The molecules of the material can be similar, or they can be dissimilar, in which case they form a heterojunction of dissimilar materials. Although the electrons and holes occupy adjacent molecules, they are still bound by the Coulomb interaction, however, smaller than that of the Frenkel excitons but certainly higher than the thermal energy at room temperature (25 meV). As a result, these excitons possess strong permanent electric dipole moments and can have values as large as 10-25 Debye. These excitons occur primarily in the organic and molecular crystals and also in transition metal oxides. Furthermore, conversion of the Frenkel excitons into the CT excitons is possible at the interface of the materials. Like Frenkel excitons, the CT excitons will either be in a singlet or in a triplet spin state configuration. Due to the long lifetime and permanent electric dipole moment, these excitons are highly appealing for optoelectronic devices.

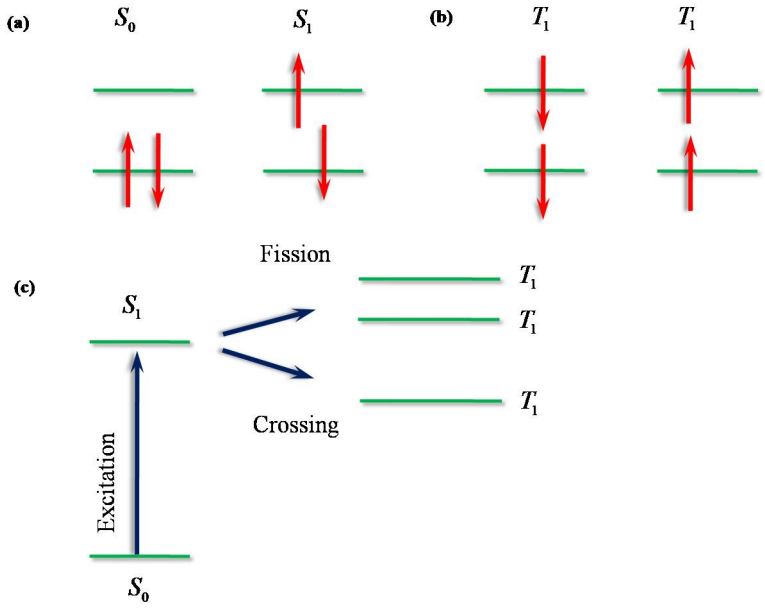

FIGURE 1.9: (a) Singlet exciton S_1, (b) Triplet exciton T_1, and (c) Absorption of photons generates singlet exciton that undergoes fission generating two triplet excitons. Alternatively, the intersystem crossing is possible to form the triplet excitons.

1.8.1.2 Classification based on spin state and spatial confinement

(a) Singlet and Triplet Excitons

Within the molecular orbital picture of the formation of excitons in the organic semiconductors, the excitons can feature the spin states, either singlet or triplet for spin multiplicity $S = 0$ or $S = 1$, respectively. The singlet excitons, consisting of an electron and a hole with opposite spin orientation, have low binding energy ($\lesssim$ 0.5 eV) with diffusion length on the order of nanometers, while they move faster through the Förster mechanism. In contrast, the triplet excitons, consisting of electron and hole with the same spin orientation, have high binding energy in the range $\sim$ 0.5 to $<$ 1 eV with diffusion length on the order of micrometers and move slower through the Dexter mechanism.[61] Unlike the singlet excitonsthat

are directly produced by the absorption of photons, the triplet excitons are produced through the fission of singlet excitons by which one singlet exciton splits to form two triplet excitons without a spin-flip involved in the process.[62–64] A representation of this process is shown in Fig. 1.9. Also, the triplet excitons can be generated from singlet excitons via intersystem crossing involving a spin-flip, which is generally slow due to weak spin–orbit coupling in the organic materials.[65, 66] However, once formed, the reverse intersystem crossing requires a spin-flip which is less favorable, and thus the triplet excitons are relatively long-lived than the singlet excitons. The singlet exciton diffusion length is typically on the order of a few nanometers, whereas the value may exceed over a hundred nanometers for triplet excitons.

(b) Direct and Indirect Excitons

Usually, the excitons in a semiconductor have a very short lifetime due to the small spatial separation between the Coulomb bound electron and hole. When both electron and hole are confined in the same potential well, a direct exciton will be formed. Such excitons have a very short lifetime ($< 10^{-9}$ s) and do not possess static dipole moment. If, however, they are localized in different wells, an indirect exciton will be formed. The indirect excitons can have a large spatial separation between the electron and hole, and thus possess static dipole moment and have a much longer lifetime ($\sim 10^{-6}$ s to 10^{-9} s). The lifetime of indirect excitons depends significantly on the width and the barrier separating the potential wells.[67, 68] A schematic representation of the formation of such excitons is

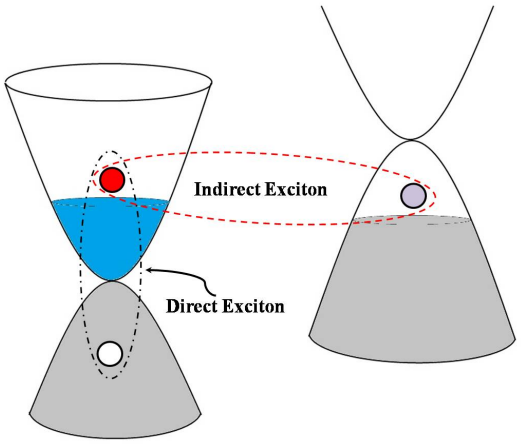

FIGURE 1.10: Schematic representation of exciton formation. A direct exciton is due to the trapping of both electron and hole in the same potential well, and indirect exciton is due to the confinement of an electron and a hole in adjacent potential wells.

shown in Fig. 1.10.

(c) Intra- and Interlayer Excitons

An emerging class of excitons that manifest in the multilayer 2D semiconductor materials are the intralayer and interlayer excitons.[69–72] This is shown in Fig. 1.11. In 2D semiconductor materials, it is possible to generate bound electron–hole pairs in the same layer, i.e., the intralayer excitons, or with the electrons confined in one layer and the holes in an adjacent layer leading to the interlayer excitons. Owing to weaker Coulomb binding, the interlayer excitons have a larger spatial extent than the intralayer excitons, and thus possess a large static dipole moment. Interlayer excitons are predominant in the hetero-bilayers obtained out of seamless stacking of the semiconducting transitional metal dichalcogenides (TMDs) without lattice mismatch, e.g., $MoSe_2/WSe_2$. More discussion on such heterostructures is

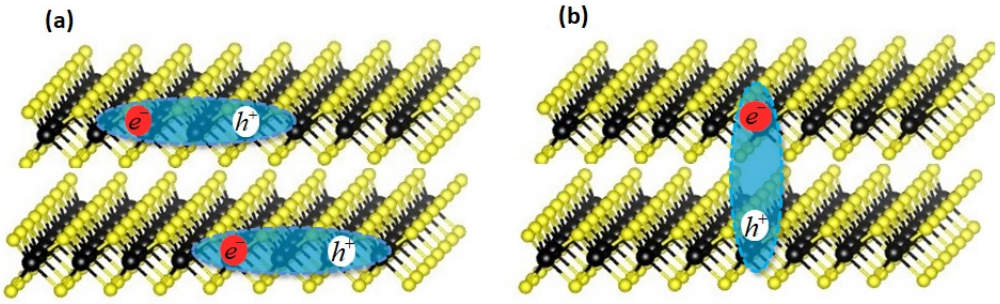

FIGURE 1.11: Schematic representation of (a) intralayer and (b) interlayer excitons in the bilayer semiconductor material.

relegated to the next subsection.

1.8.2 Transfer of excitons

Transfer of excitons between the neighbouring molecular sites takes place through either of the two main mechanisms, viz., Förster or Dexter,[73, 74] presented in Fig. 1.12. In the Förster process, energy exchange takes place between the donor and acceptor molecules which, however, requires a significant overlap of the emission spectrum of the donor molecule with the absorption spectrum of the acceptor. Thus, this mechanism is also called Förster resonant energy transfer, which is a primary mechanism for the transfer of singlet excitons when the donor and acceptor molecules are within a few nanometer ranges. In contrast, a non-radiative exchange of an electron between donor and acceptor molecules takes place in the Dexter process that requires a significant overlap of the molecular orbitals between the molecules. This process enables the transfer of triplet excitons.

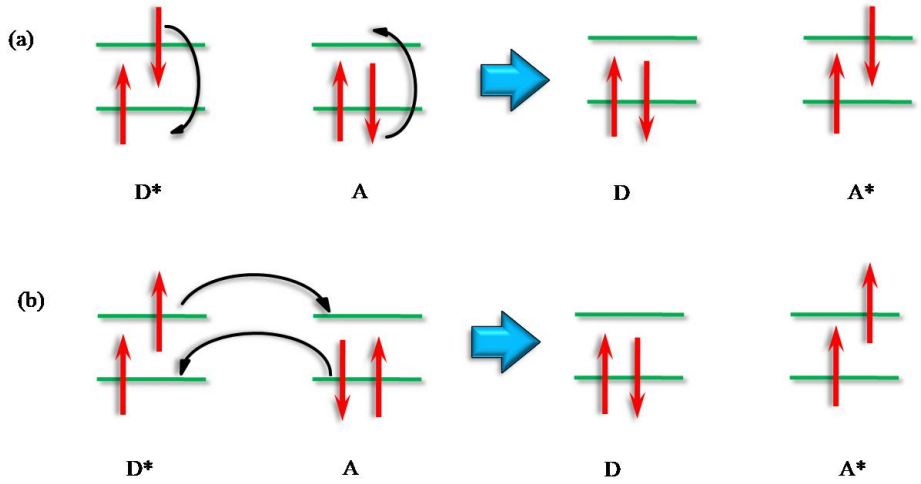

FIGURE 1.12: Representation of exciton transfer between the donor (D) and acceptor (A) through (a) Förster mechanism for singlet and (b) Dexter mechanism for triplet.

1.8.3 Transition Metal Dichalcogenides (TMDs)

Transition metal dichalcogenides (TMDCs) are a new family of 2D semiconductor materials of the form MX_2 with M as a transition metal atom (e.g., Mo or W) and X, a chalcogen atom (e.g., S, Se or Te).[75, 76] Such materials exhibit a wide range of attractive properties that include atomic-scale thickness, bandgap, spin-orbit coupling, optical, electronic and mechanical properties, making them favorable over other materials like graphene and boron nitride for applications in high-end semiconductor devices, optoelectronics and next-generation energy harvesting devices. An atomically thin monolayer of TMD (e.g., MoS_2, $MoSe_2$, WS_2 and WSe_2) typically has a thickness of 6-7 Å, which consists of a hexagonally packed layer of metal atoms sandwiched between the two layers of chalcogen atoms as depicted in Fig. 1.13. The intralayer M-X bonds within the monolayer TMD are covalent in nature, whereas the stacked structures in the multi-layer TMD are held

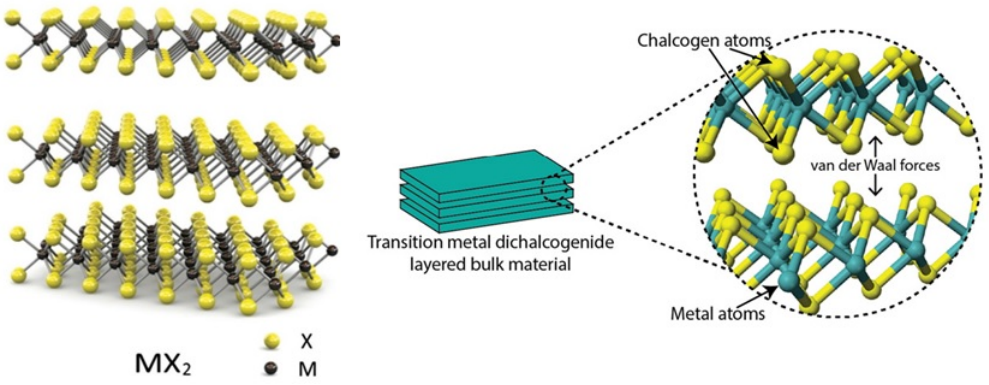

FIGURE 1.13: (a) Structure of Transition Metal Dichalcogenides (TMDs), (b) Bulk TMDs. Figure adapted from Ref. [86]

by a weak van der Waals force, thus allowing an easy cleavage into layer surfaces. Monolayers of TMDs can be stacked laterally to fabricate planar heterostructures without much lattice mismatch between them.[77, 78] This is shown in Fig. 1.14. Also, a monolayer TMD can be stacked to another TMD vertically to obtain a wide class of bilayer heterostructures of two different MX_2 such as MoS_2-WSe_2, $MoSe_2$-WS_2, $MoSe_2$-WSe_2, MoS_2-WS_2 etc.[79–82] A variety of methods have been developed to synthesize monolayer or stacked structures of TMDs.[83–85] Two of the most common methods are mechanical exfoliation from the bulk crystal and the chemical vapour deposition technique. An interesting property of TMDs is that a monolayer of TMD (e.g., MoS_2, $MoSe_2$, WS_2 and WSe_2) possesses a direct bandgap in the range 1-2eV, while the bilayers and multilayers exhibit an indirect bandgap.[87–89] However, heterostructures formed by the stacking of two different TMDs can convert the otherwise an indirect bandgap layered TMD to a direct type.[90, 91] Also, a strong geometrical confinement and a weak dielectric screening

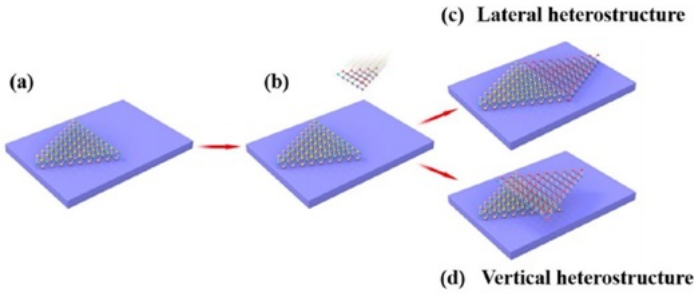

FIGURE 1.14: (a) TMD monolayer on a substrate, (b) Stacking of a second TMD layer to form (c) Lateral heterostructure, or (d) Vertical heterostructure. Figure adapted from Ref. [92]

in such 2D materials result in a strong Coulomb interaction leading to a formation of excitons upon optical excitation. In particular, in a heterobilayer TMD, the electrons are confined in one layer while the holes are in the opposite layer. The associated excitons in such heterostructures are termed interlayer excitons that exhibit intriguing properties that include a long lifetime reaching hundreds of nanoseconds and a strong permanent dipole moment in the out-of-plane direction. A novel combination of these features holds a great promise in manipulating the transport properties of the interlayer excitons in heterobilayer TMDs for the potential development of excitonic circuits, interlayer excitonic devices, and possibly a programmable quantum optical device for signal processing and optical communication with photons and excitons transforming into each other involving photoluminescence (PL) emission.[93] A study of possible control of interlayer exciton transport through stacked phenylacetylene macrocycles by manipulating the HMW phase is considered in this work.

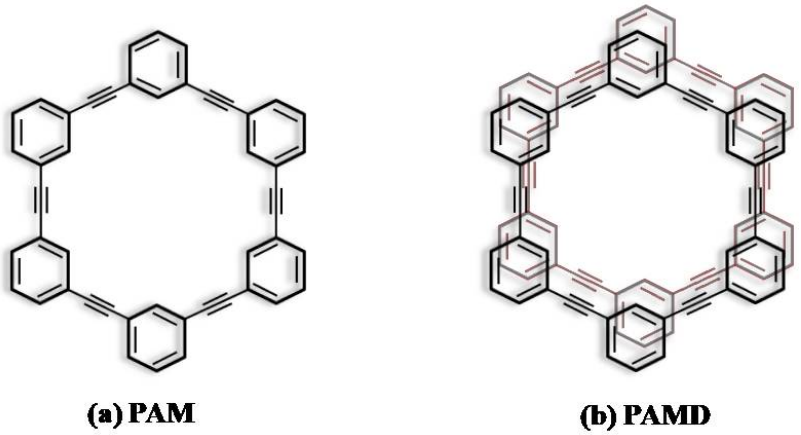

FIGURE 1.15: (a) Molecular structure of phenylacetylene macrocycle (PAM), where the peripheral moieties are excluded for simplicity, and (b) Stacked PAM dimer (PAMD).

1.8.4 Phenylacetylene Macrocycle (PAM)

PAMs are greatly extended π systems comprising multiple phenyl rings with acetylene connecting the rings to form a regular molecular framework.[94–96] They are synthesized by the cyclization of phenylacetylene oligomers.[97] Self-association of PAMs into dimers and trimers have already been demonstrated in solution involving a face-to-face, i.e., $\pi - \pi$ stacking conformation rather than an edge-to-face orientation.[98–100] Moreover, the face-to-face stacking could offer a well-ordered molecular architecture that may be used as the active components in the molecular electronic devices for the reason that a high level of molecular organization in the organic materials is known to provide high mobility of the charge carriers. A monomer and dimer PAM is shown in Fig. 1.15. The diameter of such a macrocycle, i.e., the transannular distance between the phenyl ring centres is ~ 1 nm.[95, 97] Studies reveal that the $\pi - \pi$ stacked PAM dimer (PAMD) structures are energetically favorable over other configurations with an average interplanar

distance ~ 0.4 nm.[95] Such a stacked PAM dimer sandwiched between the TMD electrodes is considered in this work as a potential setup for the possible control of interlayer exciton transport by manipulating the HMW phase of the excitons in the stacked macrocycles. This, however, requires a radial magnetic field in the plane of the macrocycles so that the dipole moment of the interlayer excitons at each location is perpendicular to the applied magnetic field. The technical details of such a setup will be discussed later in a separate Chapter.

1.8.5 Photoluminescence

Photoluminescence (PL) is an optical phenomenon in which the molecules or semiconductors re-emit light by absorbing the incident light.[101] The PL measurements usually provide the fundamental radiative characteristics of the molecular systems or semiconductors. Moreover, the study of the spectral distribution of PL provides the electronic structure of the system as the energy of the emitted photons is a direct measure of the energy difference between the associated orbitals or bands. Such measurements provide an estimate of the HOMO–LUMO gap in the molecules or the direct energy band gap in the semiconductors. PL signal generally results from the radiative recombination of the photogenerated electron-hole pairs, i.e., excitons. For a strong PL signal, radiative recombination must be dominant, which is much more efficient in the direct band gap semiconductors. A semiconductor material for our purpose that potentially exhibits a strong PL is a vertically-stacked bilayer 2D heterostructure TMDs that have a

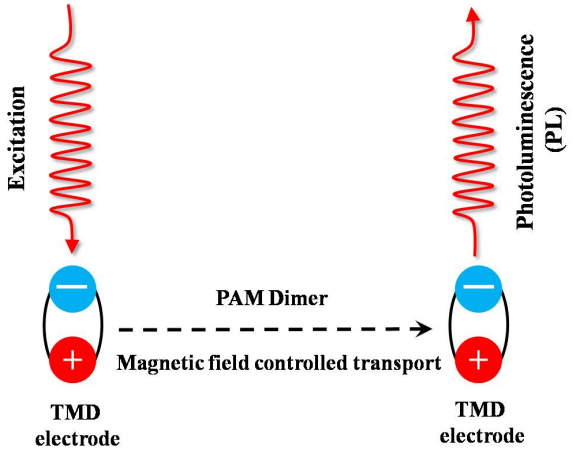

FIGURE 1.16: Laser excitation of left TMD electrode generating interlayer excitons, which diffuse through the PAM dimer to reach the right TMD electrode where they decay via radiative recombination leading to photoluminescence.

direct band gap in the range of about 0.8 eV to 2.0 eV.[90] A simple illustration of the setup for the study of the influence of field-controlled exciton transport on the photoluminescence (PL) resulting from radiative recombination of excitons is shown in Fig. 1.16. In the input electrode, the photons transform into excitons, which then diffuse through the intermediate molecular system PAM Dimer into the output electrode. The exciton transport is controlled by a radial magnetic field applied to the PAM Dimer. In the output electrode, the excitons decay predominantly through the radiative recombination of electrons and holes. PL studies can be made for understanding the influence of field-controlled excitons on the performance of exciton-based optoelectronic devices.

References

[1] Y. Aharonov and D. Bohm, Phys. Rev. **115**, 485 (1959).

[2] Y. Aharonov and A. Casher, Phys. Rev. Lett. **53**, 319 (1984).

[3] X. -G. He and B. H. J. McKellar, Phys. Rev . A **47**, 3424 (1993).

[4] M. Wilkens, Phys. Rev. Lett. **72**, 5 (1994) .

[5] G. Pascoli, C. R. Phys. **18**, 563 (2017).

[6] H. Rauch and S. A. Werner, *Neutron Interferometry: Lessons in Experimental Quantum Mechanics, Wave-Particle Duality, and Entanglement* (Oxford University Press, 2015).

[7] J. J. Sakurai, Phys. Rev. D **21**, 2993 (1980).

[8] H. C. Lefevre, C. R. Phy. **15**, 851 (2014).

[9] R. Weder, J. Math. Phys. **52**, 052109 (2011).

[10] G. Matteucci and G. Pozzi, Phys. Rev. Lett. **54**, 2469 (1985).

[11] A. Walstad, Int. J. Theo. Phys. **49**, 2929 (2010).

[12] T. C. Bachlechner and M. Kleban, Phys. Rev. B **101**, 174504 (2020). Phys. Rev. B 101, 174504

[13] A. Walstad, Int. J. Thor. Phys. **56**, 965 (2017).

[14] R. -F. Wang, Sci. Rep. **5**, 14279 (2016).

[15] R. G. Chambers, Phys. Rev. Lett. **5**, 3 (1960).

[16] A. Tonomura, T. Matsuda, R. Suzuki, A. Fukuhara, N. Osakabe, H. Umezaki, J. Endo, K. Shinagawa,Y. Sugita, and H. Fujiwara, Phys. Rev. Lett. **48**, 1443 (1982).

[17] A. Tonomura, N. Osakabe, T. Matsuda, T. Kawasaki, J. Endo, S. Yano and H. Yamada, Phys. Rev. Lett. **56**, 792 (1986).

[18] N. Osakabe, T. Matsuda, T. Kawasaki, J. Endo, A. Tonomura, s. Yano, and H. Yamada, Phys. Rev. A **34**, 815 (1986).

[19] E. L. Feinberg, Sov. Phys. Uspekhi **5**, 753 (1963).

[20] G. T. Trammel, Phys. Rev. **134**, B1183 (1964).

[21] B. Liebowitz, Nuovo Cim. **38**, 932 (1965).

[22] P. Bocchieri and A. Loinger, Il Nuovo Cimento **47 A**, 475 (1978).

[23] P. Bocchieri, A. Loinger, and G. Siragusa, Il Nuovo Cimento **51 A**, 1 (1979).

[24] S. M. Roy, Phys. Rev. Lett. **44**, 112 (1980).

[25] R. M. Herman, Fond. Phys. **22**, 713 (1992).

[26] T. H. Boyer, Phys. Rev. D **8**, 1667 (1973).

[27] T. H. Boyer, Phys. Rev. D **8**, 1679 (1973).

[28] T. H. Boyer, Fond. Phys. **30**, 893 (2000).

[29] T. H. Boyer, Fond. Phys. **30**, 907 (2000).

[30] M. Peshkin, Phys. Rep. **80**, 375 (1981).

[31] H. Essén and J. C. -E. Stén, Prog. Electromagn. Res. M **71**, 145 (2018).

[32] A. Caprez, B. Barwick, and H. Batelaan, Phys. Rev. Lett. **99**, 210401 (2007).

[33] D. Home and S. Sengupta, Am. J. Phys. **51**, 942 (1983).

[34] G. C. Hegerfeldt and J. T. Neumann, J. Phys. A: Math. Theor. **41**, 155305 (2008).

[35] P. Pearle and A. Rizzi, Phys. Rev. A **95**, 052124 (2017).

[36] K. J. Kasunic, Am. J. Phys. **87**, 745 (2019).

[37] C. Marletto and V. Vedral, Phys. Rev. Lett. **125**, 040401 (2020).

[38] M. Bunge, Found. Sci. **20**, 129 (2015).

[39] L. Vaidman, Phys. Rev. A **86**, 040101(R) (2012).

[40] R. -F. Wang, Front. Phys. **10**, 100305 (2015).

[41] R. -F. Wang, Sci. Rep. **6**, 19996 (2016).

[42] A. Cimmino, G. I. Opat, A. G. Klein, H. Kaiser, S. A. Werner, M. Arif and R. Clothier Phys. Rev. Lett. **63**, 380 (1989).

[43] W. J. Elion, J. J. Wachters, L. L. Sohn, and J. E. Mooij, Phys. Rev. Lett. **71**, 2311 (1993).

[44] H. Wei, R. Han, and X. Wei, Phys. Rev. Lett. **75**, 2071 (1995).

[45] J. P. Dowling, C. P. Williams, and J. D. Franson, Phys. Rev. Lett. **83**, 2486 (1999).

[46] T. Y. Lee, Phys. Rev. A **62**, 064101 (2000).

[47] V. M. Tkachuk, Phys. Rev. A **62**, 052112 (2000).

[48] Y. Sato and R. Packard, J. Phys. Conf. Ser. **150**, 032093 (2009).

[49] G. E. Vekstein, Eur. J. Phys. **18**, 113 (1997).

[50] V. Hinizdo, Eur. J. Phys. **33**, L3 (2012).

[51] A. L. Kholmetskii, O. V. Missevitch, and T. Yarman, Eur. J. Phys. **33**, L7 (2012).

[52] A. L. Kholmetskii, O. V. Missevitch, and T. Yarman, Prog. Electromagn. Res. B **45**, 83 (2012).

[53] S. Lepoutre, A. Gauguet, G. Trénec, M. Büchner, and J. Vigué, Phys. Rev. Lett. **109**, 120404 (2012).

[54] J. Gillot, S. Lepoutre, A. Gauguet, M. Büchner, and J. Vigué, Phys. Rev. Lett. **111**, 030401 (2013).

[55] S. Lepoutre, A. Gauguet, M. Büchner, and J. Vigué, Phys. Rev. A **88**, 043627 (2013).

[56] S. Lepoutre, J. Gillot, A. Gauguet, M. Büchner, and J. Vigué, Phys. Rev. A **88**, 043628 (2013).

[57] C. Qin and T. C. Steimle, J. Mol. Spectrosc. **281**, 1 (2012).

[58] X. Liu, G. Meijer, and J. P. -Ríos, Phys. Chem. Chem. Phys. **22**, 24191 (2020).

[59] J. Frenkel, Phys. Rev. **37**, 17 (1931).

[60] V. M. Agranovich and G. F. Bassani, *Thin Films and Nanostructures: Electronic Excitations in Organic Based Nanostructures,* (Elsevier Academic Press, Vol. 31, 2003).

[61] *Optical Properties of Materials and Their Applications,* (Wiley Series in Materials for Electronic and Optoelectronic Applications, Edited by Jai Singh, 2020).

[62] M. B. Smith and J. Michl, Chem. Rev. **110**, 6891 (2010).

[63] R. D. Pensack, E. E. Ostroumov, A. J. Tilley, S. Mazza, C. Grieco, K. J. Thorley, J. B. Asbury, D. S. Seferos, J. E. Anthony, and G. D. Scholes, J. Phys. Chem. Lett. **7**, 2370 (2016).

[64] S. N. Sanders, A. B. Pun, K. R. Parenti, E. Kumarasamy, L. M. Yablon, M. Y. Sfeir, and L. M. Campos, Chem. **5**, 1988 (2019).

[65] H. L. -Brion and Robert W. Field, *The Spectra and Dynamics of Diatomic Molecules,* (Elsevier Academic Press, 2004).

[66] D. Beljonne, Z. Shuai, G. Pourtois, and J. L. Bredas, J. Phys. Chem. A **105**, 3899 (2001).

[67] B. Miller, A. Steinhoff, B. Pano, J. Klein, F. Jahnke, A. Holleitner, and U. Wurstbauer, Nano Lett. **17**, 5229 (2017).

[68] A. I. Tartakovskii, V. B. Timofeev, V. G. Lysenko, D. Birkedal, and J. Hvam, J. Exp. Theor. Phys. **85**, 601 (1997).

[69] L. P. McDonnell, J. J. S. Viner, D. A. R. -Tijerina, P. Rivera, X. Xu, V. I. Fal'ko, and D. C. Smith, 2D Mater. **8**, 035009 (2021).

[70] M. Shah, L. M. Schneider, and A. R. -Iman, Semiconductors, **53**, 2140 (2019).

[71] E. Torun, H. P. C. Miranda, A. M. -Sánchez, and L. Wirtz, Phys. Rev. B **97**, 245427 (2018).

[72] *Excitons in Two-Dimensional Materials* (Advances in Condensed-Matter and Materials Physics - Rudimentary Research to Topical Technology, Edited by Jagannathan Thirumalai and Sergey Ivanovich Pokutnyi, IntechOpen, 2020).

[73] O. V. Mikhnenko, P. W. M. Blom, and T. -Q. Nguyen, Energy Environ. Sci., **8**, 1867 (2015).

[74] C. G. Thomson, A. -L. Lee, and F. Vilela, Beilstein J. Org. Chem. **16**, 1495 (2020).

[75] *Transition Metal Dichalcogenides Properties and Applications* (Semiconductors, Edited by M. I. Pech-Canul and N. M. Ravindra, Springer Nature Switzerland AG, 2019).

[76] J. McCarthy and Md. Nurunnabi, *Biomedical Applications of Graphene and 2D Nanomaterials,* (Elsevier Science, 2019).

[77] P. K. Sahoo, S. Memaran, F. A. Nugera, Y. Xin, T. D. Marquez, Z. Lu, W. Zheng, N. D. Zhigadlo, D. Smirnov, L. Balicas, and H. R. Gutierrez, ACS Nano **13**, 12372 (2019).

[78] S. I. Yengejeh, W. Wen, and Y. Wang, Front. Phys. **16**, 13502 (2021).

[79] Y. Guo and J. Robertson, Appl. Phys. Lett. **108**, 233104 (2016).

[80] M. Aras, C. Kılıc, and S. Ciraci, J. Phys. Chem. C **122**, 1547 (2018).

[81] Y. Shi, H. Zhang, W. -H. Chang, H. S. Shin, and L. -J. Li, MRS BULL. **40**, 566 (2015).

[82] H. Lim, S. I. Yoon, G. Kim, A. -R. Jang, and H. S. Shin, Chem. Mater. **26**, 4891 (2014).

[83] R. Lv, J. A. Robinson, R. E. Schaak, D. Sun, Y. Sun, T. E. Mallouk, and M. Terrones, Acc. Chem. Res. **48**, 56 (2015).

[84] R. Lv, H. Terrones, A. L. Elías, N. P. -Lópezc, H. R. Gutiérrez, E. C. -Silvac, L. P. Rajukumar, M. S. Dresselhaus and M. Terrones, Nano Today **10**, 559 (2015).

[85] *Preparation Methods of Transition Metal Dichalcogenides,* (Springer Series in Materials Science, Vol. 239, 2016).

[86] E. P. Nguyen, T. Daeneke, S. Zhuiykov, and K. K. Zadeh, Curr. Protoc. Chem. Biol. **8**, 97 (2016).

[87] K. F. Mak, C. Lee, J. Hone, J. Shan, and T. F. Heinz, Phys. Rev. Lett. **105**, 136805 (2010).

[88] S. Ahmad and S. Mukherjee, Graphene **3**, 52 (2014).

[89] H. R. Gutierrez, N. P. -Lopez, A. L. Elías, A. Berkdemir, B. Wang, R. Lv, F. L. -Urías, V. H. Crespi, H. Terrones, and M. Terrones, Nano Lett. **13**, 3447 (2013).

[90] X. Hu, L. Kou, and L. Sun, Sci. Rep. **6**, 31122 (2016).

[91] N. Lu, H. Guo, L. Li, J. Dai, L. Wang, W. -N. Mei, X. Wu, and X. Cheng Zeng, Nanoscale **6**, 2879 (2014).

[92] H. Qi, L. Wang, J. Sun, Y. Long, P. Hu, F. Liu, and X. He, Crystals **8**, 35 (2018).

[93] W. Choi, N. Choudhary, G. H. Han, J. Park, D. Akinwande, and Y. H. Lee, Mater. Today **20**, 116 (2017).

[94] S. Höger, Angew. Chem. Int. Ed. **44**, 3806 (2005).

[95] B. Traber, T. Oeser, and R. Gleiter, Eur. J. Org. Chem. **2005**, 1283 (2005).

[96] Y. Li, J. Zhao, X. Yin, and G. Yin, Chem. Phys. Chem. **7**, 2593 (2006).

[97] J. S. Moore, J. Zhang, Z. Wu, D. Venkataraman, and S. Lee, Macromol. Symp. **77**, 295 (1994).

[98] A. S. Shetty, J. Zhang, and J. S. Moore, J. Am. Chem. Soc. **118**, 1019 (1996).

[99] S. Maity, G. N. Patwari, R. Sedlak, and P. Hobza, Phys. Chem. Chem. Phys. **13**, 16706 (2011).

[100] R. Katoono, K. Kusaka, Y. Saito, K. Sakamoto, and T. Suzuki, Chem. Sci. **10**, 4782 (2019).

[101] I. Pelant and J. Valenta, *Luminescence Spectroscopy of Semiconductors,* (Oxford University Press, 2012).

Chapter2

The Quantum Topological Phase Shifts: A Unified Framework[†]

Abstract

The locality of the quantum topological effects, viz., Aharonov-Bohm (AB), Aharonov-Casher (AC) and He-McKellar-Wilkens (HMW) is presented as the local interaction between the hierarchy of multipole moments of the particles and the respective orders of external potentials. This leads to a coherent description of various topological effects as exclusively local phenomena. The absence of force led us to consider that the AB effect is truly non-classical, which agrees with the understanding that the topological effects in the quantum mechanical systems are the energy-based effects.

[†]This chapter is based on a research article under review.
Yam P. Rai and Dhurba Rai, "A Unified View On The Quantum Topological Phase Shifts."

2.1 Background

A remarkable prediction that a physically observable effect can occur without a force is certainly a new departure from the classical mechanics where force is the primary cause for every effect. This is the case with the Aharonov-Bohm (AB)effect,[1] proposed in 1959, where the interference fringes formed by the interfering charged particles get shifted by the electromagnetic potentials although the charged particles never come in direct contact with the fields, and hence no force on the particles. Nevertheless, in the electric (or scalar) AB effect, the charged particles pass through time-dependent scalar electric potential, while in the magnetic (or vector) AB effect, they traverse through spatially varying magnetic vector potential outside a long current-carrying solenoid. With no force acting on the particles, the non-classical explanation for the magnetic AB (hereafter AB) effect is that the vector potential $\vec{A}$ enters into the canonical momentum of the charged particle leading to the phase shift of the particle wavefunction that affects the interference fringes. A subtle explanation for this is the non-local interaction between the charged particle and magnetic field, while the latter remains confined within the solenoid. Although the very existence of the AB effect is demonstrated in the electron holography interferometry experiments by Tonomura et al.,[2, 3] theory behind the effect[1, 4] has generated two long-standing fundamental issues. First, since $\vec{A}$ is the only quantity present at each location of the moving charged

particles, the associated interaction must be local. However, if we stick to the classical concept of electromagnetic field interaction then the AB effect is non-local with a magnetic field interacting with the charged particles from a finite distance away. Second, since $\vec{A}$ is causing the local interaction and enters the Schrödinger equation for the particles, the status of $\vec{A}$ must be elevated to a quantity of fundamental importance, from erstwhile, a merely an auxiliary mathematical entity. This inherently suggests that the magnetic vector potential $\vec{A}$, though non-gauge invariant, may be regarded as a physical quantity more fundamental than the magnetic field $\vec{B}$.[5]

In fact, one often questions whether the AB effect is a genuine demonstration of a non-local interaction or just a manifestation of an extraordinary property of $\vec{A}$ previously not known in classical electrodynamics. Also, the theory behind the AB effect has far-reaching consequences in quantum mechanics (QM),[1, 4, 6] however, current theoretical understanding is divided between, the proponents favoring the AB effect as a quantum mechanical effect,[7] while the opponents consider the effect rather classical.[8] Also, what causes the AB effect, as to whether vector potential[1, 4] or electromagnetic interaction energy,[9–11] including the question of whether the AB effect is a local [12] or non-local effect[13] is not yet settled, though some alternative explanations are reported over the time.[14–19] It must be noted, however, that from the very beginning,[20, 21] the theoretical explanations for the AB effect are challenged and doubted as a classical effect. Among others,[22–25] the classical force-based explanation due to Boyer[26, 27]

got louder in 2000 when he presented a clear and sound semi-classical theory behind the AB effect.[28, 29] Such considerations can be viewed as an elegant attempt to understand a quantum effect, classically, while the only non-classical idea that Boyer employed is the de Broglie relation ($\lambda = h/p$) for the matter waves. As envisaged, the charged particle passing by a solenoid S that confines the magnetic field in its interior exerts a force $\vec{F}_{Sq}$ on the solenoid. An equal reactionary force $\vec{F}_{qS}$ ($= -\vec{F}_{Sq}$) then acts back on the charged particle causing relative displacement along the direction of motion that results in a shift in the position of the fringes in the interference pattern. A true surprise of this reactionary force-based semi-classical theory is the exact quantum mechanical expression for the phase shift obtained by AB.[1] This surprising match of phase shift has generated a renewed interest among the opponents.

Focusing on the issue of whether the AB effect is local or non-local, we consider electric potential associated with the motional electric field that the charged particles experience while traversing through a region filled with spatially varying $\vec{A}$, and no magnetic fields whatsoever. Such is the region outside a long, narrow and tightly wound solenoid with current held fixed. Intuitively, if a time varying vector potential induces an electric field at a location of a particle at rest, then a particle moving through a region of spatially varying vector potential perceives an electric field due to a change in vector potential at each location of the particle in motion. It is with the electric potential associated with the motional electric field the charged particle couples, leading to the locality of the AB effect

considered in this work. While one may think that the consideration of motional electric potential is only an intermediate relief in elucidating the locality of the AB effect, however, it provides a firm ground for understanding other various topological phases as exclusively local effects. Also, the consideration makes some of the prevailing notions in the theory of AB effect, rather secondary. These include the back-action reactionary force[28] and the magnetic interaction energy,[7, 10] as both require a magnetic field of the moving charged particles to interact with the solenoid. The reactionary force corresponding to the magnetic interaction energy is the basis of Boyer's semi-classical theory of phase shift.[27, 28] However, a detailed study has found the variation of magnetic interaction energy too insignificant to cause any reactionary force on the particle thereby making the region outside the solenoid essentially force-free,[7] which could be one of the possible reasons leading to the null result in a time delay experiment.[30] Amid this setback, some proponents favoring the AB effect as a purely non-classical but local effect insist that it is the local magnetic field interaction energy that causes the phase shift. The phase acquired by the charged particles is given by the time integral of the interaction energy.[10–12]

2.2 Scope of the Work

In this work, we provide insight into the local coupling of a charge with motional electric potential leading to the AB effect, thereby avoiding the complexity and the question of non-locality,[13] field penetration,[12] shielding efficiency,[12] magnetic

interaction energy,[7, 10, 12] and the back-action force on the particles.[28, 29] In so far as shielding is concerned, the AB effect is a case of a perfect shielding with no fields reaching each other; the moving charged particle and the current-carrying solenoid.[31] However, in the case of an imperfect shielding, the magnetic field of the moving charge may reach the solenoid, though the magnetic field of the solenoid remains confined within its interior. As a result, the current-carrying solenoid experiences a Lorentz force and the reactionary force acts on the moving charge.[28, 29] When calculated, the transverse components of the force are found to be significant in comparison to the longitudinal components. Interestingly, the transverse components in each interfering path act along the same direction. These deflecting transverse forces, however, cause the entire envelope of the interference pattern to shift but this is not the AB effect wherein the position of the fringes shifts within the envelope of the interference pattern when a confined magnetic flux is introduced between the interfering paths.[27, 32] This led us to consider that the AB effect is the case of a perfect shielding with no classical counterpart, which otherwise could have been demonstrated as due to force on the charged particles. Thus, discarding the force-based approach,[28, 29] we here consider the interaction energy approach discussed in the literature,[7, 9–12] however, with a subtle conceptual difference that in our consideration, the interaction energy is that associated with the local coupling of charge with the motional electric potential outside the solenoid.

This chapter is structured as follows. In Sec. 4.3, we outline the different

topological phases and briefly review their duality connections to the AB effect with due attention to the dual AB effect. In Sec. 4.4, we address the persisting issues of the AB effect. Based on the local charge-potential interaction, we provide a generalized insight into the persisting issues in question encompassing the other topological effects. In Sec. 4.5, we discuss the AB setup for the case of perfect and imperfect shielding of the magnetic fields. Phase shift even in the ideal case of a perfect shielding led us to consider that the AB phase shift is not a classical effect. The last section gives the summary of the work.

2.3 Different Topological Phases and their Relation to the AB Phase Shift

Two years after the marvelous and conclusive experimental demonstration of the AB effect,[3] Aharonov and Casher,[33] in 1984, predicted analogous phase difference between the counter-propagating neutral particles with non-zero magnetic moment $\vec{m}$ in a radial electric field $\vec{E}$ produced by a line of electric charges. Yet another, dual effect, for an electric dipole moment $\vec{d}$ moving around a radial magnetic field $\vec{B}$ is predicted by He and McKellar in 1993,[34] and independently by Wilkens in 1994.[35] In an attempt at providing a unified description of the AB, Aharonov-Casher (AC) and He-Mckellar-Wilkens (HMW) effects, Dowling et al.[36] analyzed the Maxwell electromagnetic duality relations between these effects and predicted a companion dual Aharonov-Bohm (DAB) effect for the

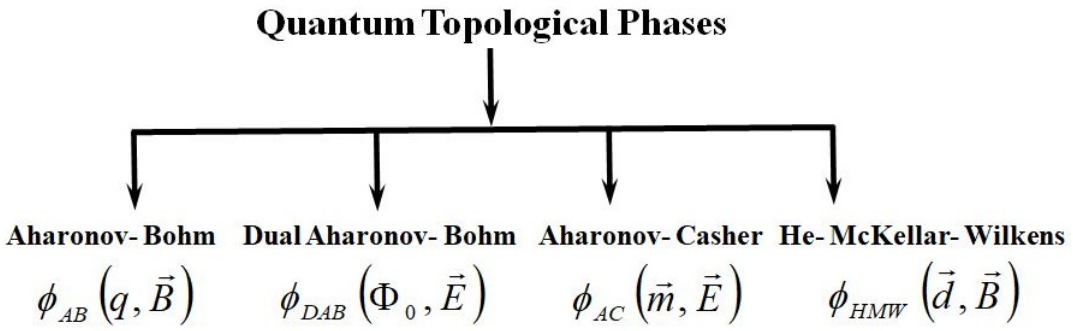

FIGURE 2.1: Different quantum topological phases.

moving magnetic monopoles. All these effects have now been experimentally verified,[3, 37–39] including the DAB with magnetic fluxon which,[40] however, is viewed as the manifestation of the AC effect.[40, 41] The defining property of these effects is that the phase difference is independent of the velocity of the particles which makes it topological in nature with no force acting on the particles whatsoever. It must be noted, however, that in the AC/HMW effects, the neutral particles possessing magnetic/electric dipole moments do pass through the electric/magnetic fields, while in the AB/DAB effects, the electric/magnetic charged particles (q, g) pass through the field-free region around the confined magnetic/-electric fluxes, which makes them a unique pair of dual topological effects. A chart of different topological phases is shown in Fig. 2.1. Of interest to us here is the duality relationship between the four topological phases with due attention to the DAB phase shift of fluxon (Φ_0) as this can be exploited for controlling the motion of fluxon in the fluxon-based superconducting devices.[42–44] The electromagnetic duality relationship between the AC phase, $\phi_{AC} = (1/\hbar c^2) \oint (\vec{m} \times \vec{E}) \cdot \vec{dl}$, and the HMW phase, $\phi_{HMW} = (1/\hbar) \oint (\vec{B} \times \vec{d}) \cdot \vec{dl}$, is well known for the pair transformations consisting of the fields and moments, i.e., $(\vec{E} \to c\vec{B}, \vec{m} \to -c\vec{d})$ and $(c\vec{B} \to -\vec{E},$

$c\vec{d} \rightarrow \vec{m}$). Similar duality pair transformations involving source charges (q, g) (that are connected by the Dirac quantization condition, $qg/2\pi\epsilon_0 c^2 = n\hbar$), viz., ($c\vec{B} \rightarrow -\vec{E}$, $q \rightarrow c\epsilon_0\Phi_0$) and ($\vec{E} \rightarrow c\vec{B}$, $c\epsilon_0\Phi_0 \rightarrow -q$) would connect the AB phase,

$$\phi_{AB} = \frac{q}{\hbar}\int \vec{B}\cdot\vec{ds}, \tag{2.1}$$

to the DAB phase in a physically accessible form,

$$\phi_{DAB} = -\frac{\epsilon_0\Phi_0}{\hbar}\int \vec{E}\cdot\vec{ds}, \tag{2.2}$$

where $\Phi_0 = h/q$ is a unit flux quantum, i.e., a fluxon, which can be considered as a quantum particle[40] that manifests as a localized magnetic vortex in the superconductors exposed to the external magnetic fields.[45] The DAB phase shift in this form for the fluxon in motion around a confined electric field is a true dual AB effect that may be exploited in the interference-based superconducting device setups.[40, 46] From the theoretical standpoint, the DAB phase shift expressed in Eq. (2.2) is more attractive than the one that employs magnetic monopole and/or electric vector potential.[36, 40, 46]

To make the connection between the AB and AC phase shifts, and that between DAB and HMW, we write the AC and HMW phase shifts in the surface integral forms

$$\phi_{AC} = \frac{1}{\hbar c^2}\int (\vec{\nabla}\times(\vec{m}\times\vec{E}))\cdot\vec{ds}, \tag{2.3}$$

and

$$\phi_{HMW} = \frac{1}{\hbar}\int (\vec{\nabla} \times (\vec{B} \times \vec{d})) \cdot \vec{ds}. \tag{2.4}$$

For the constant moments $(\vec{m}, \vec{d})$ that move in a plane perpendicular to the line of charges (q, g) producing cylindrically symmetric radial fields $(\vec{E}, \vec{B}) \sim (1/r)\hat{r}$, all other terms in the expansion of the curls

$$\vec{\nabla} \times (\vec{m} \times \vec{E}) = (\vec{E} \cdot \vec{\nabla})\vec{m} - \vec{E}(\vec{\nabla} \cdot \vec{m}) - (\vec{m} \cdot \vec{\nabla})\vec{E} + \vec{m}(\vec{\nabla} \cdot \vec{E}), \tag{2.5}$$

$$\vec{\nabla} \times (\vec{B} \times \vec{d}) = (\vec{d} \cdot \vec{\nabla})\vec{B} - \vec{d}(\vec{\nabla} \cdot \vec{B}) - (\vec{B} \cdot \vec{\nabla})\vec{d} + \vec{B}(\vec{\nabla} \cdot \vec{d}), \tag{2.6}$$

vanish except $\vec{m}(\vec{\nabla} \cdot \vec{E})$ and $\vec{d}(\vec{\nabla} \cdot \vec{B})$. The terms, $(\vec{m} \cdot \vec{\nabla})\vec{E}$ and $(\vec{d} \cdot \vec{\nabla})\vec{B}$ vanish because the fields do not vary in the dipole direction. It is evident that with the replacements, $\vec{m}(\vec{\nabla} \cdot \vec{E})$ by $-c^2\epsilon_0\Phi_0\vec{E}$, and $\vec{d}(\vec{\nabla} \cdot \vec{B})$ by $-q\vec{B}$, in conjunction with the duality transformations (c$\vec{B} \to -\vec{E}$, $q \to c\epsilon_0\Phi_0$) and ($\vec{E} \to c\vec{B}$, $c\epsilon_0\Phi_0 \to -q$), the RHS in the above expansions reduce to

$$\vec{\nabla} \times (\vec{m} \times \vec{E}) = \vec{m}(\vec{\nabla} \cdot \vec{E}) \equiv -c^2\epsilon_0\Phi_0\vec{E} \to -c^2(-q/c)(c\vec{B})), \tag{2.7}$$

$$\vec{\nabla} \times (\vec{B} \times \vec{d}) = -\vec{d}(\vec{\nabla} \cdot \vec{B}) \equiv q\vec{B} \to (c\epsilon_0\Phi_0)(-\vec{E}/c). \tag{2.8}$$

Physically, this can be understood as a "reference frame correspondence". For instance, to an observer at rest on a frame attached to a charge q, whose circulation produces the current and the associated magnetic moment $\vec{m}$ in the AC setup, the line of charge producing a cylindrically radial electric field $\vec{E}$ in the AC setup

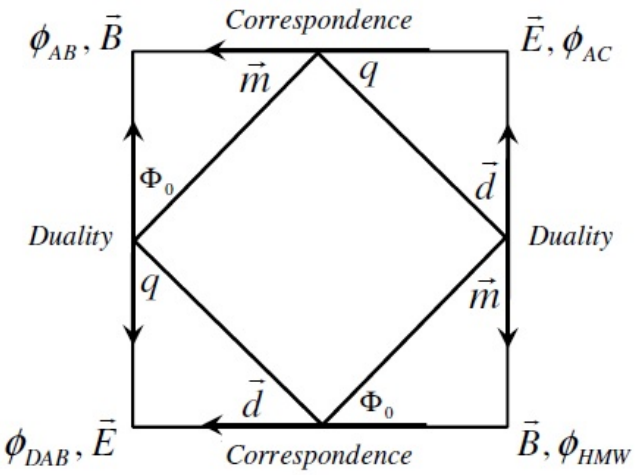

FIGURE 2.2: Relations among the four quantum topological phases. The pair $\phi_{(AB,DAB)}$ are related by duality transformations, and so are $\phi_{(AC,HMW)}$, while $\phi_{(AB,AC)}$ and $\phi_{(DAB,HMW)}$ are related through the "reference frame correspondence" as the charge and moment are not related by a dual rotation.

appears as a column of circulating charge with the induced magnetic field $\vec{B}$ confined inside. This essentially corresponds to a charge q encircling the solenoid, i.e., the AB configuration. Also, with a consideration of the magnetic monopoles that entail a perfect symmetry between the electricity and magnetism, the correspondence between the HMW and DAB can be inferred. Thus, with Eqs. (2.7, 2.8), the (AC, HMW) phase shifts in Eqs. (2.3, 2.4) reduce correspondingly to the (AB, DAB) phase shifts in Eqs. (2.1, 2.2). So, unlike (AB↔DAB) and (AC↔HMW) that are related by a dual rotation, (AC→AB) and (HMW→DAB) are related by a "reference frame correspondence", Eqs. (2.7, 2.8).

We summarize the relations among the four topological phases in a crossed-square diagram shown in Fig. 2.2. Entries $(q, \vec{d})$ and $(\Phi_0, \vec{m})$ at rest in the inner square produce the corresponding fields $\vec{E}$ and $\vec{B}$, in which the entries $(\Phi_0, \vec{m})$ and $(q, \vec{d})$ acquire topological phase when set in motion. From these, all

else would follow, and we believe that there should be no more topological phases other than that associated with the higher moments.[47] In the following section, we provide generalized insight into the persisting issues of the AB effect encompassing the AC and HMW effects, and provide the energy-based interpretation.

2.4 Persisting Issues in the AB Effect and the Energy-based Interpretation

Here we provide insights into the persisting issues concerning the AB effect from the perspective of interaction energy. The issues are presented in Fig. 2.3. Firstly, considering the magnetic field as the only existing interactive field, the AB phase shift can only be understood in terms of action at a distance, which violates the principle of locality. The AB effect thus appears to manifest non-locality which, however, is different from that associated with the violation of the Bell inequalities.[48] Nevertheless, a quantitative understanding of non-locality has remained elusive so far.[49–51] Instead, as locally only vector potential $\vec{A}$ is present, we stress on the local interaction between the hierarchy of multipole moments (charge, moments, quadrupole) of the particle with the respective orders of external potentials (potential, field, field-gradients). This leads to a coherent description of various topological effects as exclusively local phenomena with the associated interaction energy, either non-gauge invariant, i.e., $U = qV'$, for the AB phase, or gauge invariant, e.g., $U = -\vec{m} \cdot \vec{E}'$, for the AC phase, and $U = -\vec{d} \cdot \vec{B}'$,

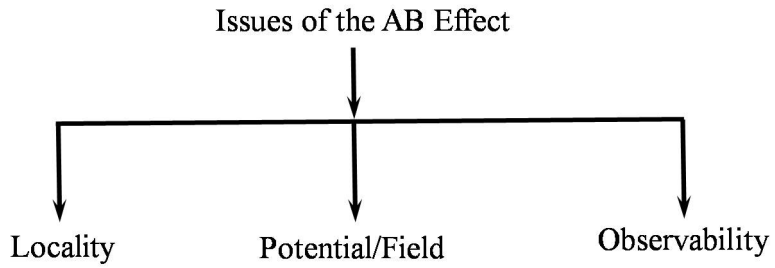

FIGURE 2.3: Persisting issues in the AB effect.

for the HMW phase, where prime labels the local motional potential and fields. It must be noted that the vector potential $\vec{A}$ that is generally accepted as non-unique has nothing to do with the question of locality. Nevertheless, in a strict sense, $\vec{A}$ can be fixed employing some convenient gauge fixing conditions, e.g., Coulomb gauge, $\vec{\nabla} \cdot \vec{A} = 0$. An alternative to this is to gauge transform $\vec{A}$ for an optimum value $\vec{A}_{opt} = \vec{A} + \vec{\nabla}\chi_{opt}$, that makes the magnetic field energy density $\frac{1}{2}\vec{A}_{opt} \cdot \vec{J}_{Source}$, equal to that otherwise obtained from $\vec{B}$, i.e., $\frac{1}{2\mu_0}|\vec{B}|^2$, where $\vec{J}_{Source}$ is the constant current density of the source of the magnetic field. However, the result differs substantially when the energy density is calculated exclusively from $\vec{A}$, thereby allowing a non-zero value for the energy density outside the solenoid.[52] Secondly, the above consideration of local interaction provides better insight into the issue as to whether or not potential is more fundamental than the field. In the AB effect, it is the charge q of the particle that couples with the motional electric potential V', which can be expressed in terms of the vector potential $\vec{A}$. Viewed in a lab-frame, the current density $\vec{J}_q$ associated with the moving charge couples with the vector potential $\vec{A}$. So, it is natural that the vector potential $\vec{A}$ is more fundamental than the field $\vec{B}$. However, in the case of the AC/HMW effects, it

is the magnetic/electric dipole moment that couples with the motional magnetic/electric field, and thus the field is more important. Further justification can be found considering a quadrupole moment that couples with the field gradients, and thus the field gradients are more important than the field or potential.[35] Finally, any attempt to avoid the problem of action at a distance entails accepting the vector potential $\vec{A}$ as a physical field that influences the phase of the wavefunction of the charged particle which, however, is not unique (not gauge invariant) and therefore not considered a physical observable. Nevertheless, $\vec{A}$ can be fixed through a gauge fixing condition, or more rigorously through a gauge transformation requiring the magnetic energy density calculated from $\vec{A}$ alone is equal to that obtained independently from $\vec{B}$ within a specified tolerance. We stress that the vector potential $\vec{A}$ is a fuzzy quantity (sometimes even called a fuzzy current, Ref. [53]) due to its imprecise value consequent to the tolerance limit in the determination of energy density. We will not push this perception too far, but it facilitates comprehension of the physical reality of $\vec{A}$. Interestingly, we note in passing that some non-gauge invariant quantities can be associated with physical observables.[54] We summarize the afore-discussed issues encompassing the AC and HMW effects in Table 2.1.

Focusing on the interaction leading to the AB phase effect, we note that the most general expression for the electric field experienced by a particle moving

TABLE 2.1: Persisting issues in the AB effect from the perspective of the interaction energy including the AC and HMW effects. The corresponding potential and fields involved are $V' = -\vec{v}\cdot\vec{A}$, $\vec{E}' = \vec{v}\times\vec{B}$ and $\vec{B}' = -\vec{v}\times\vec{E}/c^2$. Refer to the text for details.

Issues	Energy-based interpretation
(i) Locality	Local interaction with potential/field
	(a) non-gauge invariant interaction, e.g., AB effect.
	(b) gauge invariant interaction, e.g., AC/HMW effects.
(ii) Potential/Field	Depends on multipole moments
	(a) q couples with potential $V' = -\vec{v}\cdot\vec{A}$, $\Rightarrow \vec{A}$ is important in AB effect.
	(b) $(\vec{m}, \vec{d})$ couples with field $(\vec{B}', \vec{E}')$, $\Rightarrow$ Field important in AC/HMW.
(iii) Physical reality	Local interaction with
	(a) a seemingly fuzzy quantity $\vec{A}$ in the AB effect.
	(b) the ordinary quantities $(\vec{E},\vec{B})$ in the AC/HMW effects.

with velocity $\vec{v}$ is

$$\vec{E} = -\vec{\nabla}V - \frac{\partial\vec{A}}{\partial t} + \vec{v}\times\vec{B}, \tag{2.9}$$

where V is electric potential. The last term represents an electric field, $\vec{E}' = \vec{v}\times\vec{B}$, due to relative motion in magnetic field $\vec{B} = \vec{\nabla}\times\vec{A}$, which forms the basis of the Lorentz force $\vec{F} = q\vec{E}' = q(\vec{v}\times\vec{B})$, acting on the charged particle. Since $\vec{\nabla}(\vec{v}\cdot\vec{A}) = \vec{v}\times\vec{B} + (\vec{v}\cdot\vec{\nabla})\vec{A}$, the electric field in Eq. (2.9) can also be expressed in the form

$$\vec{E} = -\vec{\nabla}V - \frac{d\vec{A}}{dt} + \vec{\nabla}(\vec{v}\cdot\vec{A}). \tag{2.10}$$

In this form, the second term represents the overall time dependence of $\vec{A}$. For the AB setup, $V = 0$, $\frac{\partial \vec{A}}{\partial t} = 0$, while the convective derivative leads to $\frac{d\vec{A}}{dt} = (\vec{v} \cdot \vec{\nabla})\vec{A}$. Also, since $\vec{v} \times \vec{B} = 0$ as $\vec{B} = 0$ outside the solenoid, $\vec{\nabla}(\vec{v} \cdot \vec{A}) = (\vec{v} \cdot \vec{\nabla})\vec{A}$. The AB setup is such that $\frac{d\vec{A}}{dt} = \vec{\nabla}(\vec{v} \cdot \vec{A}) = (\vec{v} \cdot \vec{\nabla})\vec{A}$. Thus, there is no electromagnetic field, i.e., $\vec{E} = 0$, $\vec{B} = 0$, outside the solenoid, and hence no force acting on the moving charged particle. What is important to note here is that the charge q couples with the motional potential $V' = -\vec{v} \cdot \vec{A}$, associated with the motional electric field, represented by the third term in Eq. (2.10). The interaction energy corresponding to the charge-potential coupling is $U = qV' = -q\vec{v} \cdot \vec{A}$ and the classical Lagrangian of the charge is $L_{classical} = T - U = 1/2mv^2 + q\vec{v} \cdot \vec{A} = 1/2mv^2 + L_{int}$. Following the path integral formulation of QM, the transition amplitude for a particle to go from point 'a' to 'b', bypassing the solenoid along a certain path Γ, is the same as the transition amplitude if it would go along the same path with solenoid removed, however, with a multiplicative phase factor $exp(i/\hbar \mathcal{S}_{int})$, determined by the action, $\mathcal{S}_{int} = \int_{a,\Gamma}^{b} L_{int}\, dt = \int_{a,\Gamma}^{b} \frac{\partial}{\partial \vec{v}} L_{int} \cdot \vec{dl}$. In the wave mechanics, this is the phase picked up by the wavefunction of the particle that can be inferred by comparing the solutions of the Schrödinger equations in the absence and presence of the solenoid. Thus, the phase difference between the charged particles moving from point 'a' to 'b' along the paths (Γ, Γ') enclosing the solenoid is $\phi = \phi_\Gamma - \phi_{\Gamma'} = (q/\hbar) \oint \vec{A} \cdot \vec{dl}$, which is the AB phase shift in Eq. (2.1).

2.5 The AB setup with Perfect and Imperfect Shielding

It is natural that a moving charge induces a magnetic field, however, its consideration in the study of the AB effect purely depends on the model representing the AB setup. Ignoring the magnetic field due to a moving charge is equivalent to a case of a perfect shielding, so that neither the field due to a moving charge reaches the solenoid, nor the field of the solenoid leaks out to reach the moving charge as this is the defining property of a long, narrow and tightly wound solenoid. However, in the case of an imperfect shielding, the magnetic field of the moving charge may reach the solenoid, thereby influencing the current in the solenoid and the field within, with a possible back action thereof. We here begin with the perfect shielding case.

2.5.1 Perfect shielding

In this case, the magnetic field of the moving charged particles does not reach the solenoid. Also, anyway, the magnetic field inside the long solenoid will not leak into its exterior to interact with the interfering charges. So, in such a perfect setup, there is no external force on the solenoid, $\vec{F}_{Action} = 0$, and hence, no reaction force on the charge, $\vec{F}_{Reaction} = 0$. Also, there is no electromagnetic force on the moving charge as each term in the most general expression of electric field (Eq. (2.9)) is

identically zero for the AB setup, so $\vec{F}_q = q\vec{E} = 0$. However, as the interaction energy corresponding to the charge-potential coupling is velocity dependent, i.e., $U = qV' = -q\vec{v} \cdot \vec{A}$, one may be tempted to determine the force on the charge as $\vec{F}_q = -\vec{\nabla}U + \frac{d}{dt}\left(\frac{\partial U}{\partial \vec{v}}\right)$ which, however, is just $q\vec{E}$. Thus, there is no force acting on the charge. The AB effect in this case is purely a non-classical effect associated with the influence of charge-potential coupling on the phase picked up by the wavefunction of the charged particles that affect the interference fringes. In so far as shielding is concerned, some even doubt that the shielding in Tonomura's experiment acts only one way preventing the leakage of internal static field, while ineffective in shielding the external time-varying magnetic field of the moving charged particles.[12] We here stress that since the charged particles remain outside the solenoid, the consideration of local interaction of charge with motional electric potential is certainly a better choice over that based on the interaction energy resulting from the overlap of magnetic fields inside the solenoid.[7, 10, 12] Perhaps this magnetic field interaction energy is not accessible to the charged particles moving outside the solenoid.

2.5.2 Imperfect shielding

In this case, the magnetic field $\vec{B}_q$ of the moving charged particles reaches the current-carrying solenoid, and thus the solenoid experiences a force. This is viewed as the force exerted by the moving charge on the solenoid, which is estimated to

be,[21, 30]

$$\vec{F}_{Action} = -q\vec{\nabla}(\vec{v}\cdot\vec{A}) = -q\frac{d\vec{A}}{dt}. \tag{2.11}$$

In obtaining the second equality, use has been made of the fact that $\vec{B} = 0$ outside the solenoid and the dependence of $\vec{A}$ on time t is only implicit. Microscopically, this force perturbs the motion of the electrons in the solenoid and thus the current through the solenoid changes. This results in a change in the magnetic moment $\vec{m}_S$ of the solenoid and thus the interaction energy corresponding to the dipole-field coupling, $U_{MB} = -\vec{m}_S \cdot \vec{B}_q = -q\vec{v}\cdot\vec{A}$, changes.[8] A simple derivation of the interaction energy U_{MB}, i.e., the dipole-field coupling energy is as follows.

Consider a charge q moving non-relativistically past a long, narrow and tightly wound current-carrying solenoid S positioned at the origin. Assuming that the magnetic field inside the solenoid remains confined exclusively within its volume (other than those at the two ends), the charge moves in a field-free region, and thus no interaction in the exterior of the solenoid. However, this is not the case for an external magnetic field that may penetrate the solenoid, thereby interacting with the field within the solenoid. The interaction energy can be calculated, either as magnetic overlap energy $U_{BB} = \int(\vec{B}_q \cdot \vec{B}_S)d\tau$,[7, 8] or as dipole-field coupling, $U_{MB} = -\vec{m}_S \cdot \vec{B}_q$.[8] We here choose the latter as it is technically simple and easy to evaluate than the overlap energy involving volume integration.

The charge under consideration moves with velocity $\vec{v}$ in the XY plane

while the solenoid is stationary with its axis coinciding with the z-axis. Viewed from the perspective of charge, the solenoid passes by the charge with velocity $-\vec{v}$, which facilitates an easy determination of the geometric relations required in the calculation of the interaction energy. This is shown in Fig. 2.4 with solenoid passing by the charge q at a distance r ($\gg R$) away from the charge. The magnetic field that the solenoid perceives at a location ($r' = r/sin\theta, \theta$) is

$$\vec{B}_q = -\frac{\mu_0 q}{4\pi}\frac{\vec{v}\times\hat{r'}}{r'^2} = -\frac{\mu_0 q}{4\pi}\frac{\vec{v}\times\hat{r'}}{r^2}sin^2\theta. \tag{2.12}$$

If n is the number of turns per unit length of the solenoid, then the elemental length $|dz| = rd\theta/sin^2\theta$ of the solenoid has $n|dz|$ number of turns. Thus, the magnetic moment of the elemental length of the solenoid of radius R carrying a constant current I is $d\vec{m} = n|dz|I\pi R^2\hat{z}$. Therefore, the interaction energy corresponding to the coupling of $d\vec{m}$ with $\vec{B}_q$ in the rest frame of the solenoid is

$$\begin{aligned} dU_{MB} &= -d\vec{m}\cdot\vec{B}_q, \\ &= -n\frac{\mu_0}{4r}qIR^2\vec{v}\cdot(\hat{z}\times\hat{r'})\ d\theta, \\ &= -n\frac{\mu_0}{4r}qIR^2\vec{v}\cdot\hat{\phi}\ sin\theta\ d\theta, \end{aligned} \tag{2.13}$$

and the net interaction energy is

$$U_{MB} = \int_{\theta=0}^{\theta=\pi} dU_{MB} = -q\frac{\mu_0}{2r}nIR^2\vec{v}\cdot\hat{\phi} = -q\vec{v}\cdot\vec{A}, \tag{2.14}$$

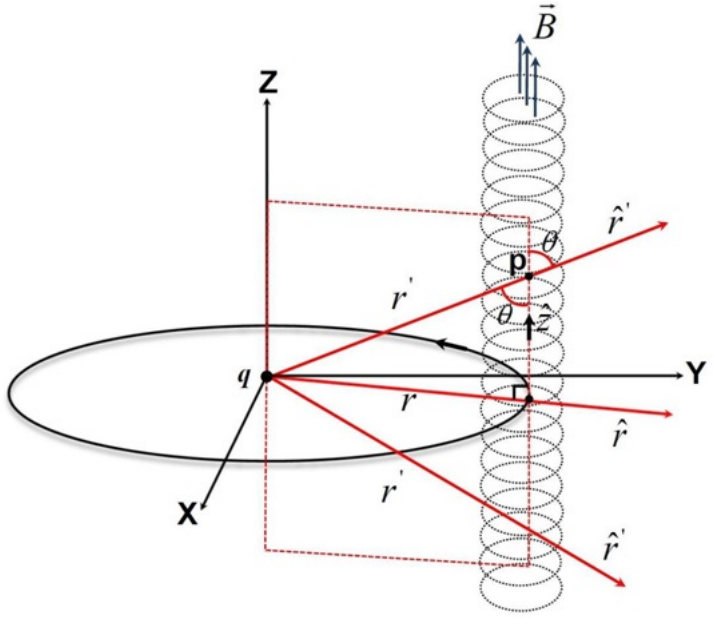

FIGURE 2.4: Schematic view of relative motion of a solenoid *w.r.t* a charged particle q. For the charged particle moving with velocity $\vec{v}$ around the solenoid at rest, the solenoid moves with velocity $-\vec{v}$ *w.r.t* the charged particle.

where $\vec{A} = \frac{\mu_0}{2r} nIR^2\hat{\phi}$ is identified as the vector potential outside ($r > R$) the solenoid. The force associated with this dipole-field coupling energy is

$$\begin{aligned} \vec{F}_{MB} &= -\vec{\nabla}U_{MB} + \frac{d}{dt}\left(\frac{\partial U_{MB}}{\partial \vec{v}}\right), \\ &= q\vec{\nabla}(\vec{v}\cdot\vec{A}) - q\frac{d\vec{A}}{dt}. \end{aligned} \tag{2.15}$$

Also, the magnetic field $\vec{B}_q$ that overlaps with the magnetic field $\vec{B}_S$ inside the solenoid changes. This results in a change in the field-field interaction energy, $U_{BB} = \int \left(\vec{B}_q \cdot \vec{B}_S\right) d\tau = q\vec{v}\cdot\vec{A}$.[7, 8] The associated force is

$$\begin{aligned} \vec{F}_{BB} &= -\vec{\nabla}U_{BB} + \frac{d}{dt}\left(\frac{\partial U_{BB}}{\partial \vec{v}}\right), \\ &= -q\vec{\nabla}(\vec{v}\cdot\vec{A}) + q\frac{d\vec{A}}{dt}. \end{aligned} \tag{2.16}$$

Therefore, the total force on the solenoid is

$$\vec{F}_{S,total} = \vec{F}_{Action} + \vec{F}_{MB} + \vec{F}_{BB} = -q\frac{d\vec{A}}{dt}. \tag{2.17}$$

Assuming that Newton's third law holds good, the reaction force is

$$\vec{F}_{Reaction} = -\vec{F}_{S,total} = q\frac{d\vec{A}}{dt}. \tag{2.18}$$

Therefore, the net force acting on the charge is

$$\begin{aligned} \vec{F} &= \vec{F}_q + \vec{F}_{Reaction}, \\ &= q\frac{d\vec{A}}{dt} = q\vec{\nabla}(\vec{v}\cdot\vec{A}). \end{aligned} \tag{2.19}$$

Thus, there is a force on the charged particle in the case of imperfect shielding. Boyer estimated this force considering U_{BB} alone, i.e., $\vec{F} = \vec{F}_{Reaction} = -\vec{F}_{BB}$, with $\vec{F}_{BB} = -\vec{\nabla}U_{BB} = -q\vec{\nabla}(\vec{v}\cdot\vec{A})$.[28] At this juncture, one may wonder if the AB phase shift ϕ_{AB} can be related to the force $\vec{F}$ on the charged particle. We answer this in the negative by analyzing the components of the force for which we consider the charged particle q to move with a velocity $\vec{v} = v_x\hat{i} + v_y\hat{j}$, in the XY plane, bypassing the solenoid placed at the origin $(0,0)$ with its axis coinciding the z-axis. For a long solenoid of cross-sectional area $\mathcal{A} = \pi R^2$, with the magnetic field $\vec{B}_0 = \mu_0 nI\hat{z}$, confined within its volume, the vector potential outside the

solenoid ($r > R$) is

$$\vec{A} = \frac{B_0\mathcal{A}}{2\pi r}\hat{\phi} = \frac{B_0\mathcal{A}}{2\pi r^2}(-y\hat{i} + x\hat{j}). \tag{2.20}$$

The force components, $F_x = q\nabla_x(\vec{v}\cdot\vec{A})$ and $F_y = q\nabla_y(\vec{v}\cdot\vec{A})$, are thus

$$F_x = \frac{qB_0\mathcal{A}}{2\pi}\left[\frac{1}{(x^2+y^2)}\left(-y\frac{\partial v_x}{\partial x} + x\frac{\partial v_y}{\partial x}\right) + \frac{2xyv_x + (y^2-x^2)v_y}{(x^2+y^2)^2}\right], \tag{2.21}$$

$$F_y = \frac{qB_0\mathcal{A}}{2\pi}\left[\frac{1}{(x^2+y^2)}\left(-y\frac{\partial v_x}{\partial y} + x\frac{\partial v_y}{\partial y}\right) + \frac{-2xyv_y + (y^2-x^2)v_x}{(x^2+y^2)^2}\right]. \tag{2.22}$$

For a constant velocity $\vec{v} = v_0\hat{j}$, Eq. (2.22) reduces to that in Refs. [28, 30], however, the opposite sign indicates that $\vec{F}$ is a reactionary force. Moreover, as the particles approach the solenoid from laterally opposite sides $\pm x$, the transverse components $F_{\pm x}$ of the force become increasingly significant over its longitudinal component F_y, which remains true even if we consider the effect of the force on the velocity v_0, though $F_{+x} \neq F_{-x}$ in that case. Precisely at $y = 0$ plane, $F_{\pm x} = -\frac{qB_0\mathcal{A}}{2\pi}\frac{v_0}{x^2}$, while $F_y = 0$. Consequently, the charged particles suffer lateral displacement causing the entire envelope of the interference pattern to shift, but this is not the AB effect wherein the position of the fringes shift within the envelope of the interference pattern when a confined magnetic flux is introduced between the interfering paths.[27, 32] Boyer's analysis of longitudinal component F_y, while completely ignoring the deflecting transverse component F_x, would result in a relative displacement between the charges passing on the opposite sides of the

solenoid that precisely determines the AB phase shift.[28] This surprising match between the reactionary force-based phase shift and the genuine AB phase shift led to performing an experiment aimed at measuring the possible time delay between the particles traversing opposite sides of the solenoid, however, the null results proved sufficient to rule out any forces that otherwise could have acted on the particle.[30] The genuine AB phase shift corresponding to a perfect shielding case (AB type I effect,[55]) is thus not a classical effect based on the reactionary force associated with the imperfect shielding (Boyer type II effect,[26]).

Our stance here is that all the AB experiments performed to date, either represent perfect shielding, thereby no force and time delay, or the observed fringe shift, though unlikely, is the entire interference pattern shift due to deflecting transverse force with no time delay that may otherwise arise from the longitudinal force. Should there be a genuine phase shift, no force should act on a particle whatsoever, while all force-based effects manifest the entire interference pattern shift rather than a shift in the position of the fringes within the interference pattern. We summarize the physical effects of various combinations of force and field in Table 2.2.

TABLE 2.2: Physical effects for various combinations of field and force. See Refs. [26, 55, 56].

	AB		Boyer	
	Type I	Type II	Type I	Type II
Fields	$\vec{E}$, $\vec{B} = 0$	$\vec{E}$, $\vec{B} \neq 0$	$\vec{E}$, $\vec{B} \neq 0$	$\vec{E}$, $\vec{B} = 0$
Force	$\vec{F} = 0$	$\vec{F} = 0$	$\vec{F} \neq 0$	$\vec{F} \neq 0$
Effects	AB, DAB	AC, HMW	Pattern shift	Fringe shift
Shielding	Perfect	–	–	Imperfect

However, we stress that the Boyer type II effect is the entire interference pattern shift due to the deflecting transverse force that plays a decisive role in the case of an imperfect shielding.

2.6 Summary and Concluding Remarks

In summary, we consider the hierarchical local interaction of the multipole moments of the particles with the various orders of potential, leading to the various topological phases. The consideration leads to a coherent description of various topological phases as exclusively local effects. Furthermore, the consideration aids in the quest to determine whether the potential or field is more important. The AB effect is due to the local interaction of charge with electric potential associated with the motional electric field, so the potential is more important than the field. However, the AC and HMW effects are associated with the local interaction of the dipole moment with the field, so the field is important. In an attempt at generalizing the duality relations among the various effects, the pair effects (AB & AC) and (DAB & HMW) are found to relate only through "correspondence", as the charge and moment are not related by a dual rotation. It turns out that among the most studied effects, the AB phase shift is the case of a perfect shielding with no fields reaching the charged particle and the solenoid, and hence no force on the charged particles. The absence of force led us to consider that the AB phase shift is truly a non-classical effect, which further suggests that the AB phase shift is an energy-based effect rather than a force-based effect. However, the reactionary

force in the case of imperfect shielding causes the entire envelope of the interference pattern to shift which, however, is not the AB effect wherein the position of the fringes shifts within the envelope of the interference pattern.

References

[1] Y. Aharonov and D. Bohm, Phys. Rev. **115**, 485 (1959).

[2] A. Tonomura, T. Matsuda, R. Suzuki, A. Fukuhara, N. Osakabe, H. Umezaki, J. Endo, K. Shinagawa, Y. Sugita, and H. Fujiwara, Phys. Rev. Lett. **48**, 1443 (1982).

[3] A. Tonomura, N. Osakabe, T. Matsuda, T. Kawasaki, J. Endo, S. Yano, and H. Yamada, **56**, 792 (1986).

[4] Y. Aharonov and D. Bohm, Phys. Rev. **123**, 1511 (1961).

[5] R. A. Mulder, Found. Phys. **51**, 48 (2021).

[6] M. Peshkin, Phys. Rep. **80**, 375 (1981).

[7] H. Essén and J. C. -E. Sténe, Prog. Electro. Res. M **71**, 145 (2018).

[8] K. T. McDonald, "Classical Aspects of the Aharonov-Bohm Effect", 2019.

[9] L. Vaidman, Phys. Rev. A **86**, 040101(R) (2012).

[10] R. -F. Wang, Front. Phys. **10** 100305 (2015).

[11] R. -F. Wang, Sci. Rep. **6**, 1 (2016).

[12] K. Kang, Phys. Rev. A **91**, 05116 (2015).

[13] Y. Aharonov, E. Cohen, and D. Rohrlich, Phys. Rev. A **93**, 042110 (2016).

[14] D. Home and S. Sengupta, Am. J. Phys. **51**, 942 (1983).

[15] G. C. Hegerfeldt and J. T. Neumann, J. Phys. A: Math. Theor. **41**, 155305 (2008).

[16] P. Pearle and A. Rizzi, Phys. Rev. A **95**, 052124 (2017).

[17] K. J. Kasunic, Am. J. Phys. **87**, 745 (2019).

[18] C. Marletto and V. Vedral, Phys. Rev. Lett. **125**, 040401 (2020).

[19] C. R. de Oliveira and R. G. Romano, Found. Phys. **50**, 137 (2020).

[20] E. L. Feinberg, Usp. Fiz. Nauk, **78**, 53 (1963).

[21] G. T. Trammel, Phys. Rev. **134**, B1183 (1964).

[22] P. Bocchieri and A. Loinger, Il Nuovo Cimento **47 A**, 475 (1978).

[23] P. Bocchieri, A. Loinger, and G. Siragusa, Il Nuovo Cimento **51 A**, 1 (1979).

[24] S. M. Roy, Phys. Rev. Lett. **44**, 111 (1980).

[25] R. M. Herman, Fond. Phys. **22**, 713 (1992).

[26] T. H. Boyer, Phys. Rev. D **8**, 1667 (1973).

[27] T. H. Boyer, Phys. Rev. D **8**, 1679 (1973).

[28] T. H. Boyer, Fond. Phys. **30**, 893 (2000).

[29] T. H. Boyer, Fond. Phys. **30**, 907 (2000).

[30] A. Caprez, B. Barwick, and H. Batelaan, Phys. Rev. Lett. **99**, 210401 (2007).

[31] P. L. Saldanha, Phys. Rev. A **104**, 032219 (2021).

[32] S. Olariu, Rev. Mod. Phys. **57**, 339 (1985).

[33] Y. Aharonov and A. Casher, Phys. Rev. Lett. **53**, 319 (1984).

[34] X. -G. He and B. H. J. Mckellar, Phys. Rev. A **47**, 3424 (1993).

[35] M. Wilkens, Phys. Rev. Lett. **72**, 5 (1994).

[36] J. P. Dowling, C. P. Williams, and J. D. Franson, Phys. Rev. Lett. **83**, 2486 (1999).

[37] A. Cimmino, G. I. Opat, A. G. Klein, H. Kaiser, S. A. Werner, M. Arif, and R. Clothier, Phys. Rev. Lett. **36**, 380 (1989).

[38] S. Lepoutre, A. Gauguet, G. Trénec, M. Büchner, and J. Vigué, Phys. Rev. Lett. **109**, 120404 (2012).

[39] J. Gillot, S. Lepoutre, A. Gauguet, M. Büchner, and J. Vigué, Phys. Rev. Lett. **111**, 030401 (2013).

[40] W. J. Elion, J. J. Wachters, L. L. Sohn, and J. E. Mooiji, Phys. Rev. Lett. **71**, 2311 (1993).

[41] B. Reznik and A. Aharonov, Phys. Rev. D **40**, 4178 (1989).

[42] S. Savel'ev and F. Nori, Physica C **1**, 179 (2002).

[43] J. E. Villegas, S. Savel'ev, F. Nori, E. M. Gonzalez, J. V. Anguita, R. Garcá, and J. L. Vicent, Science **302**, 1188 (2003).

[44] H. Hilgenkamp, V. V. Moshchalkov, and P. Kes, Science **302**, 1159 (2003).

[45] T. Matsuda, S. Hasegawa, M. Igarashi, T. Kobayashi, M. Naito, H. Kajiyama, J. Endo, N. Osakabe, and A. Tonomura, Phys. Rev. Lett. **62**, 2519 (1989).

[46] O. Yamaashita and S. Tomiyoshi, Phys. Lett. A **309**, 138 (2003).

[47] C. -C. Chen, Phys. Rev. A **51**, 2611 (1995).

[48] R. Healey, Philos. Sci. **64**, 18 (1997).

[49] F. J. Tipler, Proc. Natl. Acad. Sci. **111**, 11281 (2014).

[50] R. B. Griffiths, Phys. Rev. A **101**, 022117 (2020).

[51] W. Sulis, Front. Phys. **8**, 1 (2020).

[52] H. E. Puthoff, Eur. J. Phys. **37**, 055203 (2016).

[53] N. Ida, *Engineering Electromagnetics* (3rd ed, Springer-Verlag, NY, 2015).

[54] B. Berche, D. Malterre, and E. Medina, Am. J. Phys. **84**, 616 (2016).

[55] Y. Aharonov, Proc. Int. Symp. *Foundations of Quantum Mechanics* (Tokyo, 1983) p. 10-19.

[56] H. Batelaan and A. Tonomura, Phys. Today **62**, 38 (2009).

Chapter3

Quantum Mechanical Phase of a Moving Electric Dipole in a Static Magnetic Field[†]

Abstract

The quantum mechanical phase of an electric dipole moving in a static magnetic field is studied in the light of the original concept proposed by He and McKellar in 1993, and independently by Wilkens in 1994. An elementary approach to the alternative derivation of the He-McKellar-Wilkens (HMW) phase is presented. It is shown that the Lagrangian of the moving dipole with explicit consideration of the interaction between the current associated with the moving electric dipole and the magnetic vector potential would lead to the same expression for the phase

[†]This chapter is based on a research article:
Yam P. Rai and Dhurba Rai, "On the He–McKellar–Wilkens phase of an electric dipole", Ann. Phys. **383**, 196 (2017).

shift. Conditions for the observation of the HMW phase are investigated, and a practical setup is proposed for its observation with the magnetic field alone.

3.1 Background

A startling prediction of a new quantum effect requires an in-depth understanding of previously unknown or unaccounted interaction mechanisms. In 1959, Aharonov and Bohm (AB) [1] predicted the phase difference between the counter-propagating electrons through a magnetic field-free region outside a long current-carrying solenoid. The AB phase is $\phi_{AB} = \frac{1}{\hbar} \oint \vec{A} \cdot \vec{dl}$, where $\vec{A}$ is a circumferential vector potential outside the long current-carrying solenoid. In contrast to being, the magnetic vector potential, a mere supplementary mathematical object introduced for the description of magnetic fields, the interpretation of this quantum phenomenon highlighted the fundamental importance of vector potential in quantum mechanics. The AB effect not only revealed the physical reality of vector potential but also engendered a whole set of analogous quantum effects like the Aharonov-Casher (AC) effect [2], Casella effect [3], He-McKellar-Wilkens (HMW) effect [4, 5] and the associated additional effect studied by Spavieri.[6–8] In an attempt at providing a unified description of these effects, Dowling et al.[9] established the Maxwell electromagnetic duality relations between the various quantum mechanical phase shift effects. These effects have been experimentally verified including the HMW phase shift that was measured a decade ago by Lepoutre et al.[10–12]

Our interest in this work is the HMW phase collected by a moving electric dipole $\vec{d}$ in a static magnetic field $\vec{B}$ given by $\phi_{HMW} = \frac{1}{\hbar} \oint \left(\vec{B} \times \vec{d}\right) \cdot \vec{dl}$. A

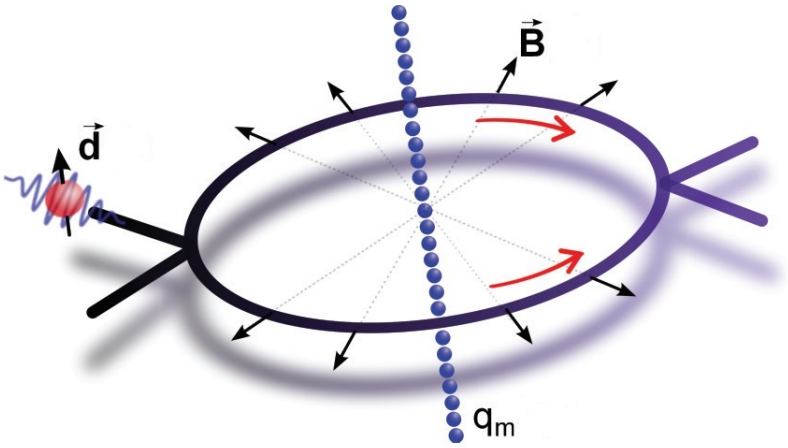

FIGURE 3.1: The HMW setup wherein the counter-propagating electric dipoles $\vec{d}$ in a radial magnetic field $\vec{B} \sim \hat{r}/r$ produced by a line of magnetic monopoles q_m acquire a phase difference ϕ_{HMW} independent of the shape of the path and the velocity of the moving dipoles. Figure adapted from Ref. [10].

schematic diagram of the HMW setup is presented in Fig. 3.1. It took almost two decades for experimental observation of this phase after its first prediction by He and McKellar in 1993,[4] and independently by Wilkens in 1994.[5] The principal obstacle to the experimental test of the HMW phase was the requirement of a radial magnetic field necessary for zero classical force and torque on the moving dipole, [5, 13–17] i.e., force $\vec{F} = \vec{v} \times \left\{ \vec{\nabla} \times \left(\vec{B} \times \vec{d} \right) \right\} = 0$ and torque $\vec{\tau} = \vec{d} \times \left(\vec{v} \times \vec{B} \right) = 0$, where $\vec{v}$ is the velocity of the moving dipole. Starting with Wilkens' configuration [5] consisting of a pierced magnetic sheet mimicking the required radial magnetic field confined within the hole, varieties of field configurations [9, 13, 18–20] were proposed for experimental observation of the HMW phase. It is only in 2012, Lepoutre et al.[10] observed the long-sought HMW effect in a polarized Li atom interferometer with an interaction region consisting of the electric and magnetic fields similar to that initially proposed by Wei et al.[18] A practical setup employed by Lepoutre et al. is shown in Fig. 3.2 where crossed-electric and magnetic

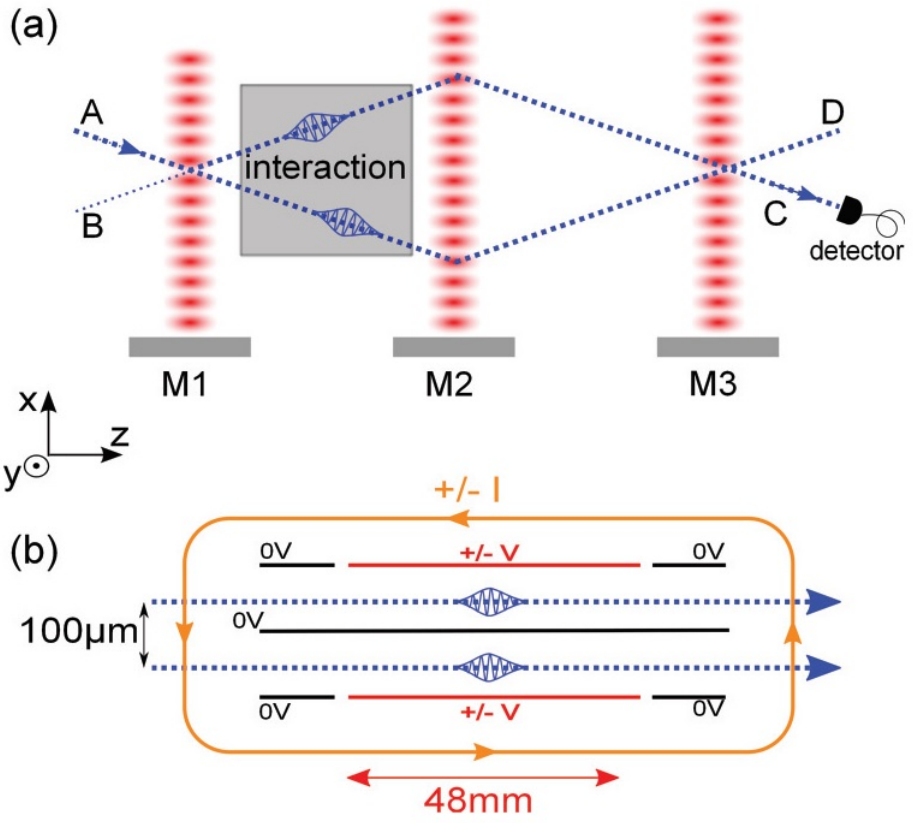

FIGURE 3.2: Experimental setup due to Lepoutre et al.[11] consisting of Mach-Zehnder atom interferometer. (a) The interaction region where the Li atomic beams (dotted lines) interact in the presence of the crossed-electric and magnetic fields. (b)The electric fields are produced by two parallel plate capacitors through which the interfering atomic beams pass. Two rectangular coils labelled as $\pm I$ (electric currents) produce the vertical magnetic field.

fields are used for the observation of the HMW phase. The measured value of the HMW phase shift of 27 $m$rad is reported to be 31% larger than the expected value and the discrepancy is attributed to the limitations of their experimental model involves extraction of the HMW phase which the Li atoms pickup in addition to that due to the stray effects, viz., AC, Zeeman, and Stark effects. However, there is a significant improvement in the determination of the HMW phase in the subsequent measurements. [11, 12] Also recently, Chen et al.[21] have proposed a dc SQUID-like device to test the HMW effect in the interference of the excitons in

the bilayer exciton condensates observed in semiconductor heterostructures and bilayer graphene. No other effects contribute to the interference making the setup unique for the study of the HMW effect in the excitonic interference.

On the theoretical front, Spavieri in 1998, made a critical examination of the HMW phase.[6] He found that a rigorous gauge-invariant Lagrangian of the moving electric dipole leads to an additional term $\frac{1}{\hbar}\oint \vec{\nabla}\left(\vec{d}\cdot\vec{A}\right)\cdot\vec{dl}$ in the HMW phase. This additional term, hereafter labeled as ϕ_S, is topological in nature as it does not depend on the shape of the encircling path and it is non-dispersive, i.e., independent of particle velocity. The question of whether or not ϕ_S even exists has been debated. [7, 22] It is argued in Ref. [7] that ϕ_S is non-zero in the Wilkens' configuration while the total phase shift $\phi = \phi_{HMW} + \phi_S$ is zero. Looking for a more practical scheme for experimental verification of the HMW phase, Tkachuk [19] considered an electric dipole encircling a long and thin ferromagnetic wire magnetized in opposite direction from the endpoints with magnitude varying linearly along the wire. The central part of such a magnetized wire would essentially produce a radial magnetic field suitable for testing the HMW phase. The delicious ingenuity of the proposed configuration lies in the fact that the additional term in the HMW phase is identically zero, i.e., $\phi_S = \frac{1}{\hbar}\oint \vec{\nabla}\left(\vec{d}\cdot\vec{A}\right)\cdot\vec{dl} = 0$ for any orientation of the electric dipole $\vec{d}$. At this juncture, it must be noted however that a term so profound in the analysis must have some significance, and thus deserve a detailed investigation.

3.2 Scope of the Work

The work aims to investigate the interaction of moving electric dipole with static magnetic field $\vec{B}$ and the associated vector potential $\vec{A}$, thereby revealing the physical origin of the additional term in the HMW phase, and explore situations where this is non-zero. It is both interesting and important to consider the way such an additional term, so prominent in the analysis, can be verified. This work is also intended to explore the various field configurations underscoring the necessity of inverse radial dependence of magnetic field for the observation of the HMW phase. We here propose a practical setup that provides essentially a radial magnetic field with inverse radial dependence that is important for the observation of the HMW effect. The setup is intended to serve a two-fold purpose: first, to observe the original HMW phase with a magnetic field alone, and second, to determine the HMW phase avoiding the associated stray effects when simultaneous crossed-electric and magnetic fields are used. This chapter is organized as follows. In Sec. 3.3, we present an elementary approach to realize the HMW phase. In Sec. 3.4, we re-derive the HMW phase using the Lagrangian of an electric dipole in motion considering explicitly the associated currents. Section 3.5 discusses the net force and torque on the dipole moving through magnetic field $\vec{B}$ and the associated vector potential $\vec{A}$. Sec. 3.6 discusses the HMW phase in various field configurations. In Sec.3.7, we present the practical setup for the realization of HMW effect followed by Sec. 3.8 that gives a summary of the work presented in

this chapter.

3.3 Elementary Approach to the HMW Phase

A unique feature of the various intriguing effects such as Sagnac, AB, AC, and HMW is the relative phase shift of interfering waves caused by rotation or electromagnetic interaction. The Sagnac effect is a phase-coherent effect in atom (or optical) interferometers in which rotation of the interferometer with respect to an inertial reference frame causes the counter-propagating waves path lengths to differ by an amount proportional to the angular velocity ω and area S enclosed by the interfering paths, resulting in an interference fringe shift.[23] The AB effect is caused by charge q coupling with vector potential $\vec{A}$ in a multiply-connected region without a magnetic field. The AC effect is caused by the interaction of a magnetic dipole $\vec{m}$ with the Lorentz transformed effective magnetic field $\vec{B}' \cong -\vec{v} \times \vec{E}/c^2$ in a co-moving frame traversing a magnetic field-free region, just as its Maxwell counterpart, the HMW effect, is caused by the interaction of an electric dipole $\vec{d}$ with the Lorentz transformed effective electric field $\vec{E}' \cong \vec{v} \times \vec{B}$ in a co-moving frame traversing an electric field-free region. The phase shifts are expressed as a

closed line integral of vector fields, i.e.,

$$\phi_{Sag} = \frac{m}{\hbar}\oint \vec{v}\cdot\vec{dl} = \frac{2m}{\hbar}\int \vec{\omega}\cdot\vec{dS} = \frac{2m}{\hbar}\omega S, \tag{3.1}$$

$$\phi_{AB} = \frac{q}{\hbar}\oint \vec{A}\cdot\vec{dl} = \frac{q}{\hbar}\int \vec{B}\cdot\vec{dS} = \frac{q}{\hbar}\Phi, \tag{3.2}$$

$$\phi_{AC} = \frac{1}{\hbar c^2}\oint \left(\vec{m}\times\vec{E}\right)\cdot\vec{dl}, \tag{3.3}$$

$$\phi_{HMW} = \frac{1}{\hbar}\oint \left(\vec{B}\times\vec{d}\right)\cdot\vec{dl}. \tag{3.4}$$

It must be noted here that the Sagnac and AB phases are expressed in the surface integral form that is directly accessible to experimental measurements. In Eq. (3.1), m is the inertial mass of a particle ($m = h/\lambda c$ for photon) and $\vec{v}$ is the linear velocity of rotation of the interferometer,[24] while Φ in Eq. (3.2) is magnetic flux piercing the surface S. We note in passing that the surface S enclosed by the closed contour is multiply-connected, and not one-sided manifold (e.g., Möbius strip) for which Stoke's theorem is not applicable. The Sagnac-based atom or optical interferometers provide the most accurate measure of the angular velocity of a rotating device. In recent years, the Sagnac effect is studied in the context of electron coherence in mesoscopic rings and carbon nanotube loops, wherein Sagnac interference is either due to rotation-induced path difference,[25, 26] or because of band velocity difference between the electrons.[27, 28]

It's worth noting that the Sagnac phase shift can be obtained from the AB phase shift using the two-fold analogy between the Coriolis force in the rotating

frame and the Lorentz force on a charged particle, as well as the canonical momentum in a rotating frame and the charged particle's momentum.[29] The hidden momentumHidden Momentum $\vec{p}_{hidden}$, which is part of the canonical momentum $\vec{p} = \partial L/\partial \vec{v}$, determines the Sagnac and AC phases.[30–32] However, as pointed out by Spavieri,[32] the HMW phase of an electric dipole travelling through a magnetic field is determined by electromagnetic momentum $\vec{p}_{em}$. For (AC, Sagnac) and (AB, HMW), the interaction energy leading to the aforesaid phases can be expressed as $U = -\vec{v} \cdot \vec{p}_{hidden}$ and $-\vec{v} \cdot \vec{p}_{em}$, respectively. The electromagnetic momentum $\vec{p}_{em}$ of an electric dipole $\vec{d}$ in a magnetic field $\vec{B}$ given by vector potential $\vec{A}$ such that $\vec{B} = \vec{\nabla} \times \vec{A}$ is $\vec{p}_{em} = (\vec{d} \cdot \vec{\nabla})\vec{A}$, and hence the interaction energy is $U = -\vec{v} \cdot \vec{p}_{em} = -\vec{v} \cdot (\vec{d} \cdot \vec{\nabla})\vec{A}$. The correctness of the interaction energy can, however, be confirmed by looking at the interaction in the dipole's rest frame. To this effect, it must be noted that the interaction cannot be represented solely in terms of the field $\vec{B}$ since the dipole is travelling through a region where both $\vec{B}$ and $\vec{A}$ are non-zero. The effective electric field experienced by the electric dipole is $\vec{\vec{E}}' = (\vec{v} \times \vec{B}) + (\vec{v} \cdot \vec{\nabla})\vec{A} = \vec{\nabla}(\vec{v} \cdot \vec{A})$ because $\vec{A}$ varies at the rate $(\vec{v} \cdot \vec{\nabla})\vec{A}$ along the path traversed by the dipole. As a result, the interaction energy is $U = -\vec{d} \cdot \vec{\vec{E}}' = -(\vec{d} \cdot \vec{\nabla})(\vec{v} \cdot \vec{A}) = -\vec{v} \cdot (\vec{d} \cdot \vec{\nabla})\vec{A}$. A simple vector identity is used in obtaining this expression, and the fact that $\vec{v}$ and $\vec{d}$ are not explicitly dependent on the x, y, z coordinates has been used. The phase acquired by the circling electric

dipole as a result of the above interaction is

$$\phi = \frac{1}{\hbar}\oint -\frac{\partial U}{\partial \vec{v}}\cdot \vec{dl}, \tag{3.5}$$

$$= \frac{1}{\hbar}\oint (\vec{d}\cdot\vec{\nabla})\vec{A}\cdot\vec{dl}, \tag{3.6}$$

$$= \frac{1}{\hbar}\oint \left(\vec{B}\times\vec{d}\right)\cdot\vec{dl} + \frac{1}{\hbar}\oint \vec{\nabla}\left(\vec{d}\cdot\vec{A}\right)\cdot\vec{dl}. \tag{3.7}$$

This is the HMW phase obtained by Spavieri[6, 7].The very existence of the second term in the above HMW phase, i.e., Spavieri term, was debated.[7, 22] As argued,[22] any closed line integrals of a gradient field $\vec{\nabla}\left(\vec{d}\cdot\vec{A}\right)$ vanish, or equivalently $\vec{\nabla}\times\vec{\nabla}\left(\vec{d}\cdot\vec{A}\right)$ is zero, which however is true when the scalar field $\left(\vec{d}\cdot\vec{A}\right)$ is a single-valued function.[33] However, if $\vec{A}$ is multi-valued, the closed line integrals of $\vec{\nabla}\left(\vec{d}\cdot\vec{A}\right)$ do not vanish. In a study by Spavieri,[7] it is proven that in the Wilkens' configuration of a dipole travelling through a magnetic sheet, the second term is non-zero while the total shift, i.e., Eq. (3.7) is zero. In Tkachuk's proposed setup,[19] the second term is identically zero for any dipole orientation. However, we are in the view that the second term is merely a mathematical curiosity with no physical importance. Nevertheless, if a setup with a monotonic gradient of $(\vec{d}\cdot\vec{A})$ is properly built-in a segment of the interferometer loop, the second term may take on a non-vanishing value. It's tempting to think of this in terms of the gradient of $(\vec{d}\cdot\vec{A})$ in the physically accessible volume of a frustum torus depicted in Fig. 3.3, which may require a suitable modification to allow for a sharp fall of $\vec{A}$ at the ends. Any potential implications that may be revealed in various torus field configurations are discussed in the last chapter concerning the future prospects of

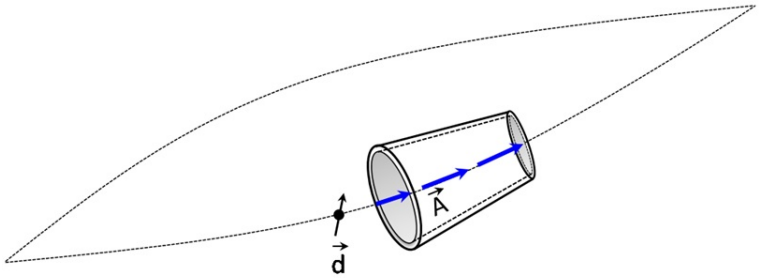

FIGURE 3.3: A current-carrying frustum torus with one of the arms of a neutral particle interferometer passes through it. Magnetic field $\vec{B}$ is contained within the coil, whereas vector potential $\vec{A}$ has a gradient both in length and cross-section.

the work carried out in this thesis. We now discuss the origin of the second term in the following section by deriving the HMW phase from the Lagrangian of the dipole, considering explicitly the interaction of the currents associated with the moving dipole with vector potential $\vec{A}$.

3.4 Lagrangian Approach to the HMW Phase

In the Lagrangian considered by Wilkens [5] and others [13, 15], only the dipole-field interaction is taken into account. Since the interaction is the same in the rest frame of the moving dipole as it is in the lab frame, the dipole-field interaction could be viewed either as $\vec{d} \cdot \vec{E}'$ in the rest frame of the dipole, with the Lorentz transformed field $\vec{E}' = \vec{v} \times \vec{B}$, or as $\vec{m}' \cdot \vec{B}$ interaction in the lab frame, where $\vec{m}' = \vec{d} \times \vec{v}$. Thus, the Lagrangian of the moving electric dipole in the magnetic

field is

$$L = \frac{1}{2}mv^2 + \vec{m}' \cdot \vec{B}, \tag{3.8}$$

$$= \frac{1}{2}mv^2 + \vec{v} \cdot \left(\vec{B} \times \vec{d}\right). \tag{3.9}$$

The canonical momentum is

$$\vec{p} = \frac{\partial L}{\partial \vec{v}} = m\vec{v} + \left(\vec{B} \times \vec{d}\right) = \vec{p}_{mech} + \vec{p}_{em}. \tag{3.10}$$

The phase shift associated with the dipole-field interaction is given by $\frac{1}{\hbar}\oint \vec{p}_{em} \cdot \vec{dl}$, which is the HMW phase expressed in Eq. (3.4). In contrast, Spavieri considered the charge-potential interaction in the same way as in the AB effect considering a point charge dipole ($\pm q$), and within the dipole approximation, the Lagrangian of the moving electric dipole is expressed as [6, 7]

$$L = \frac{1}{2}mv^2 + \vec{v} \cdot \left[\left(\vec{d} \cdot \vec{\nabla}\right)\vec{A}\right]. \tag{3.11}$$

Since, for a constant dipole moment, $\vec{\nabla}\left(\vec{d} \cdot \vec{A}\right) = \left(\vec{d} \times \vec{B}\right) + \left(\vec{d} \cdot \vec{\nabla}\right)\vec{A}$, the Lagrangian can be expressed as

$$L = \frac{1}{2}mv^2 + \vec{v} \cdot \left[\left(\vec{B} \times \vec{d}\right) + \vec{\nabla}\left(\vec{d} \cdot \vec{A}\right)\right]. \tag{3.12}$$

With the canonical momentum, $\vec{p} = \partial L/\partial \vec{v} = m\vec{v} + \left[\left(\vec{B} \times \vec{d}\right) + \vec{\nabla}\left(\vec{d} \cdot \vec{A}\right)\right]$, the phase shift corresponding to the charge-potential interaction is the HMW phase

expressed in Eq. (3.7). The first term in the interaction term of the above Lagrangian leads to the HMW phase ϕ_{HMW} and the second term gives rise to the Spavieri phase ϕ_S. Just the additional term in the HMW phase was the subject of debate as it is not obvious to be identified other than being a component of the electromagnetic momentum associated with the interaction of electric dipole with the static magnetic field.[34]

In this work, we aim to provide a unified description that takes into account dipole-field interaction and the currents associated with the dipole in motion that couple with the magnetic vector potential and obtain the same Lagrangian as due to Spavieri. Instead of a point charge dipole, as viewed by Spavieri,[6] we consider an electric dipole $\vec{d}$ at $\vec{r}(t)$ as a charge dispersion with an effective charge density given by $\rho(\vec{r}') = -\big(\vec{d}\cdot\vec{\nabla}_{\vec{r}'}\big)\delta(\vec{r}'-\vec{r})$, which when moves with velocity $\vec{v} = \frac{d\vec{r}}{dt}$ gives rise to polarization current $\vec{J}_P(\vec{r}') = -\vec{d}\big(\vec{v}\cdot\vec{\nabla}_{\vec{r}'}\big)\delta(\vec{r}'-\vec{r})$.[35] A representative sketch of charge density distribution in a physical dipole is shown in Fig. 3.4. Moreover, in the lab frame, a moving electric dipole is equivalent to a magnetic dipole and the associated magnetization current is $\vec{J}_M = -\vec{\nabla}_{\vec{r}'}\times\big[\big(\vec{v}\times\vec{d}\big)\delta(\vec{r}'-\vec{r})\big]$. Therefore, considering both the currents, the effective current density is [35]

$$\begin{aligned}
\vec{J} &= \vec{J}_M + \vec{J}_P, \\
&= -\big[\vec{\nabla}_{\vec{r}'}\times\big[\big(\vec{v}\times\vec{d}\big)\delta(\vec{r}'-\vec{r})\big] + \vec{d}\big(\vec{v}\cdot\vec{\nabla}_{\vec{r}'}\big)\delta(\vec{r}'-\vec{r})\big], \\
&= -[\delta(\vec{r}'-\vec{r})[\vec{\nabla}_{\vec{r}'}\times(\vec{v}\times\vec{d})] - (\vec{v}\times\vec{d})\times\vec{\nabla}\delta(\vec{r}'-\vec{r}) + \vec{d}(\vec{v}\cdot\vec{\nabla}_{\vec{r}'})\delta(\vec{r}'-\vec{r})], \\
&= -\vec{v}\big(\vec{d}\cdot\vec{\nabla}_{\vec{r}'}\big)\delta(\vec{r}'-\vec{r}). \qquad (3.13)
\end{aligned}$$

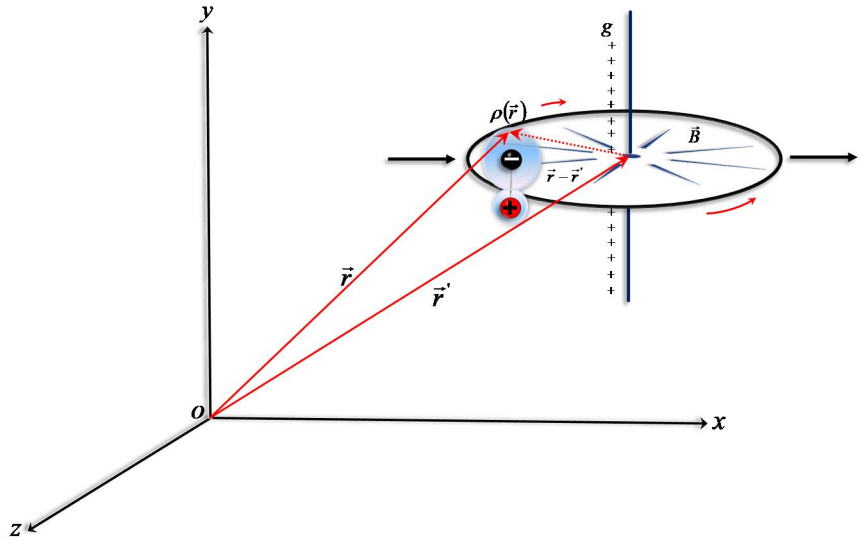

FIGURE 3.4: Representation of charge density distribution in a physical dipole.

The vector identity for curl, as well as the property of delta function, are used in simplifying the above expression for the total current density, $\vec{J}$. It should be noted that the coupling of current $\vec{J}_M$ with vector potential $\vec{A}$ results in the dipole-field interaction, which can be viewed either as $\vec{d} \cdot \vec{E}'$ in the dipole's rest frame, with Lorentz transformed electric field $\vec{E}' = \vec{v} \times \vec{B}$, or as $\vec{m}' \cdot \vec{B}$ interaction in the lab frame, where $\vec{m}'$ is the Lorentz transformed magnetic moment given by

$\vec{m}' = \vec{d} \times \vec{v}$. This can be explicitly shown as

$$\begin{aligned}
&\int \vec{J}_M(\vec{r}') \cdot \vec{A}(\vec{r}') d^3\vec{r}', \\
&= -\int \vec{\nabla}_{\vec{r}'} \times \big[\big(\vec{v} \times \vec{d}\big)\delta(\vec{r}' - \vec{r})\big] \cdot \vec{A}(\vec{r}') d^3\vec{r}', \\
&= -\int \big(\vec{v} \times \vec{d}\big)\delta(\vec{r}' - \vec{r}) \cdot \big[\vec{\nabla}_{\vec{r}'} \times \vec{A}(\vec{r}')\big] d^3\vec{r}', \\
&= -\int \big(\vec{v} \times \vec{d}\big) \cdot \vec{B}(\vec{r}')\delta(\vec{r}' - \vec{r}) d^3\vec{r}', \\
&= \big(\vec{d} \times \vec{v}\big) \cdot \vec{B}(\vec{r}), \\
&= \vec{m}' \cdot \vec{B}.
\end{aligned} \tag{3.14}$$

Once again the vector identity for curl, as well as the property of delta function, are used in obtaining the above result. Therefore, the Lagrangian of the moving electric dipole with an effective $\vec{J} \cdot \vec{A}$ interaction is

$$\begin{aligned}
L &= \frac{1}{2}mv^2 + \int \vec{J}(\vec{r}') \cdot \vec{A}(\vec{r}') d^3\vec{r}', \\
&= \frac{1}{2}mv^2 - \int \big[\vec{v}\big(\vec{d} \cdot \vec{\nabla}_{\vec{r}'}\big)\delta(\vec{r}' - \vec{r})\big] \cdot \vec{A}(\vec{r}') d^3\vec{r}', \\
&= \frac{1}{2}mv^2 - \int \vec{d} \cdot \vec{\nabla}_{\vec{r}'}\delta(\vec{r}' - \vec{r})\big(\vec{v} \cdot \vec{A}(\vec{r}')\big) d^3\vec{r}', \\
&= \frac{1}{2}mv^2 + \vec{d} \cdot \vec{\nabla}\big(\vec{v} \cdot \vec{A}\big), \\
&= \frac{1}{2}mv^2 + \vec{v} \cdot \big(\vec{d} \cdot \vec{\nabla}\big)\vec{A}, \\
&= \frac{1}{2}mv^2 + \vec{v} \cdot \big[\big(\vec{B} \times \vec{d}\big) + \vec{\nabla}\big(\vec{d} \cdot \vec{A}\big)\big].
\end{aligned} \tag{3.15}$$

This is the Lagrangian derived in Refs. [6, 7] with the interaction term leading to the phase shift given in Eq. (3.7). The ingenuity of the present consideration lies

in the fact that the term $\vec{\nabla}\big(\vec{d}\cdot\vec{A}\big)$ is now identified as electromagnetic momentum associated with the interaction of polarization current $\vec{J}_P$ with the vector potential $\vec{A}$ giving rise to the Spavieri phase ϕ_S, whereas the electromagnetic momentum $\big(\vec{B}\times\vec{d}\big)$ due to dipole-field interaction leads to the HMW phase ϕ_{HMW}. One of the most important aspects of the preceding analysis is that the $\vec{J}\cdot\vec{A}$ interaction accounts for effects associated with both $\vec{B}$ and $\vec{A}$, with the latter being particularly important in the AB-like effect when $\vec{B}$ is zero. We now demonstrate that the net force and torque on the moving electric dipole in the HMW setup are zero, and thus the HMW phase acquired by the electric dipole is purely topological in nature.

3.5 Force and Torque on a Moving Electric Dipole

The classical Lorentz forceexperienced by an electric dipole $\vec{d}$ moving with velocity $\vec{v}$ in the static magnetic field $\vec{B}$ can be determined from the associated current density $\vec{J}$ as [36]

$$\begin{aligned}
\vec{F} &= \int \vec{J}(\vec{r}')\times\vec{B}(\vec{r}')d^3\vec{r}',\\
&= -\int \big[\vec{v}\big(\vec{d}\cdot\vec{\nabla}_{\vec{r}'}\big)\delta(\vec{r}'-\vec{r})\big]\times\vec{B}(\vec{r}')d^3\vec{r}',\\
&= -\int \big(\vec{d}\cdot\vec{\nabla}_{\vec{r}'}\big)\delta(\vec{r}'-\vec{r})\big(\vec{v}\times\vec{B}(\vec{r}')\big)d^3\vec{r}',\\
&= \big(\vec{d}\cdot\vec{\nabla}\big)\big(\vec{v}\times\vec{B}\big),\\
&= \big(\vec{d}\cdot\vec{\nabla}\big)\vec{E}'.
\end{aligned} \tag{3.16}$$

where $\vec{E}' = \vec{v} \times \vec{B}$ is the Lorentz transformed electric field in the rest frame of dipole. Instead, one might be tempted to use $\vec{E}' = \big(\vec{v} \times \vec{B}\big) + \big(\vec{v} \cdot \vec{\nabla}\big)\vec{A}$ to represent the effective electric field in Eq. (3.16), however, the second term of the resultant expression can be expressed in the form $\vec{v} \times \big[\vec{\nabla} \times \vec{\nabla}\big(\vec{d} \cdot \vec{A}\big)\big]$, which is zero. The foregoing expression resulting from the second term can be realized using a vector identity, viz., $\vec{C} \times \big(\vec{\nabla} \times \vec{D}\big) = \vec{\nabla}\big(\vec{C} \cdot \vec{D}\big) - \vec{D} \times \big(\vec{\nabla} \times \vec{C}\big) - \big(\vec{C} \cdot \vec{\nabla}\big)\vec{D} - \big(\vec{D} \cdot \vec{\nabla}\big)\vec{C}$. For, $\vec{C} = \vec{v}$ and $\vec{D} = \vec{\nabla}\big(\vec{d} \cdot \vec{A}\big)$, this identity reduces to $\big(\vec{d} \cdot \vec{\nabla}\big)\big(\vec{v} \cdot \vec{\nabla}\big)\vec{A}$, while care should be taken in maintaining the correct order of operations involving $\vec{\nabla}$ in the resulting terms. We now write the force in the form obtained from the Lagrange's equation of motion, viz.,

$$\frac{d}{dt}\left(\frac{\partial L}{\partial t}\right) = \vec{\nabla} L. \tag{3.17}$$

For the Lagrangian expressed in Eq. (3.15), and making use of the convective derivative,i.e., $\frac{d}{dt} = \frac{\partial}{\partial t} + (\vec{v} \cdot \vec{\nabla})$, the Lagrange's equation of motion leads to force

$$\vec{F} = \vec{v} \times \big[\vec{\nabla} \times \big(\vec{B} \times \vec{d}\big)\big], \tag{3.18}$$

$$= \vec{v} \times \big(\vec{d} \cdot \vec{\nabla}\big)\vec{B}. \tag{3.19}$$

We note that Eq. (3.16) reduces to Eq. (3.19) for a constant $\vec{v}$ and $\vec{d}$. It is clear from Eq. (3.19) that a uniform field does not exert force on the dipole. In the HMW setup, the magnetic field does not vary in the dipole direction, i.e., $\big(\vec{d} \cdot \vec{\nabla}\big)\vec{B} = 0$, and thus the dipole experiences no force.

For a permanent electric dipole in the effective electric field $\vec{E}'$, the classical torque on the dipole is

$$\vec{\tau} = \vec{d} \times \vec{E}' = \vec{d} \times \left(\vec{v} \times \vec{B}\right). \tag{3.20}$$

Thus, so long as the dipole orients perpendicular to both $\vec{v}$ and $\vec{B}$, the torque is zero. This configuration of the triad $(\vec{v}, \vec{d}, \vec{B})$ is important in the HMW setup. However, in the case of induced dipole due to externally applied electric field $\vec{E}$, the effective field $\vec{E}' = \vec{E} + \left(\vec{v} \times \vec{B}\right)$, orients the dipole $\vec{d}$ along its direction, and the torque is always zero. Therefore, the phase acquired by the electric dipole in the HMW setup is purely topological in nature. It should be noted that the electric dipole should not be subjected to the classical force or torque while observing the HMW phase.

We here summarize the conditions for the configurations of the triad $(\vec{v}, \vec{d}, \vec{B})$ that make both force and torque zero in the HMW setup. A careful look at the above Eqs. (3.18)-(3.20) reveals that for a finite phase accumulation with a zero force and torque, the configuration in the HMW setup should be such that for

(1) a permanent dipole in a radial magnetic field, the dipole must be oriented in a direction perpendicular to both $\vec{B}$ and $\vec{v}$, i.e., $\vec{d} \perp \left(\vec{B}, \vec{v}\right)$, while for,

(2) an induced dipole, the magnetic field must be oriented in a direction perpendicular to both $\vec{d}$ and $\vec{v}$, i.e., $\vec{B} \perp \left(\vec{d}, \vec{v}\right)$.

It should be noted that any geometrical restriction on the diads $\left(\vec{B}, \vec{v}\right)$ and $\left(\vec{d}, \vec{v}\right)$

would prevent the HMW phase from being path independent. We evaluate these conditions in various configurations in the following section, and we propose a realistic radial field arrangement for observing the original HMW phase with a magnetic field alone.

3.6 HMW Phase in Various Field Configurations

Several experimental setups with various field configurations have been presented in the past for observing the HMW phase.[5, 13, 18, 19] However, Wilkens' configuration is still important for the following two reasons.[5]

(1) First, the magnetic field produced by the pierced magnetic sheet at the hole mimics the radial field produced by a line of magnetic charge, and

(2) Second, there is no electric field in the setup, which would otherwise cause stray effects linked with the Stark effect.

As shown in the preceding section that for an electric dipole, $\vec{d} = d\hat{z}\perp(\vec{B}, \vec{v})$, moving in the xy plane around a line of magnetic charge with density λ per unit length that produces a radial magnetic field given by

$$\vec{B} = \frac{B_o}{r}\hat{r}; \qquad B_o = \frac{\mu_o}{2\pi}\lambda, \tag{3.21}$$

the classical force and torque on the dipole are zero, which is essential for the topological nature of the HMW phase. We note in passing that in cold atom experiments, it is feasible to recreate a radial magnetic field caused by a line of

magnetic charge.[37] The vector potential corresponding to the above magnetic field can be written as

$$\vec{A} = \frac{\mu_o}{2\pi}\lambda\theta\hat{z}, \tag{3.22}$$

where θ, an azimuthal angle. It must be noted that θ is a multi-valued function that experiences a finite discontinuity of magnitude 2π as we go around the origin. However, for such a vector potential the gradient $\vec{\nabla}\left(\vec{d}\cdot\vec{A}\right)$ reduced to $-\left(\vec{B}\times\vec{d}\right)$, and thus the HMW phase expressed in Eq. (3.7) vanishes as discussed in Ref. [6]. At this point, it must be made clear that the multi-valued vector potential expressed in Eq. (3.22) is only a mathematical construction that makes the second term in Eq. (3.7), non zero. As argued, no vector potential with $\vec{\nabla}\times\vec{A} = \frac{B_o}{r}\hat{r}$ actually exists making $\vec{\nabla}\cdot\vec{B} = 0$ globally for Maxwell's equations to hold true.[22]

Several practical schemes were proposed for the observation of the HMW phase, however, both electric and magnetic fields are employed for the purpose. In a setup proposed by WHW,[18] the induced electric dipole $\vec{d}$ encircles a charged wire in the xy plane. The charged wire is oriented along the z direction that produces radial electric field in the xy plane, while a uniform magnetic field $(\vec{B}\perp\left(\vec{d},\vec{v}\right))$ is applied parallel to the wire along z direction. Due to the radial nature of the electric field, the orientation of the induced dipole changes along the path of the dipole, however, the requirement of the radial magnetic field for the observation of the HMW phase is eliminated in the setup. Although such field configurations

in a setup appear simple, it is only in 2012, Lepoutre et al.[10–12] experimentally observed the HMW phase. In their setup, the electric field configuration due to the central plate of the capacitor, when shrink to a wire, reduces to that of the WHW configuration. However, the problem in the experimental setup is the extraction of the HMW component from the total phase shift as the electric field-induced effects, e.g., Stark and the AC effects may contribute to the total phase shift. Also, since a uniform magnetic field is employed, the observed HMW phase shift is aesthetically different from the original HMW phase that was proposed to observe in a radial magnetic field alone. In yet another configuration due to Lee,[13] a uniform magnetic field is shown to induce the HMW phase. For a uniform field $\vec{B} = B\hat{x}$, the HMW phase acquired by a permanent electric dipole, $\vec{d} = d\hat{z}$ oriented in a direction perpendicular to both $\vec{B}$ and $\vec{v}$ can be considered as the electromagnetic dual of the phase studied by Casella involving a magnetic dipole in a uniform electric field.[3] It is to be noticed that crossed-electric and magnetic fields are commonly used to avoid the need for a radial magnetic field. For instance, in a recent experiment by Kumiya et al.,[38] uniform electric and magnetic fields are used in Ca atom interferometer leading to the HMW phase of 3.0 ± 2.1 mrad.

In this work, we emphasise the importance of an inverse radial nature of the magnetic field for observing the original HMW phase. The required radial magnetic field for the purpose can be generated in a variety of ways. For instance,

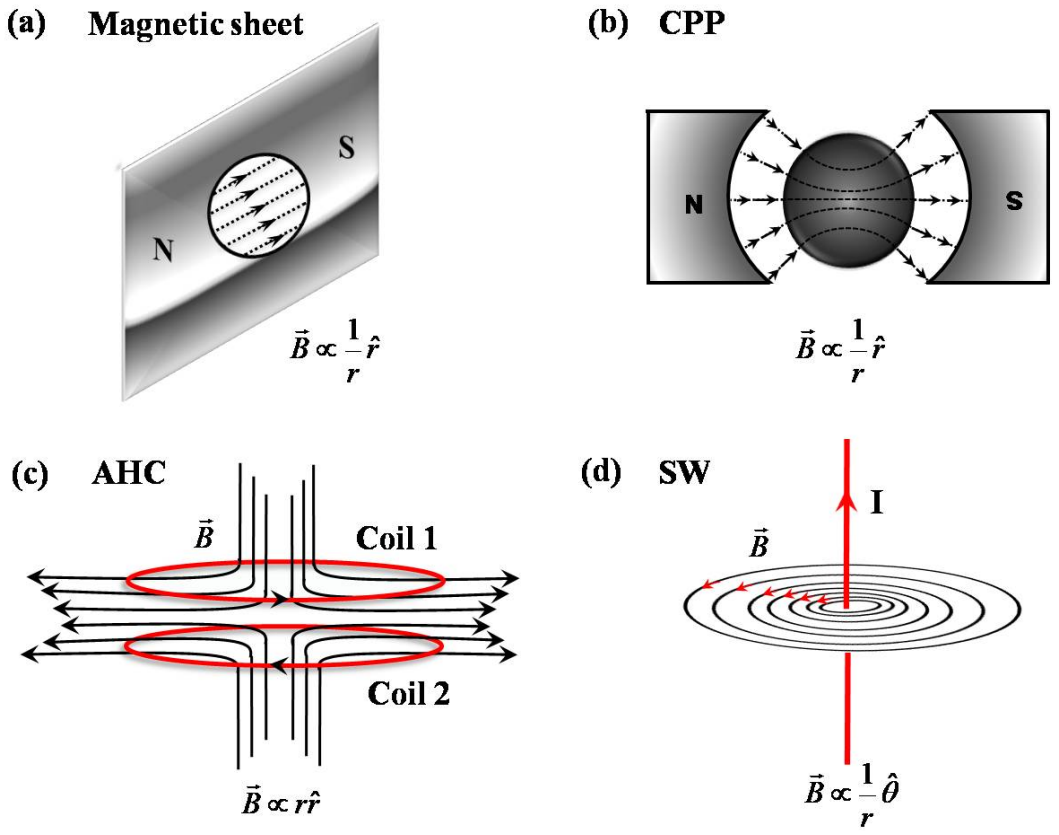

FIGURE 3.5: Field configuration in (a) Wilkens' magnetic sheet,[5] (b) Curved pole pieces (CPP),[40] (c) Anti-Helmholtz coil (AHC),[39] and (d) Straight wire (SW)

the radial magnetic field that exists in the air gap between the magnetised cylindrical curved pole pieces (CPP) and a soft iron cylindrical core, is essentially radial. Starting with Wilkens' field configuration, various other field configurations are presented in Fig. 3.5. A practical setup for the observation of the HMW phase employing CPP in the interferometric paths is discussed in the next section. Also, one may exploit the Meisner effect in a superconducting material to produce a planar radial magnetic field in a narrow gap between a superconductor disc and one end of a long current-carrying solenoid. The diverging magnetic flux out of

the solenoid's end does not penetrate the superconductor disc cooled to a temperature below the critical temperature of the material, and thus the field lines spread out in a radial pattern parallel to the narrow gap. As such, a planar radial magnetic field $\vec{B} \propto r\hat{r}$ can be obtained in an anti-Helmholtz coil (AHC) used in the study of 2D ferrofluid patterns.[39] However, in such a radial field with dipole $\vec{d} = d\hat{z}\perp(\vec{B}, \vec{v})$, and motion confined in the xy plane, $\left(\vec{B} \times \vec{d}\right) \propto r\hat{\theta}$. This results in non-zero force, while the torque vanishes. The phase accumulated by the dipole contains a component due to non-zero force, hence such a magnetic field does not belong to our consideration. Nevertheless, a slight modification in the AHC setup would yield a radial field with $\vec{B} \propto \frac{1}{r}\hat{r}$. For instance, a ferromagnetic rod may be coaxially placed in the AHC setup generating a field configuration similar to that proposed by Tkachuk.[19] It must be mentioned here that even if the field has $\frac{1}{r}$ dependence but is not radial, as is the case in a long current-carrying straight wire (SW) oriented along z-axis, for which $\vec{B} \propto \frac{1}{r}\hat{\theta}$ and thus, $\left(\vec{B} \times \vec{d}\right) \propto \frac{1}{r}\hat{r}$. The HMW phase is zero for such a field configuration. The varieties of field configurations discussed above are summarized in Table 3.1.

A moment's reflection shows that the force is zero in all configurations except that in the AHC setup, while torque is zero in all cases. Finally, we stress that the inverse radial dependence of the magnetic field is crucial for observing the original HMW phase with the magnetic field alone.

TABLE 3.1: Various field configurations for the (a) AC and (b) HMW phases. For the AC phase, $\vec{m}\perp(\vec{E},\vec{v})$, while for the HMW phase, $\vec{d}\perp(\vec{B},\vec{v})$, except in the WHW configuration in which case $\vec{B}\perp(\vec{d},\vec{v})$.

Configuration	$\vec{E}$	$\vec{B}$	ϕ	Comment	Ref.
(a) AC	$\frac{1}{r}\hat{r}$	0	$\neq 0$	Radial $\vec{E}$	[2]
Casella	Uniform	0	$\neq 0$	Equiv. to AC	[3]
(b) Wilkens	0	$\frac{1}{r}\hat{r}$	$\neq 0$	Dual of AC	[5]
WHW	$\frac{1}{r}\hat{r}$	Uniform	$\neq 0$	$\vec{E}$ radial, not $\vec{B}$	[18]
Lee	0	Uniform	$\neq 0$	Dual of Casella	[13]
CPP	0	$\frac{1}{r}\hat{r}$	$\neq 0$	Radial $\vec{B}$	[40]
AHC	0	$r\hat{r}$	$\neq 0$	Non-zero force	[39]
SW	0	$\frac{1}{r}\hat{\theta}$	0	Non radial $\vec{B}$	

3.7 Practical Setup for the Realization of the Original HMW Effect

In this section, we present a feasible setup that provides the radial magnetic field suitable for the observation of the HMW phase of a permanent electric dipole. This field configuration is in the spirit of the original HMW phase with a magnetic field alone. As shown in Fig. 3.6, the magnetic field in a space between the magnetised cylindrical curved pole pieces (CPP) and a soft iron cylindrical core at the center, is essentially a cylindrical symmetric radial field, i.e., $\vec{B} \propto \frac{1}{r}\hat{r}$.[40] Such a simple arrangement is common in the electric motors and moving coil galvanometers but has never been proposed before when a radial magnetic field with inverse radial dependency is required to realise the HMW phase in a Wilkens-type interferometric setup. For a dipole oriented along the z-axis in the cylindrical symmetric radial magnetic field, $\left(\vec{B}\times\vec{d}\right) \propto \frac{1}{r}\hat{\theta}$, the force on the dipole is zero,

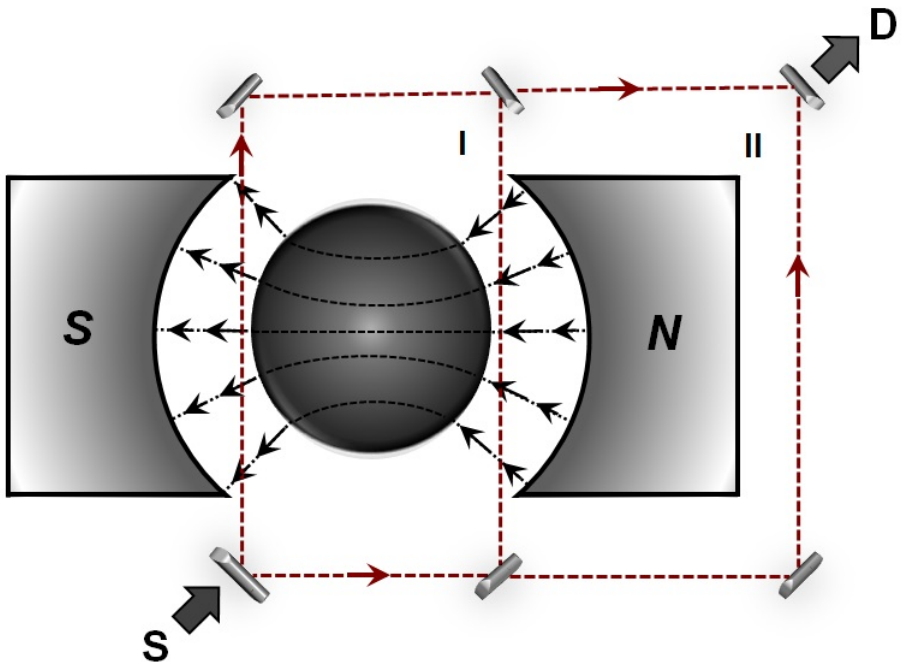

FIGURE 3.6: Top view of interferometric paths (I, II) of a permanent electric dipole through a radial magnetic field, $\vec{B} \propto \frac{1}{r}\hat{r}$ in a space between the cylindrical curved pole pieces and a soft iron core at the center. Path I encloses both converging and diverging fields while path II encloses either of the fields. The permanent electric dipole $\vec{d} = d\hat{z}$ is oriented in a direction perpendicular to the interferometric plane with a source (S) and detector (D) of the dipoles.

while its motion in the xy plane results in zero torque. As shown in the figure, two interferometric paths I and II are considered. The path I has two interferometric arms through the radial magnetic field, whereas path II only has one. It is evident from the figure that there is no HMW phase shift for the path I due to passage through both convergent and divergent radial fields. However, since path II has only one interferometric arm through either a convergent or divergent field, the dipole acquires a finite HMW phase. It must be mentioned here that several aspects of the proposed setup have a direct impact on the observability of the HMW phase. This include, minimization of flux leakage, appropriate spacing between the pole pieces and the iron core, number of turns and current through

the windings. Optimal selections of these would increase the prospects of phase measurement. Another parameter of paramount importance in the observability of the HMW phase is the strength of the electric dipole moment. A suitable choice for a permanent electric dipole would be the alkali halide molecules (MX; M=K,Rb,Cs and X=Cl,Br,I) that have dipole moments over 10 Debye.[41] Also, by applying a homogeneous electric field axially, one can enhance the dipole moment without changing its orientation, however, the resulting configuration will be identical to the WHW configuration [18] with a role reversal of the electric and magnetic fields. A subtle choice is to make use of excitons that have permanent dipole moments over 100 Debye.[42] A detailed study of the HMW effect involving excitons would offer entirely new perspectives on excitonic quantum interference in molecular and nanoscale excitonic devices.[43, 44] This is the subject of interest in the next chapter.

3.8 Summary and Concluding Remarks

In conclusion, the HMW phase of a moving electric dipole in a static magnetic field is investigated. By explicitly considering the interaction between the currents associated with the moving dipole and the vector potential corresponding to the magnetic field, we deduced the Lagrangian of the moving dipole leading to the HMW phase. The conditions for observing the HMW phase in various field configurations are explored, with a focus on the verification of the original HMW phase that was proposed to observe in a radial magnetic field alone. A simple

experimental setup, consisting of magnetized cylindrical curved pole-pieces with a ferromagnetic core at the center that provides a radial magnetic field with an inverse radial dependence is proposed for the observation of the original HMW phase. The study of magnetic field effects is important when dealing with the coherence of neutral particles endowed with electric dipole moment in an open quantum ring. This opens up whole new avenues of dipole current control in the possible HMW effect-based devices.

References

[1] Y. Aharonov and D. Bohm, Phys. Rev. **115**, 485 (1959).

[2] Y. Aharonov and A. Casher, Phys. Rev. Lett. **53**, 319 (1984).

[3] R. C. Casella, Phys. Rev. Lett. **65**, 2217 (1990).

[4] X. -G. He and B. H. J. McKellar, Phys. Rev . A **47**, 3424 (1993).

[5] M. Wilkens, Phys. Rev. Lett. **72**, 5 (1994).

[6] G. Spavieri, Phys. Rev. Lett. **81**, 1533 (1998).

[7] G. Spavieri, Phys. Rev. A **59**, 3194 (1999).

[8] G. Spavieri, Phys. Lett. A **310**, 13 (2003).

[9] J. P. Dowling, C. P. Williams, and J. D. Franson, Phys. Rev. Lett. **83**, 2486 (1999).

[10] S. Lepoutre, A. Gauguet, G. Trénec, M. Büchner, and J. Vigué, Phys. Rev. Lett. **109**, 120404 (2012).

[11] S. Lepoutre, A. Gauguet, M. Büchner, and J. Vigué, Phys. Rev. A **88**, 043627 (2013).

[12] S. Lepoutre, J. Gillot, A. Gauguet, M. Büchner, and J. Vigué, Phys. Rev. A **88**, 043628 (2013).

[13] T. –Y. Lee, Phys. Rev. A **62**, 064101 (2000).

[14] G. E. Vekstein, Eur. J. Phys. **18**, 113 (1997).

[15] V. Hnizdo, Eur. J. Phys. **33**, L3 (2012).

[16] A. L. Kholmetskii, O. V. Missevitch, and T. Yarman, Eur. J. Phys. **33**, L7 (2012).

[17] A. L. Kholmetskii, O. V. Missevitch, and T. Yarman, Prog. Electro. Res. B **45**, 83 (2012).

[18] H. Wei, R. Han, and X. Wei, Phys. Rev. Lett. **75**, 2071 (1995).

[19] V. M. Tkachuk, Phys. Rev. A **62**, 052112 (2000).

[20] Y. Sato and R. Packard, J. Phys. Conf. Ser. **150**, 032093 (2009).

[21] W. Chen, P. Horsch, and D. Manske, Phys. Rev. B **87**, 214502 (2013).

[22] M. Wilkens, Phys. Rev. Lett. **81**, 1534 (1998).

[23] H. Rauch and S. A. Werner, *Neutron Interferometry: Lessons in Experimental Quantum Mechanics, Wave-Particle Duality, and Entanglement* (OUP Oxford, 2015).

[24] L. A. Page, Phys. Rev. Lett. **35**, 543 (1975).

[25] C. P. Search, J. R. E. Toland, and M. Zivkovic, Phys. Rev. A **79**, 053607 (2009).

[26] J. R. E. Toland and C. P. Search, Phys. Lett. A **374**, 923 (2010).

[27] G. Refael, J. Heo, and M. Bockrath, Phy. Rev. Lett. **98**, 246803 (2007).

[28] W. Bishara, G. Refael, and M. Bockrath, Phys. Rev. B **78**, 165405 (2008).

[29] J. J. Sakurai, Phys. Rev. D **21**, 2993 (1980).

[30] S. M. Al-Jaber, X. Zhu, and W. C. Henneberger, Eur. J. Phys. **12**, 268 (1991).

[31] S. A. Werner, Class. Quantum Grav. **11**, A207 (1994).

[32] G. Spavieri, Nuov Cim B **111**, 1069 (1996).

[33] D. Pandres, JR., J. Math. Phys. **3**, 602, (1962).

[34] D. J. Griffiths, Am. J. Phys. **60**, 979 (1992).

[35] V. Hnizdo, Am. J. Phys. **80**, 645 (2012).

[36] J. D. Jakson, *Classical Electrodynamics* (3rd ed, Now York, John Wiley & Sons, 1999).

[37] G. J. Conduit, Phys. Rev. A **86**, 021605(R)(2012).

[38] T. Kumiya, A. S. Akentyev, Y. Mori, J. Ichimura, and A. Morinaga, Phys. Rev. A **93**, 023637 (2016).

[39] R. M. Oliveira, J. A. Miranda, and E. S. G. Leandro, Phys. Rev. E **77**, 016304 (2008).

[40] J. Chiasson, *Modeling and High-Performance Control of Electric Machines* (Wiley-IEEE Press, 2005), pp. 6, 254.

[41] Jr. R. D. Nelson, Jr. D. R. Lide, and A. A. Maryott, *Selected Values of Electric Dipole Moments for Molecules in the Gas Phase,* (National Standard Reference Data Series, NBS, 1970).

[42] R. Anankine, S. Dang, M. Beian, E. Cambri, C. G. Carbone, A. Lemaître and F. Dubin, New J. Phys. **20**, 073049 (2018).

[43] S. -K. Hong, S. W. Nam and K. -H. Yeon, Nanotechnology **19**, 155402 (2008).

[44] M. T. Lusk, C. A. Stafford, J. D. Zimmerman, and L. D. Carr, Phys. Rev. B **92**, 241112 (2015).

Chapter4

Magnetic Field-Based Exciton Current Control In The Stacked PAM Junctions[†]

Abstract

A practical realization of exciton transport control exploiting the He-McKellar-Wilkens (HMW) phase in stacked phenylacetylene macrocycle (PAM) junctions is examined. Numerical calculations suggest the sensitivity of the exciton transport to the applied magnetic field in a model 1D continuum ring system and a stacked PAM molecular ring structure. Despite the fact that a number of parameters have a direct impact on the exciton transport through a ring junction, a properly designed setup would significantly increase the prospect of exciton transport controlled by the applied magnetic field.

[†]Part of this chapter is based on a research article:
Yam P. Rai and Dhurba Rai, "On the He–McKellar–Wilkens phase of an electric dipole", Ann. Phys. **383**, 196 (2017).

4.1 Background

The concept of molecular ring junction devices, which may have substantial functionality given a wide diversity of molecular ring configurations,[1–3] has emerged in response to theoretical and experimental interest in quantum interference-based electronic devices.[4–7] The possible magnetic field control of electron transport through nano-size rings under a weak coupling condition has been investigated theoretically,[8–10] however, no experimental confirmations are available to date. The concept was then evolved to include molecular-scale rings, and it was investigated under various circumstances for potential control of electron conduction through such rings by an externally applied magnetic field. The most important prerequisite for the goal is that the molecules must have degenerate energy levels in order for them to be separated by the asymemtric geometry connection of the contact leads (or electrodes) to the ring and the energy gaps between the levels that are altered by the magnetic field.[11, 12]

Our goal in this Chapter is the investigation of potential magnetic field control of exciton current exploiting the He-McKellar-Wilkens (HMW) phase acquired by a moving exciton by virtue of its electric dipole. The observation of the HMW phase itself necessitates a significant dipole moment of the neutral particle, among other things, as was discussed in the introduction chapter. The search for a suitable and stable molecule that may be used to exploit the HMW phase and possibly make use of the HMW phase for device applications is still

ongoing because the molecular electric dipole moment greatly exceeds that of the neutral particles.[13] Alternately, since excitons are neutral particles with significant dipole moments as already discussed in the introduction chapter, we may consider employing them instead. Along this line, the possibility of using bilayer exciton condensates to demonstrate the HMW phase has been reported in the literature.[14] The choice of using excitions for large dipole moments is particularly appealing since the continuous generation of excitons using a continuous-wave (CW) laser is possible and the suitable materials for the purpose are a wide class of bilayer heterostructures of transition metal dichalcogenides (TMDs)that have a wide range of energy gap ($\sim$ 1.3 to 2.8 eV) and can be suitably modulated by scaling down their thickness from multilayer to monolayer.[15, 16] The excitons so generated are then diffused into the volume of the material and eventually lost due to electron-hole recombination, thereby releasing photons that can be accessed through photoluminescence (PL) spectroscopy.[17] A sketch of the theme undertaken in this work is shown in Fig. 4.1. Quite intrestingly the whole journey of excitons from its creation to annihilation can be tracked using the state-of-the-art spectroscopic techniques currently available.[18, 19] In particular, the indirect excitons induced in the bilayer heterostructure materials by photo excitation have the requisite properties, such as a large dipole moment, long diffusion length, and long lifetime. Additionally, in such materials, the exciton production is efficient due to the large photon absorption power of the materials associated with the characteristic direct energy gap in most cases, which can be suitably tuned by changing the stacking order. The use of an electric field through a gate electrode

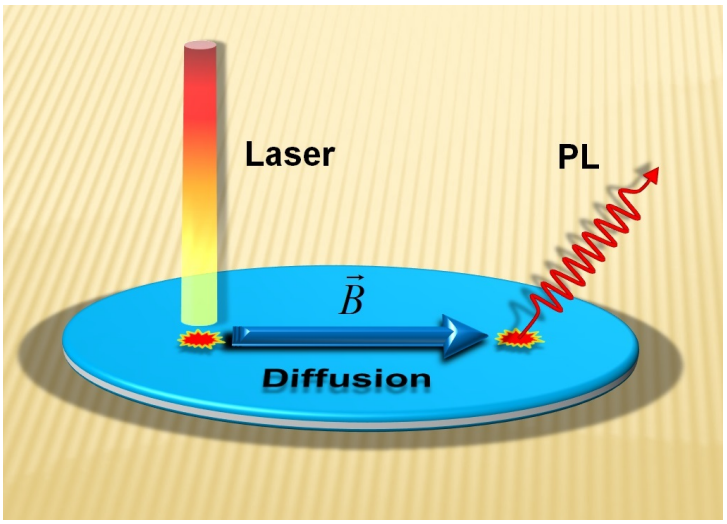

FIGURE 4.1: Optical excitation-driven diffusion of excitons with magnetic field control of PL emission.

is an efficient and well-established method of controlling exciton transport.[20, 21]

Concerning our work, we focus on the magnetic field aspects of exciton current control. The influence in the energy spectrum of an exciton in a mesoscopic quantum ring threaded by a magnetic flux has been thoroughly studied in the last decades in the context of the Aharonov-Bohm (AB) effect.[22–28] The exciton energy spectrum in the magnetic field bears a remarkable resemblance with the energy spectrum of a charged particle in the ring.[29] This motivates us to consider the possible magnetic field-based control of exciton transport across a ring structure junction along the lines of magnetic field influence on the electron transport across ring junctions as discussed in Refs.[8–12]. However, it must be mentioned here that the magnetic field influence on the energy spectra of an electric dipole or excitons confined in the quantum rings is the manifestation of the AB effect of spatially separated constituent $\pm q$ charges.[22–28] In contrast, concerning our work, the feasibility of magnetic field control of exciton transport

across ring junction lies on the modulation of the HMW phase pick-up by the interfering electric dipoles in the ring,[30] though the HMW phase can be shown to be obtained from the AB phases of the constituent charged particles,[14, 31] however, they are fundamentally different as discussed in Chapter 2. We here explore this in a molecular ring junction.

Numerous models have been proposed to study various aspects of exciton transport.[14, 32–38] For instance, the exciton currents in photosynthetic systems have been studied with the two-site and Fenna-Matthews-Olson (FMO) models, wherein currents are calculated using the quantum master equation in Lindblad form.[38] Of interest to us is how to make them move in a molecular system [33, 35, 38] or bilayer structures [14, 34, 36] as they are electrically neutral. We here consider a diffusion model for exciton transport across a molecular ring bridging the bilayer heterostructure TMD contact leads. Excitons are generated by a CW laser in the input contact that acts as the exciton source reservoir. The excitons then diffuse through the bridging ring molecule, which we considered a stacked phenylacetylene macrocycle (PAM), to reach the output TMD lead (sink reservoir) where they are annihilated and PL emission takes place. The diffusion of excitons from source to sink reservoirs set exciton current through the bridging PAM ring. The details of the proposed setup are discussed later in the section concerned.

Considering the diffusion length of inter-layer excitons ($L_D > 1\mu$m, [39]) and the size of the PAM ring (diameter $\sim$ 1 nm, [40, 41]), the proposed setup has an incredibly small gap between the TMD contact leads, and thus the transport

of excitons across the PAM can be considered to take place ballistically without energy loss. The Landauer formulation accurately describes the electron and heat transport through the molecular junctions when such coherent transport is the primary mechanism.[42–44] In a precise analogy to the electron transport, Xiong et al. [45] have studied the excitation energy transfer (EET) and the exciton current in the photosynthetic systems within the Landauer formalism with tight-binding Hamiltonians describing the exciton reservoirs and a pigment network for exciton transport. The exciton currents are evaluated by summing the exciton transmission probabilities over all the excitonic transfer channels within the relevant energy window. We here consider a tight-binding model Hamiltonian describing the stacked PAM ring molecule bridging the TMD contact leads. It is possible to perform a perspective study of the PL caused by the excitons' diffusion into the sink reservoir and the influence the applied magnetic field in the PAM ring have on the PL spectrum, similar to the study of electric field influence on the PL spectrum of excitons trapped in a quantum ring.[46]

4.2 Scope of the Work

The 2D TMDs exhibit remarkable electrical and optical properties.[47] Most importantly, the energy band gap can be altered from indirect to direct when the bulk material or multilayers are scaled down to monolayers.[48] However, the bilayer heterostructure TMDs are found to have a direct band gap.[48] The long-lived nature of the interlayer excitons generated in the bilayer heterostructure TMDs has

a diffusing ability of over a hundred nanometers distance.[39] The tunable band gap in such materials is accompanied by strong PL and large binding energy and dipole moment of the excitons, making them a promising candidate for a variety of optoelectronics and excitonic devices.[49]

In this work, we model a bilayer heterostructure TMD as an input contact lead, injecting indirect excitons excitons produced by a CW laser into the stacked PAM ring molecule and dissipating the excitons in the output bilayer heterostructure TMD on the other end. A radial magnetic field is applied in the plane of the PAM ring. Discussion on the various practical setups feasible for producing the required radial magnetic field was covered in Chapter 3. The applied magnetic field modulates the HMW phase acquired by the moving excitons, thereby affecting their interference at the output lead. However, in order for the otherwise degenerate energy levels of the ring molecule to be tuned by an applied magnetic field, the contact leads to the bridging molecule must be connected in a geometrically asymmetric configuration.[11, 12] The control over exciton transport through the ring junction is made possible by the magnetic field-tuning of the transmission spectrum that essentially changes the energy gap between the already split energy levels associated with the geometrically asymmetric connection of the contact leads to the ring. This, however, is not possible for a symmetrical connection of the contact leads to the ring. The underlying consideration has its root in the remarkable resemblance of the magnetic field effect on the energy spectrum of an

exciton confined in a ring with that of a charged particle in the ring.[29, 50] Looking from the perspectives of photon absorption for exciton generation in the input lead to the PL emission in the output lead that is tuned by the applied magnetic field in the ring, the underlying mechanism may be viewed as manipulating light with a magnetic field.[51] Such a setup may lead to the development of efficient exciton-based optoelectronic devices for optical communications.

The structure of the chapter is as follows. Section 4.3 presents the conceptual framework outlining the model for exciton formation in the input lead, exciton transport across the stacked PAM ring molecule, and exciton diffusion into the output lead with a possibility for the PL spectroscopic studies. In Section 4.4, we provide the numerical findings for a model 1D continuum ring and PAM ring junction, where the applied magnetic field effectively controls the exciton transport across the ring. Section 4.5 provides an overview of the work and its implications for further research are covered.

4.3 Theoretical Framework

We now present the theoretical models employed in our study of exciton transport and control in the molecular ring junction. We delve into the mechanisms of exciton diffusion from input to output leads, their transport across the stacked PAM ring molecule and a possible PL study, invariably under the steady-state

condition. Separating the model into three steps, as shown below, makes the entire process easier to comprehend.

4.3.1 Exciton generation and diffusion

Excitons are generated by a CW laser excitation in the input contact lead made up of a bilayer heterostructure $MoSe_2$-WSe_2. As long as the laser pumping is continuous, the interlayer excitons are generated continuously in the input lead. The bilayer $MoSe_2$-WSe_2 is a 2D material where WSe_2 monolayer is stacked on $MoSe_2$ monolayer with interlayer separation $\sim 0.40 - 0.70$ Å depending on the stacking configurations (AA, AA′ etc.) [52–55] and the interaction between the layers is a weak van der Waals interaction. Thus, it is possible to easily produce such bilayers by various methods such as artificial stacking, mechanical exfoliation, tear-and-stack and mechanical transfer.[56, 57] With the cutting-edge technologies that are currently accessible, it is possible to fabricate a monolayer TMD-PAM-TMD junction and stacked it on top of another monolayer TMD-PAM-TMD junction to produce the bilayer TMD-stacked PAM junction. The average interplanar separation in the stacked PAM is $\sim$ 0.4 nm.[41] The energy band gap of a bilayer $MoSe_2$-WSe_2 is $\sim$1.3 eV [58] while the individual $MoSe_2$ and WSe_2 monolayers have a band gap in the range $\sim 1.4 - 1.6$ eV.[59] Other heterostructures like MoS_2-WS_2, $MoSe_2$-WS_2, MoS_2-WSe_2, etc can be considered for the purpose.

The peculiar band gaps of these materials are particularly appealing for extraordinarily strong light-matter interactions as desired for applications in

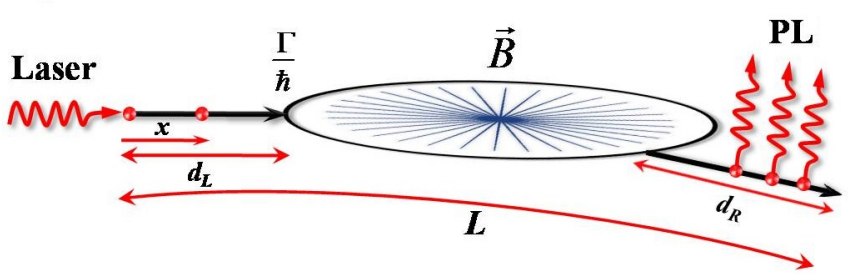

FIGURE 4.2: Laser excitation of the input contact lead and PL at the output lead with a possible magnetic field-based control of exciton transport through a molecular ring exploiting the modulation of the HMW phase acquired by the excitons. The excitons are injected into the ring at a tunneling rate $\Gamma/\hbar$ and a radial magnetic field $\vec{B}$ is applied in the molecular plane. $L < L_D$ ($L = d_L + L_M + d_R$) is the effective size of the setup and L_M is the dimeter of the molecular ring.

the optoelectronics devices operating in the visible to near-infrared wavelength regime.[60–62] Thus, upon photo-excitation, electrons and holes are generated, however, the majority of the electrons reside in the $MoSe_2$ layer and holes in the WSe_2 layer. As a result, the interlayer excitons are generated in the bilayer input lead. However, due to their longer lifetime $\tau > 1$ ns [63, 64] and high density in the laser focussed region, the exciton cloud extends well beyond the excitation region making them diffuse over several hundred nanometers. With the separation of electrons and holes into their respective quantum wells in the interlayers, indirect excitons form electric dipoles with dipole moment in the range $\sim 20 - 35$ Debye that is aligned perpendicular to the bilayer's plane. It is the gradient in dipole-dipole interaction potential that causes exciton diffusion from the region of high density to low.

We consider a laser light incident on the edge surface of the input bilayer TMD lead at $x = 0$ as depicted in Fig. 4.2. The input lead occupies the space

$x > 0$ and extends to $x = d_L$, such that the length d_L is large compared to the penetration depth $(1/\alpha)$ of the light, where α is the absorption coefficient of the bilayer TMD. Since the excitons are continuosly generated by photo excitation, the rate equation for exciton diffusion in 1D can be modeled as [65–67]

$$\frac{d}{dt}n(x,t) = D\frac{d^2}{dx^2}n(x,t) - \frac{1}{\tau}n(x,t) - R_A n^2(x,t) + G(x,t), \tag{4.1}$$

where n is the exciton density, D is the diffusion coefficient associated with exciton diffusion in the TMD material, τ is exciton lifetime, R_A is the Auger recombination coefficient, G is the light-induced exciton generation rate per unit length around x in the x-direction. Accordingly, the first term describes exciton density diffusion, the second term denotes recombination rate, while the third term describes Auger recombination (non-radiative) process. Assuming that each photon absorption causes an exciton generation and no exciton-exciton annihilation through the Auger recombination process, the exciton generation at any point x in the material can be related to the incident photon rate J_0 as $G(x,t) = G_0 e^{-\alpha x} = J_0 \alpha e^{-\alpha x}$,[67] where G_0 is the generation rate at per unit length at $x = 0$ and α is the photon absorption coefficient of the material. Given the laser power (P in μW) and wavelength (λ in nm), J_0 (photons/second) can be determined as $J_0 = 5 \times 10^9 \times P \times \lambda$. Since our concern in the present work is the steady-state transport, the exciton diffusion equation reduces to

$$\frac{d^2}{dx^2}n(x) - \frac{1}{D\tau}n(x) = -\frac{J_0\alpha}{D}e^{-\alpha x}. \tag{4.2}$$

Solving for exciton density, we get

$$n(x) = C_1 e^{\frac{x}{\sqrt{D\tau}}} + C_2 e^{-\frac{x}{\sqrt{D\tau}}} - \frac{J_0 \alpha \tau e^{-\alpha x}}{(D\tau\alpha^2 - 1)}. \tag{4.3}$$

To determine the constants C_1 and C_2, we make use of the boundary conditions, viz., at a large distance from the excitation region, the density of the excitons is zero, i.e., the exciton density is negligibly small, i.e., $n(x)\Big|_{x=+\infty} = 0$, for which Eq. 4.3 requires $C_1 = 0$. Also, due to continuous generation, the exciton density has diminishing gradient at $x = 0$, i.e., $\frac{dn(x)}{dx}\Big|_{x=0} = 0$. This condition may be identified as a non-quenching surface at $x = 0$. Thus, Eq. 4.3 leads to

$$C_2 = \frac{\sqrt{D\tau} J_0 \alpha^2 \tau}{(D\tau\alpha^2 - 1)}, \tag{4.4}$$

Therefore, the exciton density distribution is

$$n(x) = \frac{J_0 \alpha \tau}{(1 - D\tau\alpha^2)} \left[e^{-\alpha x} - \alpha \sqrt{D\tau} e^{-\frac{x}{\sqrt{D\tau}}} \right]. \tag{4.5}$$

For no diffusion ($D = 0$), this equation essentially gives the exciton density profile along the excitation path with exponentially diminishing light intensity. As discussed in the preceding section, we consider ballistic diffusion across the PAM ring molecule for $L_M << L_D$, where L_M denotes the size of the PAM ring molecule bridging the input-output leads. The exciton diffusion length L_D is related to the diffusion coefficient as $L_D = \sqrt{D\tau}$.

Transport calculations within the Landauer formulation require electronic coupling strength between the continuum energy states in the contact leads and the discrete energy levels of the bridging molecule, which can be interpreted in terms of the tunneling rate ($\Gamma/\hbar$) of the particles from the input lead to molecule and then to the output lead. In the electron transport problems in molecular junctions, one generally considers Γ on the order of a few tens to hundreds of meV,[68] while the detailed calculation would require the details of overlap integrals between the atomic orbitals of the lead and the molecular orbitals at the interface and also the density of continuum states in the lead. The present consideration is the optical excitation-driven diffusion of the excitons. For diffusion governed by Fick's law, one may consider a phenomenological model for a heuristic determination of the rate of exciton diffusion into the PAM ring as

$$k_D = -D\frac{dn(x)}{dx}\Big|_{x=d_L}, \tag{4.6}$$

$$= \frac{J_0 D\tau\alpha^2}{(1-D\tau\alpha^2)}\left[e^{-\alpha d_L} - e^{-\frac{d_L}{\sqrt{D\tau}}}\right]. \tag{4.7}$$

It is tempting to consider, for calculation purposes, a suitably scaled k_D playing the same role as Γ (or the electron transfer rate k) does in the typical electron transport problem, however, precisely identifying it as the coupling of continuum states of the bilayer TMD leads to the discrete energy levels of the stacked PAM ring would be an overstatement and overinterpretation. For low Γ electron conduction, Γ scales linearly with k,[69] however, we are not aware of any work relating k_D with Γ. This could be the basis of our future endeavour. Also, our analysis and consideration

can be thought of as operating in the wide-band approximation, where the rate at which each exciton enters the ring is independent of energy.

4.3.2 Exciton transport through stacked PAM ring

Once the excitons are mounted in the molecular ring, their conduction through various transmission channels in the molecular ring is largely decided by the quantum interference effect and coupling strength to the exit lead R. For the reason stated in the preceding sections, we consider geometrically asymmetric connection of the contact leads to the ring and consider symmetric coupling strengths, $\Gamma_L = \Gamma_R = \Gamma$. Limiting ourselves to the ballistic and elastic transport of excitons in the setup, the Landauer formalism provides a reliable mechanism for exciton transport, just as it does for electron and heat transport across the molecular junctions.[44] The central quantity in the Landauer formalism is the calculation of the transmission probability function $T(E)$. Before delving into the technical details of its calculation, we first discuss the tight-binding models adopted for our purpose. Various tight-binding models for excitons have been proposed.[70, 71] We begin with the Hamiltonian of the setup as

$$\hat{H} = \hat{H}_M + \hat{H}_K + \hat{H}_{KM}, \tag{4.8}$$

where the different sub-Hamiltonians characterise the different regions of the setup. The Hamiltonian $\hat{H}_M$ accounts for excitons in the ring molecule M, $\hat{H}_K$ for the

contact leads ($K = L, R$) that act as exciton reservoirs, while $\hat{H}_{KM}$ represents the coupling between the ring molecule and the contact leads. In second quantization form

$$\hat{H}_M = \sum_{i \in M} \epsilon_i \hat{d}_i^\dagger \hat{d}_i - \sum_{\langle ij \rangle \in M} \left(t_{ij} \hat{d}_i^\dagger \hat{d}_j + h.c. \right), \tag{4.9}$$

where $\hat{d}_i$ and $\hat{d}_i^\dagger$ destroys and creates an exciton at site i in the molecule, respectively. As is typical in the tight-binding theory, ϵ_i denotes the on-site energy and t_{ij} is the hopping integral between the nearest-neighbor sites (i, j) in the molecule. Likewise,

$$\hat{H}_K = \sum_{i \in K} \epsilon_i \hat{c}_i^\dagger \hat{c}_i, \quad K = L, R, \tag{4.10}$$

where ϵ_i is the on-site energy of excitons in the source and sink reservoirs, and $\hat{c}_i^\dagger$ and $\hat{c}_i$ are the creation and annihilation operators. The last term in the total Hamiltonian is

$$\hat{H}_{KM} = \sum_{i \in M, j \in K} \left(v_{ij} \hat{d}_i^\dagger \hat{c}_j + h.c. \right), \tag{4.11}$$

where the coupling matrix elements v_{ij} describe the strength of interaction between the continuum energy states in the contact leads and the excitonic states of the molecule. This is related to the energy level broadening function $\Gamma_{K,ij}(E) = 2\pi \sum_{k \in K} v_{ki}^* v_{kj} \rho(E)$, where $\rho(E)$ is the density of states in the contact leads. As shown in Fig. 4.3, a radial magnetic field $\vec{B} \sim \hat{r}/r$ is applied in the molecular plane of the ring. In analogy to electron transport problem,[11] magnetic field enters in the calculation through the hopping integral t_{ij} which gets modified as

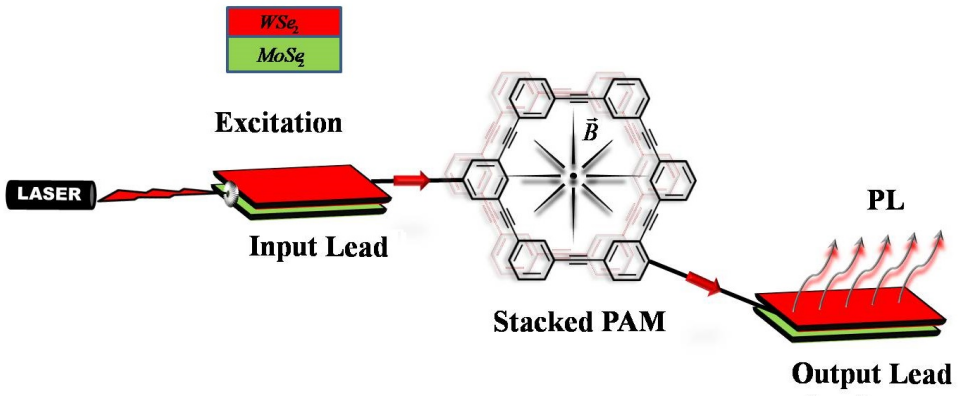

FIGURE 4.3: Schematic representation of a stacked PAM junction setup.

[14, 30]

$$t_{ij} \rightarrow t_{ij} e^{i\frac{2\pi}{|e|}(\Delta\Phi_d)_{ij}/\Phi_0}, \tag{4.12}$$

where $(\Delta\Phi_d)_{ij} = \int_{\vec{r}_i}^{\vec{r}_j} (\vec{B} \times \vec{d}) \cdot \vec{dl}$ and $\Phi_0 = h/|e|$ is the flux quantum. The phase $\Delta\phi_{HMW} = \frac{2\pi}{|e|}(\Delta\Phi_d)_{ij}/\Phi_0$ can be identified as the HMW phase acquired by the dipole $\vec{d}$ while hopping from site i to j. A driven open system with a flow of particles in and out constitutes a non-equilibrium system. In such a case, as widely used in the electron and heat transport problems, we use the non-equilibrium Green's function (NEGF) method to assess the transmission probability function $T(E)$ under the steady-state condition. Within the NEGF method, $T(E)$ can be expressed in terms of the retarded ($G^r = [E - H_M - \Sigma_L - \Sigma_R]^{-1}$) and advanced ($G^a = [G^r]^\dagger$) Green's functions of the molecule through a relation [42, 43]

$$T(E) = Tr[\Gamma^L G^r \Gamma^R G^a], \tag{4.13}$$

where the trace is taken in the finite basis set of the molecule. In the above expression, Γ^L and Γ^R are the tunneling or coupling matrices that represent the coupling

between the molecule with left and right contact leads, respectively. They are usually expressed in terms of the self-energies of the contact leads as, $\Gamma^K = i[\Sigma_K - \Sigma_K^\dagger]$. The self-energies come into play on account of the effect the bulk contact leads have on the bridging molecule. As a consequence, the molecular energy levels get broadened, thereby affecting the transport characteristics. With all relevant expressions in place, the steady-state excitonic particle current I is obtained by summing up transmission contribution from all possible energy channels in the energy window (E_{Min}, E_{Max}), i.e., [42–44]

$$I = \frac{1}{h} \int T(E) dE. \tag{4.14}$$

This consideration is an exact analogue of the Landauer current for electron and heat transport in the coherent elastic limit at 0 K temperature. The finite temperature calculations, however, require the details of exciton's occupation of energy levels in the leads subject to Bose-Einstein statistics, which is not covered in the present analysis.

4.3.3 Steady-state photoluminescence

The annihilation of excitons in the bilayer heterostructure TMD output contact lead is accompanied by a characteristic PL associated with the radiative electron-hole recombinations. The PL intensity is proportional to the number of excitons in the output lead. To calculate this, we solve the diffusion equation under the

steady-state condition, i.e.,

$$D\frac{d^2}{dx^2}n(x) - \frac{1}{\tau}n(x) + G_{0R}\,\delta(x - x_0) = 0, \tag{4.15}$$

where G_{0R} is the rate at which the excitons exit the ring at $x = x_0$ molecular-lead interface. This acts as a point source of generation of excitons in the output lead, which are then freely diffused into the output lead. Solving for the exciton density distribution, Eq. 4.15 yields

$$n(x) = C_1 e^{\frac{x}{\sqrt{D\tau}}} + C_2 e^{-\frac{x}{\sqrt{D\tau}}} + \frac{\sqrt{D\tau}G_{0R}}{2D} e^{-\frac{1}{\sqrt{D\tau}}(x-x_0)}. \tag{4.16}$$

As before, the constants C_1 and C_2 are to be determined from the boundary conditions pertinent to the physical setup. At a location far from the interface in the output lead, exciton density is negligibly small i.e., $n(x)\Big|_{x=+\infty} = 0$, for which Eq. 4.16 requires $C_1 = 0$. The boundary condition at the interface is $n(x)\Big|_{x=x_0} = G_{0R}/v = I/v$, which is the ratio of exciton current I to the exciton velocity v, with which the excitons exit the ring and enter the output lead. We take a conservative estimate of velocity as $v = \sqrt{2|E|/M}$, where M is the exciton mass. However, we consider v_0 energy independent (wide-band approximation), and evaluated as, half the value at either edge of the energy window (E_{min}, E_{max}) for conduction channels, i.e., $v_0 = v(E = E_{min/max})/2$ for all excitons. Thus,

$$C_2 = \left(\frac{1}{v} - \frac{\sqrt{D\tau}}{2D}\right) G_{0R}\, e^{\frac{1}{\sqrt{D\tau}}x_0}, \tag{4.17}$$

Therefore, the exciton density distribution in the output lead is

$$n(x) = \frac{G_{0R}}{v} e^{-\frac{1}{\sqrt{D\tau}}(x-x_0)}. \tag{4.18}$$

which is a typical density profile in a free diffusion process. PL originates from the radiative recombination of excitons. Considering that all excitons have the same recombination probability through radiative decay, the entire PL intensity from the segment, $x = x_0$ to $x = d_R$, of the output lead can be obtained by integrating the density profile as [67, 72–74]

$$I_{PL} = \int_{x_0}^{d_R} n(x)dx, \tag{4.19}$$

$$= \frac{G_{0R}}{v}\sqrt{D\tau}\Big(1 - e^{-\frac{1}{\sqrt{D\tau}}(d_R - x_0)}\Big). \tag{4.20}$$

where d_R is the distance from the interface into the output lead over which the exciton recombination takes place. In a steady-state situation, for a given magnetic field value, the PL intensity is only the function of length segment d_R of the output lead over which radiative decay of excitons occurs.

4.4 Numerical Results and Discussion

To a very good approximation, an exciton can be considered a neutral particle with a finite electric dipole moment $\vec{d}$. We consider typical parameters for the calculation of transmission probability function $T(E)$ as indicated in the respective

sections while temperature is considered zero in all calculations. Exciton transport through 1D continuum ring subject to planar radial field $\vec{B} \sim \hat{r}/r$ is studied. We consider each vertically positioned phenyl pair in the stacked PAM ring as a single site in the tight-binding model considered in this work, thereby essentially reducing the stacked PAM ring to a six-site hexamer ring. Thus, the result presented here is simply intended for indicative purposes and in no way should be taken as quantitative.

4.4.1 Exciton transport through 1D continuum ring

Considering the analogy to an electron confined in a 1D ring pierced by a magnetic field $\vec{B}$, the energy spectrum of an exciton confined in a 1D ring of radius R is given by [29, 75]

$$E(m, B) = \frac{\hbar^2}{2MR^2}\big(m + \frac{\Phi_d}{\Phi_0}\big)^2, \tag{4.21}$$

where M is the mass of the exciton and $m = 0, \pm1, \pm2, ...$ represents the angular quantum number, while $\Phi_d = \frac{1}{|e|}\oint(\vec{B} \times \vec{d}) \cdot \vec{dl}$ and $\Phi_0 = h/|e|$ is the flux quantum. As discussed in Chapter 3, the HMW phase of an electric dipole requires radial magnetic field $\vec{B} \sim \hat{r}/r$, and for the configuration where the dipole moment is oriented in the direction perpendicular to both fields $\vec{B}$ and velocity $\vec{v}$, i.e., for $\vec{d} \perp (\vec{B}, \vec{v})$, $\Phi_d = \frac{2\pi}{|e|}dRB$. The HMW phase acquired by the dipole in the ring is $\phi_{HMW} = 2\pi\Phi_d/\Phi_0$. The variation of low-lying energy states ($m = \pm0, 1, 2$) of an

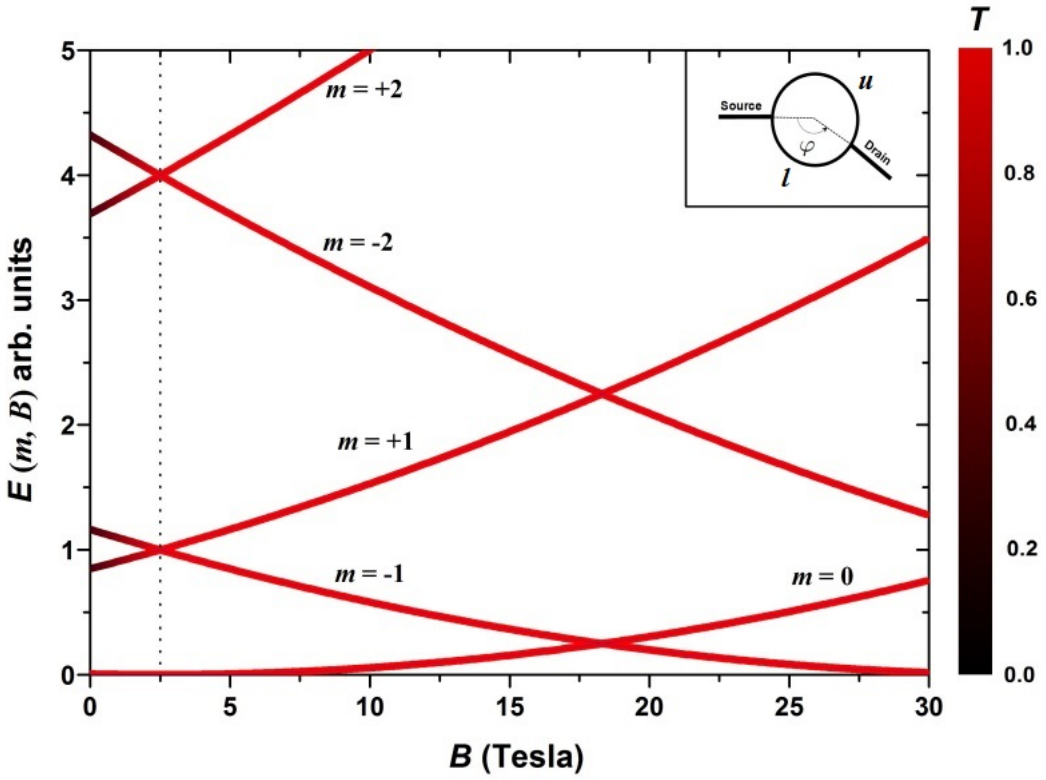

FIGURE 4.4: Low lying energy levels of an exciton confined in a 1D ring as a function of applied magnetic field for $d = 50$ Debye and $R = 10$nm. The energy levels to the left of the dotted vertical line are only indicative of how the applied magnetic field narrows the already split otherwise degenerate levels due to contacts at angular separation φ other than $n\frac{\pi}{m}$ and $(n + \frac{1}{2})\frac{\pi}{m}$. The zero of the magnetic field axis is shifted by 2.5 T to the left to show the energy level split by contact leads before the field application.

exciton confined in a 1D quantum ring as a function of the applied magnetic field is shown in Fig. 4.4 for $d = 50$ Debye and $R = 10$ nm. The transmission map along the energy curves is only for indications of the typical evolution of transmission probability and it should not by any means be considered quantitative. It illustrates how the magnetic field narrows the already separated otherwise degenerate energy levels, due to contact leads' asymmetrical connection to the ring, thereby increasing the transmission to its maximum ($T \sim 1$) at the energy level crossing or at the position of the minimum energy gap in the case of the avoided

crossing as when such circumstances arise. For the perceptive and comprehensive understanding of the events occurring at the energy levels, $T(E)$ vs E plot provides a better illustration. This is demonstrated in the next section for a stacked PAM ring junction. We may note in passing that an efficient modulation of the transmission function occurs for field values below the value for which the transmission function becomes maximum, $T \sim 1$. Whereas as stressed earlier, this is not possible in the case of symmetrically connected leads, because the symmetric connection alone does not lift the degeneracy of the energy levels. The separation of otherwise degenerate energy levels by the contact leads at zero fields is crucial, which is possible only if the contact leads are connected asymmetrically.

From the perspective of quantum interference, an exciton picks up the HMW phase in the ring and thus its wavefunction in the state m modifies to $\Psi_m(\varphi) \propto e^{i(m+\Phi_d/\Phi_0)\varphi}$. This leads the exciton transport properties to undergo Aharonov-Bohm like oscillations due to fluctuation of transmission probability T_m for state m as a function of flux Φ_d.[76] Possibility of controlling exciton transport with quantum interference alone has been discussed in Ref. [77]. Considering the counter-propagating waves, $\Psi^u_m \propto e^{i(m-\Phi_d/\Phi_0)(2\pi-\varphi)}$ in the upper arm (u) and $\Psi^l_m \propto e^{i(m+\Phi_d/\Phi_0)\varphi}$ in the lower arm (l) of the ring, the interference at the exit point φ at the output lead results in fluctuation of transmission probabilityas

$$T_m \propto |\Psi^u_m + \Psi^l_m|^2 = 2\big[1 + cos\big(2m\varphi + 2\pi\frac{\Phi_d}{\Phi_0}\big)\big], \tag{4.22}$$

where the first term in the cosine term represents the interference condition that

depends on the geometrical connection of the contact leads to the ring. Constructive interference takes place for $\varphi = n\frac{\pi}{m}$ giving rise to a pronounced resonant transmission peak at the position of the otherwise degenerate energy levels of the isolated ring, while no transmission takes place for $\varphi = (n + \frac{1}{2})\frac{\pi}{m}$, due to destructive interference. In analogy to the electron transport through a quantum ring, an interesting situation occurs when the contact leads split the degenerate energy levels for the exit lead position other than $n\frac{\pi}{m}$ and $(n + \frac{1}{2})\frac{\pi}{m}$, $n = 0, 1, 2, ...$[78] At this point, we wish to draw the attention to a fact that, at first glance, it may appear that influencing exciton transport by tuning the interference effect requires an extremely high magnetic field for Φ_d of the order of the flux quantum, Φ_0. This is not the case, though, as we will see in a moment. The transmission peaks for the split energy levels by the asymmetric connection of the contact leads in a stacked PAM ring are relatively distinct and well-resolved when the ring is coupled only weakly to the contact leads. These peaks are then tuned by the magnetic field for a transmission maximum ($T \sim 1$), which corresponds to the overlap of the transmission peaks when the field narrows down the energy gap. Thus, in a suitably designed setup, the application of a magnetic field can control the exciton transport through a molecular ring junction.

4.4.2 Exciton transport through a stacked PAM ring

For our model calculations, we consider the vertically positioned phenyl ring pairs in the stacked PAM ring structure as single sites with the associated tight-binding

parameters, viz., on-site energy $\epsilon_i = 0, \forall\ i \in M$ and the nearest-neighbor hopping integral between sites $t_{\langle ij \rangle} = 0.01, \forall\ \langle i, j \rangle \in M$ eV. The on-site energy is the energy of the particle when it occupies a specific site, while the hopping integral is the kinetic energy associated with the hopping from one site to the next. Whereas the on-site energy does not affect the calculation other than accurate positioning of the energy levels of the ring within the conductin energy window, the hopping integral is important, the more precise the better. We consider the above values in the lack of these parameters in the literature, however, one can still look into the generic features. Within the tight-binding model, the stacked PAM under consideration is essentially a hexamer with a side 0.5 nm.[40, 41] Considering the interplanar separation in the $MoSe_2$-WSe_2 to be 0.4 nm,[52] the dipole moment of the interlayer is 20 Debye. For the modulation of the transmission spectra, a radial magnetic field of strength in the range (0 to 10 Tesla) is applied in the plane of the PAM ring. Various possible setups for generating radial fields were discussed in Chapter 3.

Of most importance is the geometrically asymmetric connection of the contact leads to the stacked PAM rings. This is essential for the split of the otherwise degenerate energy levels of the stacked PAM rings. Weak contact-molecule coupling $\Gamma = 0.001$ eV [79] is considered so as to affect the relative distinct energy levels and the associated sharp transmission resonance in the ring by the applied magnetic field. The transmission spectrum $T(E)$ as a function of exciton energy E in the energy range as indicated for different field values is shown in Fig. 4.5

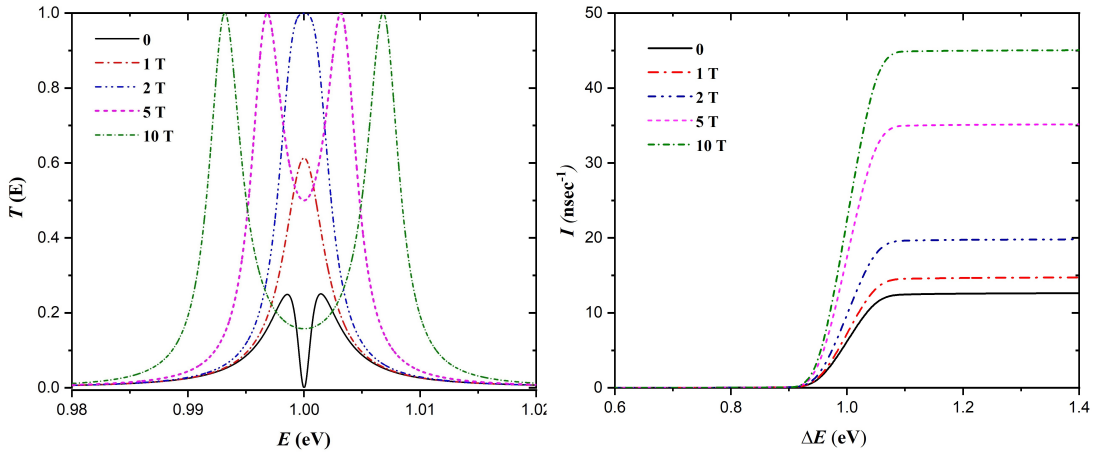

FIGURE 4.5: (a) Transmission probability as a function of energy for transmission through a frontier orbital positioned at 1 eV for different values of magnetic fields $\vec{B}$, and (b) Current as a function of energy window $\Delta E = E_{Max} - E_{Min}$ placed symetrically about 1 eV, for $\Gamma = 0.001$ eV, $D = 0.6$ cm^2 sec^{-1} and $\tau = 1.5$ nsec.

(a). As is evident from the plot, at zero field, two distinct transmission peaks arise corresponding to the split of degenerate energy levels by the geometrically asymmetric connection of the contact leads. On the field application, the energy gap narrows down and consequently, the transmission peaks come closer to each other and eventually overlap when the energy gap reduces to zero. This corresponds to $T(E) \sim 1$ in the transmission spectrum. Beyond this, the area under each transmission peak remains essentially constant. This leads to saturation in the current values as shown in Fig. 4.5 (b). Emphasis must be laid on the requirement of a weak contact-molecule coupling which together with a magnetic field can have a significant impact on current conduction. Although there are several factors that have detrimental effects on exciton transport but a suitably designed molecular ring junction device would greatly improve the prospects of exciton current control under an applied magnetic field.

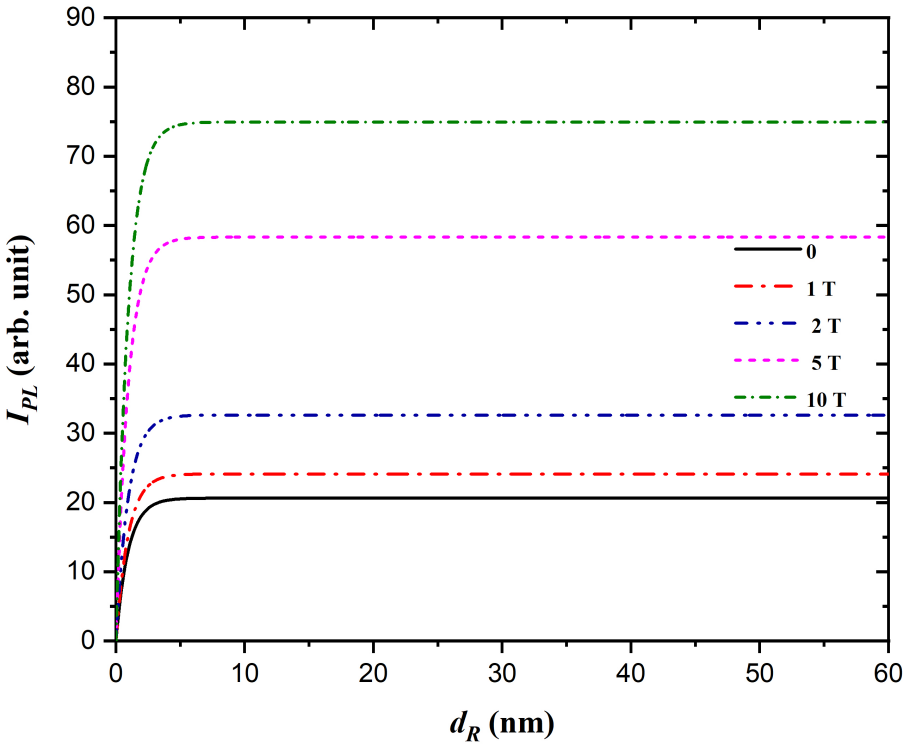

FIGURE 4.6: PL intensity as a function of length d_R of the output contact lead for different values of field strength for $\Delta E = 1$ eV.

The PL emission taking place in the output lead over the length d_R is studied. The PL intensity is plotted as a function of length segment d_R for various field strengths. This is shown in Fig. 4.6. As all the excitons reaching the output lead within their lifetime contribute to the PL intensity, the increase of PL intensity nearly linearly with d_R is expected at shorter lengths. However, for a given exciton current, the majority of the excitons are annihilated much faster than they diffuse, which causes PL saturation as d_R is increased. It is the modulation of the PL intensity by the applied magnetic field in the ring that may find potential application in the emerging field of exciton-based optoelectronic devices.

4.5 Summary and Concluding Remarks

We have considered light-driven exciton diffusion through a suitably designed bilayer TMD-PAM-TMD junction. Exciton diffusion into the stacked PAM ring molecule is studied. Once inside the ring molecule, the excitons pick up an additional phase in accordance with the HMW effect in the ring. For a low lead-molecule coupling, the modulation of the HMW phase of the excitons by the applied magnetic field has a significant effect on the transmission spectrum that affects the exciton conduction through the molecule. This is also demonstrated in the 1D continuum ring. The most basic prerequisite condition for realising this is to have a geometrically asymmetric connection of the contact leads to the ring so that the level degeneracy of the molecule is lifted by the contact leads alone. The applied field then modulates the energy gap between the split levels, affecting the exciton transport. The PL intensity resulting from the electron-hole recombination is studied and magnetic field influence is observed. The whole setup can be viewed as the magnetic field-based control of light in a molecular ring junction. A deeper study is necessary to make our findings an intuitive and compelling argument for the viability of creating excitonic devices and integrating them into circuits, which will pave a new avenue for the development of future exciton-based optoelectronic devices. Any progress on this otherwise unexplored subject and the findings will be discussed elsewhere.

References

[1] M. Mayor and C. Didschies, Angew. Chem. Int. Ed. **42**, 3176 (2003).

[2] T. Akutagawa, R. Jin. R. Tunashima. S. -ichiro Noro, L. Cronin, and T. Nakamura, Langmuir **24**, 231 (2008).

[3] M. Richaus, M. Jirasek, L. Tejerina, H. Gotfredsen, M. D. Peeks, R. Haver, H. -Wei, Jiang, T. D. W. Claridge, and H. L. Anderson, Nat. Chem. **12**, 236 (2020).

[4] S. -H. Ke and W. Yang, Nano Lett. **8**, 3257 (2008).

[5] A. S. -Souza, M. Smeu, L. Zhang, A. G. S. Filho, H. Cuo, and M. A. Ratner, J. Am. Chem. Soc. **136**, 15065 (2014).

[6] C. Ja, M. Famili, M. Carlotti, Y. Liu, P. Wang, I M. Grace, Z. Feng, Y. Wang, Z. Zhao, M. Ding, X. Xu, C. Wang, S. -J. Lee, Y. Huang, R. Chiechi, C. J. Lambert, and X. Duan, Sci. Adv. **4**, 8237 (2018).

[7] M. Carlotti, S. Soni, X. Qiu, E. Sauter, M. Zharnikov, and R. C. Chiechi, Nabiscale Adv. **1**, 2018 (2019).

[8] O. Hod, R. Baer, and E. Rabani, J. Phys. Chem. B **108**, 14807 (2004).

[9] O. Hod, E. Rabani, and R. Baer, Acc. Chem. Res. **39**, 109 (2006).

[10] O. Hod, R. Baer, and E. Rabani, J. Phys.: Condens. Matter **20**, 383201 (2008).

[11] D. Rai, Oded Hod and A. Nitzan, J. Phys. Chem. Lett. **2**, 2118 (2011).

[12] D. Rai, Oded Hod and A. Nitzan. Phys. Rev. B **85**, 155440 (2012).

[13] Jr. R. D. Nelson, Jr. D. R. Lide, and A. A. Maryott, *Selected Values of Electric Dipole Moments for Molecules in the Gas Phase* (National Standard Reference Data Series, NBS, 1970).

[14] W.Chen, P. Horsch and D. Manske, Phys. Rev. B **87**, 214502 (2013).

[15] A. V. Kolobov and J. Tominaga, *Two-Dimensional Transition-Metal Dichalocogenides* (Springer Series in Materials Science, 2016).

[16] A. Chaves, J. G. Azadani, H. Alsalman et al. NPJ 2D Mater. Appl. **4**, 29 (2020).

[17] G. M. Akselrod, P. B. Deotare, N. J. Thompson, J. Lee, W. A. Tisdale, M. C. Baldo, V. M. Menon, and V. Bulovic, Nat. Commun. **5**, 3646 (2014).

[18] C. Geogi, M. Bohmler, H. Qian, L. Novotny, and A. Hartschuh, Phys. Status Solidi B **246**, 2683 (2009).

[19] Y. Wan, A. Stradomska, J. Knoester, and L. Huang, J. Am. Chem. Soc. **139**, 7287 (2017).

[20] A. A. High, E. E. Novitskaya, L. V. Butov, M. Hanson, and A. C. Gossard, Science **321**, 229 (2008).

[21] Y. Liu, K. Dini, Q. Tan, T. Liew, K. S. Novoselov, and W. Gao, Sci. Adv. **6**, 1830 (2020).

[22] A. V. Chaplik, JETP Lett. **62**, 900 (1995).

[23] R. A. Romer and M. E. Raikh, Phys. Rev. B **62**, 7045 (2000).

[24] A. V. Chaplik, JETP Lett. **75**, 292 (2002).

[25] A. O. Govorov, S. E. Ulloa, K. Karrai, and R. J. Warburton, Phys. Rev. B **66**, 081309(R) (2002).

[26] S. E. Ulloaa, A. O. Govorova, A. V. Kalameitsevb, R. Warburtonc and K. Karraid, Physica E **12**, 790 (2002).

[27] K. Moulopoulos and M. Constantinou, Philos. Mag. **86**, 2511 (2006).

[28] M.D. Teodoro, V. L. Campo, Jr. V. L. -Richard, E. Marega et al. Phys. Rev. Lett. **104**, 086401 (2010).

[29] J. G. Analytis, S. J. Blundell, A. Ardavan, Am. J. Phys. **72**, 613 (2004).

[30] J. Yi, G. S. Jeon, and M. Y. Choi, Phys. Rev. B **52**, 7838 (1995).

[31] G. Spavieri, Phys. Rev. A **59**, 3194 (1999).

[32] D. V. Averin, A. N. Korotkov, and Y. Nazorov, Phys. Rev. Lett. **66**, 2818 (1991).

[33] M. Nakano, M. Takahata, S. Yamada, K. Yamaguchi, R. Kishi, and T. Nitta, J. Chem. Phys. **120**, 2359 (2004).

[34] J. -J. Su and A. H. MacDonald, Nat. Phys. **4**, 799 (2008).

[35] G. Panitchayangkoona, D. V. Voronineb, D. Abramaviciusc, J. R. Carama, N. H. C. Lewisa, S. Mukamele, and Gregory S. Engela, PNAS **108**, 20908 (2011).

[36] A. D. K. Finck, J. P. Eisenstein, L. N. Pfeiffer, and K. W. West, Phys. Rev. Lett. **106**, 236807 (2011).

[37] J. P. Eisenstein, A. D. K. Finck, D. Nandi, L. N. Pfeiffer, and K. W. West, J. Phys. Conf. Ser. **456**, 012009 (2013).

[38] C. Guan, N. Wu, and Y. Zhao, J. Chem. Phys. **138**, 115102 (2013).

[39] J. Choi, W. -T. Hsu, L. -S. Lu et al. Sci. Adv. **6**, 8866 (2020).

[40] J. S. Moore, J. Zhang, Z. Wu, D. Venkataraman, and S. Lee, Macromol. Symp. **77**, 295 (1994).

[41] B. Traber, T. Oeser, and R. Gleiter, Eur. J. Org. Chem. **2005**, 1283 (2005).

[42] S. Datta, *Quantum Transport in Mesoscopic Systems* (Cambridge University Press, 1995).

[43] M. Di Ventra, *Electrical Transport in Nanoscale Systems* (Cambridge University Press, 2008).

[44] N. A. Zimbovskaya, J. Phys.: Condens. Matter **28**, 183002 (2006).

[45] S. J. Xiong, Y. Xiong, and Y. Zhao, J. Chem. Phys. **137**, 094107 (2012).

[46] L. G. G. V. Dias da Silva, José M. V. -Bôas, and Sergio E. Ulloa, Phys. Rev. B **76**, 155306 (2007).

[47] M. Bernardi, C. Ataca, M. Palummo, and J. C. Grossman, Nanophotonics **6**, 479 (2017).

[48] J. Gusakova, X. Wang, L. L. Shiau, A. Krivosheeva, V. Shaposhnikov, V. Borisenko, V. Gusakov, and B. K. Tay, Phys. Status Solidi A **214**, 1700218 (2017).

[49] N. Huo, Y. Yang, and J. Li, J. Semicond. **38**, 3 (2017).

[50] N. A. J. Kleemans, J. H. Blokland, A. G. Taboada et al. Phys. Rev. B **80**, 155318 (2009).

[51] B. A. van Tiggelen and G. L. J. A. Rikken, in *Optical Properties of Nanostructured Random Media* (Topics in Applied Physics, Vol 82. Springer, Berlin, 2002) pp. 275-302.

[52] F. Zhang, W. Li, and X. Dai, Solid State Commun. **266**, 11 (2017).

[53] R. Gillen and J. Maultzsch, Phys. Rev. B **97**, 165306 (2018).

[54] W. Li, X. Lu, S. Dubey, L. Devenica, and A. Srivatava, Nat. Mat. **19**, 624 (2019).

[55] K. Tran, G. Moody, F. Wu, X. Lu et al. **567**, 71 (2019).

[56] Z. Gao, M. -Q. Zhao, Md. M. A. Ashik, A. T. C. Johnson Jr. J. Phys. Mater. **3**, 042003 (2020).

[57] A. J. Watson, W. Lu, M. H. D. Guimaraes, and M. Stohr, 2D Mater. **8**, 032001 (2021).

[58] K. Xu, Y. Xu, H. Zhang, B. Peng et al. Phys. Chem. Chem. Phys. **20**, 30351 (2018).

[59] S. Deng and L. Li, and M. Li, Physica E Low Dimens. Syst. Nanostruct. **101**, 44 (2018).

[60] W. Liu, M. Liu, H. Hand, S. Fang, H. Teng, M. Lei, and Z. Wei, Photonics Res. **6**, C15 (2018).

[61] T. Mueller and E. Malic, NPJ 2D Mater. Appl. **2**, 29 (2018).

[62] F. Li, B. Zu, W. Yang, Z. Qi, C. Ma, Y. Wang, X. Zhang, Z. Luo, D. Liang, D. Li, Z. Li, and A. Pan, Nano Res. **13**, 1053 (2020).

[63] P. Rivera, J. R. Schaibley, A. M. Jones et al. Nature Commun. **6**, 6242 (2015).

[64] R. Gillen, Phys. Status Solidi B **258**, 2000614 (2021).

[65] B. J. Mulder in *Diffusion and surface reactions of singlet excitons in anthracene* (Technische Hogeschool Eindhoven, 1967).

[66] D. Haarer and G. Castro, J. Lumin. **12**, 233 (1976).

[67] R. R. Lunt, N. C. Giebink, A. A. Belak, J. B. Benziger, and S. R. Forrest, J. Appl. Phys. **105**, 053711 (2009).

[68] Y. Komoto, S. Fujii, H. Nakamura, T. Tada, T. Nishino, and M. Kiguchi, Sci. Rep. **6**, 26606 (2016).

[69] W. Dou and J. E. Subotnik, J. Phys. Chem. A **124**, 757 (2020).

[70] H. Li, S. V. Malinin, S. Tretiak, and V. Y. Chernyak, J. Chem. Phys. **139**, 064109 (2013).

[71] P. Stepnicki and M. Matuszewski, Phys. Rev. A **88**, 033626 (2013).

[72] Y. Wu, Y. C. Zhou, H. R. Wu, Y. Q. Zhang, J. Zhou, S. T. Zhang, J. M. Zhao, Z. J. Wang, X. M. Ding, and X. Y. Hou, Appl. Phys. Lett. **87**, 044104 (2005).

[73] Y. C. Zhou, Y. Wu, L. L. Ma, J. Zhou, X. M. Ding, and X. Y. Hou, J. Appl. Phys. **100**, 023712 (2006).

[74] J. Xie, T. Inaba, R. Sugiyama, and Y. Homma, Phys. Rev. B **85**, 085434 (2012).

[75] S. Viefers, P. Koskinen, P. S. Deo, and M. Manninen, Physica E **21**, 1 (2004).

[76] R. A. Romer and M. E. Raikh, Phys. Sat. Sol. (b) **221**, 535 (2000).

[77] M. T. Lusk, C. A. Stafford, J. D. Zimmerman, and L. D. Carr, Phys. Rev. B **92**, 241112(R) (2015).

[78] J. Yi, G. Cuniberti, and M. Porto, Eur. Phys. J. B **33**, 221 (2003).

[79] K. Wang, J. Zhou, J. M. Hamill, and B. Xu, J. Chem. Phys. **141**, 054712 (2014).

Chapter5

Future Prospects

In this thesis, a variety of topics related to the Aharonov-Bohm (AB) and He-McKellar-Wilkens (HMW) phases of charged particles and electric dipoles, respectively, have been discussed. An attempt has been made to present a unified description of the various quantum topological phases, including the dual-AB and Aharonov-Casher (AC) phases of fluxon and magnetic moment. The associated quantum effects are coherently described as being an exclusively local phenomena by the local coupling of the hierarchy of multipole moments (charge, moment, quadrupole) of the particles to their corresponding orders of external potentials (potential, field, field-gradient). The AB effect is seen to be a case of a perfect shielding with no field overlapping, indicating that it is an energy-based phenomenon. The observation of the HMW phase in the presence of a radial magnetic field alone has been stressed in the context of the phase shift associated with a moving electric dipole. This then conforms to the original proposal in spirit. A practical setup for the HMW phase observation has been suggested. Observation conditions with regards to various field configurations have been discussed. Furthermore, the HMW phase is exploited in affecting the exciton transport in an

optically driven molecular ring junction. The tight-binding model-based calculations show that the sensitivity of the exciton transport properties to the applied magnetic field in a suitably designed device provides promising prospects for future exciton-based optoelectronic devices.

Although the major goal of the thesis has been achieved, deeper accessements including the analytical validations and ab initio based computational tests are highly warranted. Future works in this area are expected to involve physical demonstration, or at the very least, simulations that accurately reflect the actual physical scenario. We feel that this thesis may provide the necessary background information and a stimulating discussion for these future works. The following are some of the areas that have been identified to be worthwhile investigations.

- ☞ (1) Chapter 2: Experimental study of Boyer type-II effect to verify if the effect is actually the entire interference pattern shift to establish that the AB effect is not a force-based effect as contested otherwise.

- ☞ (2) Chapter 2: A deeper energy-based considerations may prove helpful in overcoming AB's non-locality issue to the effect that the vector potential is treated as a fuzzy physical quantity.

- ☞ (3) Chapter 3: Examination of any physical effects concerning electric dipole's motion through a monotonic gradient of the vector potential.

- ☞ (4) Chapter 3: Observation of the HMW effect solely in a magnetic field in the spirit of the original proposal.

☞ (5) Chapter 4: Ab inito based calculations of the magnetic field control of exciton transport in a light-driven exciton through a molecular ring junction.

☞ (6) Chapter 4: Experimental study of magnetic field effects on exciton current for excitonic device applications in optoelectronics and optical communications.

The aforementioned points, however, require some justifications and thus the following brief overview is important.

(1) Boyer's reactionary force-based analysis has been the most persuasive in its attempt to explain the physical cause of the AB effect. Although this could be viewed as investigating a quantum effect through classical physics, an analysis so strong, convincing and compelling cannot be ignored. The surprising result was the exact match between the force-based phase shift (Boyer type-II) and the AB phase shift. The AB phase shift was then attributed to the classical electromagnetic lag effect in account of the longitudinal component of the force causing relative displacement between the interfering charges for the phase shift. On closer inspection, the transverse component appears responsible for the shift of the entire envelope of the interference pattern, but this is not the genuine AB effect wherein only the fringe shift occurs while the envelope is maintained stationary. Any attempt to observe the classical lag effect inherently depends on the magnetic field shielding efficiency of the setup.[1] We strongly believe that the genuine AB effect corresponds to the perfect shielding case with no classical force whatsoever. Thus, a careful study is necessary to confirm that the genuine AB effect is an

energy-based effect rather than force-based.

(2) Overcoming AB's non-locality issue inevitably demands asserting the physical nature of the vector potential. It may be thought of as a fuzzy physical quantity, as stressed in this work. It may sound strange and peculiar, but the fuzziness is associated with its non-unique determination since it is non-gauge invariant. Subject to a gauge transformation, the energy considerations may be helpful in fixing the vector potential if the magnetic energy density computed from the vector potential alone is identical to that derived independently from the magnetic field within a given tolerance. We will not push this perception too far, instead expect the enthusiasts to explore along this line for any possible implications that may be unveiled and discussed in the context of the issues in question. However, working towards the reality of the vector potential demands careful consideration and compliance with the gauge symmetry.

(3) Interaction of an electric dipole with a magnetic field emanates from the coupling of dipole moment with the motional electric field, which has a component that depends on the gradient of the vector potential. Therefore, it is very encouraging to investigate the physical impacts that the different vector potential configurations have on the moving dipoles shown in Fig. 5.1. The gradient of the vector potential varies depending on the arrangement, but a highly abrupt decline in the vector potential at the ends is considered in all cases. The interferometric setups shown are reminiscent of the setup for the AB effect using ring torus.[2]

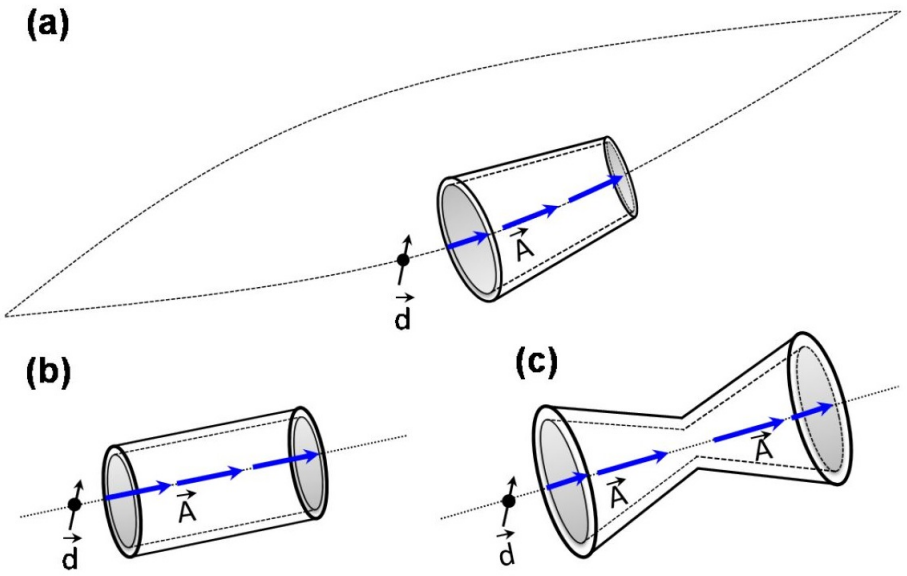

FIGURE 5.1: Dipole interferometer with one of the arms through (a) frustum torus, (b) cylindrical torus, and (c) an hourglass-shaped torus. Only the vector potentials at axial points are shown with a magnitude proportional to the length of arrows.

Should the gradient of vector potential bear any effects, the cylindrical torus and hourglass-shaped torus do not exhibit any effects because the vector potential is uniform in the case of the cylindrical torus and zero in the latter. This is because the increase in the vector potential in the first half is offset by a decrease in the other half.

(4) The original focus of the HMW effect was the observation of the quantum mechanical phase of an electric dipole in a radial magnetic field. Several field configurations were offered, including the one in the most recent experimental demonstration,[3, 4] but they did not draw attention to the need for the radial magnetic field as originally proposed. Although the use of crossed-electric and magnetic fields eliminates the requirement for a radial magnetic field for the purpose, the disadvantage of employing the crossed-electric and magnetic fields is

the emergence of the stray effects associated with the Stark effect that makes extracting the HMW phase difficult. Thus, the observation of the HMW effect in the presence of a radial magnetic field alone is still worth trying and remains a challenge. Our proposed setup could be useful to test the effect using some stable molecules with dipole moment exceeding 10 Debye.

(5) While the model-based calculations capture only the generic features of the physical situations the molecular junction devices are exposed to, the ab initio calculations are, however, computationally demanding but accurately represent the physical situations as they include many-body effects and incorporate various excitation processes. This is crucial to determine whether the sensitivity to magnetic field influence endures in the face of detrimental effects such as thermal dephasing that results in decoherence. The non-equilibrium Green's function density functional theory (NEGF-DFT) with a tight-binding formulation holds a great promise for transport computations. Simulated calculations of light-driven excitonic transport through a variety of molecular junction devices are necessary for predicting the characteristic transport features for device applications in exciton-based optoelectronic devices.

(6) Magnetic field-based control of light can be achieved in molecular ring junctions. Experimental demonstrations should be feasible with a variety of suitable 2D materials for exciton generation by photoexcitation and their field-based control of transport through the molecular rings bridging such materials accompanied

by field-modulated photoluminescence at the output. Such exciton-based devices hold great promise for technological applications as well as providing a greater understanding of happenings at the microscopic level since direct images of exciton propagation can be achieved via tip-enhanced near-field optical microscopy.

It is observed that significant progress has been made over the years in demonstrating the decades-old fundamental discoveries of the various quantum topological phases. This is important because it confirms the true nature of the fundamental interactions. It has been noted that despite their discoveries long ago, very few attempts have been made to put them into practical applications. The majority of efforts have been focused on the theoretical understanding of the quantum topological phases, while very few studies have attempted to utilise these phases. The present technologies could be refined with capabilities to fully utilise the topological phases and their associated effects for device applications.

We believe that the studies made over the years culminating in the form of a thesis represent the actual physical scenario, but a careful and thorough assessment through the experimental methodologies is indispensable to validate our findings. Undoubtedly, further research is needed, but with the rapid development of experimental techniques, we express a great hope that the results of the work carried out in the present venture will be realized. Until then some of our findings in the present endeavor may remain elusive.

References

[1] M. Becker and H. Batellan, EPL, **115**, 10011 (2016).

[2] N. J. Carron, Am. J. Phys. **63**, 717 (1995).

[3] J. Gillot, S. Lepoutre, A. Gauguet, M. Büchner, and J. Vigué, Phys. Rev. Lett. **111**, 030401 (2013).

[4] S. Lepoutre, A. Gauguet, M. Büchner, and J. Vigué, Phys. Rev. A **88**, 043627 (2013).

Index